A Brachiating Robot Controller

Jun NAKANISHI

Contents

Acknowledgements

This work could never be accomplished without many people's support who have contributed their valuable time. I would like to acknowledge all the people's help with this work.

First, I would like to thank Professor Toshio Fukuda of Center for Cooperative Research in Advanced Science and Technology at Nagoya University for having this work possible through his support, instruction and encouragement.

I am grateful to Professor Daniel E. Koditschek of the University of Michigan for his support, advice and a number of illuminating discussions particularly during my stay in his lab at the University of Michigan.

I would also like to thank the members of my thesis committee, Professor Yoshikazu Suematsu and Professor Yoshikazu Hayakawa of Department of Electronic-Mechanical Engineering at Nagoya University for their help. I am indebted to Professor Gancho Vachkov, Associate Professor Fumihito Arai, Research Associate Yasuhisa Hasegawa, Research Associate Futoshi Kobayashi, Engineering Technician Mr. Hideo Matsuura, and all of the previous and present faculty and staff members, secretaries and colleagues of Fukuda lab at Nagoya University.

I wish to express my appreciation to the colleagues of Kodlab and the staff members in Advanced Technology Laboratories at the University of Michigan as well. My special thanks to Bill Schwind and Noah Cowan of the University of Michigan for their helpful remarks and suggestions on this work as well as for their help during my stay there. I would like to thank Professor Roberto Horowitz of the University of California at Berkeley for having valuable discussions during his stay at Nagoya University on sabbatical.

I am grateful to the members of the international exchange committee and all the people who have supported my study as a graduate student at the Department of Electrical Engineering and Computer Science, the University of Michigan from fall 1995 to summer 1996 through the exchange program between School of Engineering, Nagoya University and College of Engineering, the University of Michigan under a Toyota Exchange Fund Scholarship.

Finally, I wish to express my deep appreciation to my family for their understanding and support throughout my life.

Chapter 1

Introduction

This dissertation presents our effort to develop a new controller for a two degree of freedom brachiating robot. A brachiating robot dynamically moves from handhold to handhold like a long armed ape swinging its arms as depicted in Figure 1.1. This dissertation concerns a simplified two-link robot with one actuator at the elbow connecting two arms, each of which has a gripper (see Figure 1.3). Since the grippers cannot impose torque on the handhold, this is an underactuated machine, having fewer actuators than its degrees of freedom. In spite of its relatively simple structure, designing a brachiating controller for such a system is challenging since the theory of underactuated mechanisms is not well established.

A growing number of robotics researchers have taken an interest in building machines that are required to interact dynamically with an otherwise unactuated environment in order to achieve a designated task [36]. Our interest in this work arises from general concern about how dynamically dexterous tasks can be achieved by combining physical insight into the task and the intrinsic dynamics of the system in its environment. Brachiating robots take an interesting place within this larger category of robots that juggle, bat, catch, hop and walk. A brachiating and a legged locomotion system share the requirement of an oscillatory exchange of kinetic energy and potential energy in the gravitational field. Brachiation incurs the added problem of dexterous grasps: fumbles not only fail the task but incur a potentially disastrous fall as well.

This chapter introduces the background of this work. In Section 1.1, we briefly review the literature in primatology and biomechanics of brachiation. Section 1.2 reviews the related work to our study of robot brachiation. Section 1.3 discusses the role of task encoding to achieve dynamical dexterity. In Section 1.4, from our reading of the biomechanics literature, we define variants of robot brachiation problems that we will refer to in this work.

1.1 What is Brachiation?

Brachiation—arboreal locomotion via arms swinging hand over hand through the trees—is an interesting form of locomotion unique to long armed apes as depicted in Figure 1.1. In primatology [50], apes are in the anthropoid families, which is common to man, and they are classified into two families. One of them is *Pongidae* including the gorilla, chimpanzee and orang-utan, and the other is *Hylobatidae* including the gibbon and siamang which are arboreal in habitat in tropical rain forest of Southeast Asia [50]. In fact, apes and monkeys are quite different anatomically. One of the basic differences between apes and monkeys is that apes have much greater flexibility
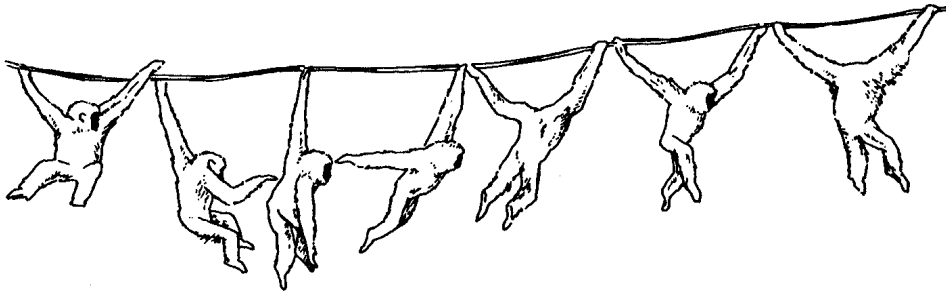
Figure 1.1: Brachiation of a gibbon: a picture taken from [70].

of movement in their long forelimbs than monkeys as depicted in Figure 1.2—with their free swinging arms that rotate at shoulders, apes can travel in arm swinging locomotion while monkeys are basically quadrupeds [18].

Historically, Keith introduced the term "brachiation" in 1899 [32] and its participial adjective "brachiating" as well according to [80]. However, the agent-noun "brachiator" had been applied by Owen at least forty years earlier (e.g. in [54]) to the "long-armed" gibbons in contrast to the orang-utan, chimpanzee and gorilla [80]. Napier reviews the historical usage of these terms "brachiation" and "brachiator," and defines the terminology based on his classification of arm-swinging locomotion of anthropoid apes and monkeys [51]. Only the gibbons and the siamangs can be regarded as "full-time" brachiators since they perform efficient brachiation by means of the suspensory activities of the forelimbs alone at almost all the time in locomotion [51]. Carpenter estimates that approximately 90% of locomotion of a gibbon is brachiation by his observation of the behavior of gibbons in his field study in Thailand [17]. While orang-utans are entirely arboreal in habitat, they climb and move cautiously with the aid by the hind limbs because of their body weight. Gorillas are essentially forest floor animals, and chimpanzees appear to take an intermediate position between gibbons and orangs in terms of brachiating forms [51]. Among all four apes, the gibbons are the best at brachiating whose slight body, elongated arms and fingers are morphologically suited to this form of locomotion [18]. Most commonly, gibbons engage in "slow brachiation," traveling at about the speed of the average human walk. But when excited or frightened, they can plunge through the forest canopy at astonishing speeds, sometimes covering 30 feet or more in a single jump without a break in "stride" (fast brachiation, ricocheting) [18].

In the studies of biomechanics of brachiation [20, 55, 56], specifically Preuschoft *et al.* identified a close correspondence between slow brachiation and the motion of a simplified pendulum [56]. Although the ape's moment of inertia varies during the swing locomotion according to its change of posture, the motion of a simplified pendulum gives a fairly good approximation. Motivated by this pendulous motion of an ape's brachiation, we will introduce the notion of "target dynamics" in which the the robot brachiation task is encoded in Chapter 2 as we will discuss.

1.2   Related Work—Dynamically Dexterous Robotics—

Consider the behaviors that we do easily and naturally, for example, manipulation of objects such as picking up and placing a cup on a table, throwing and catching a ball, as well as walk, run,
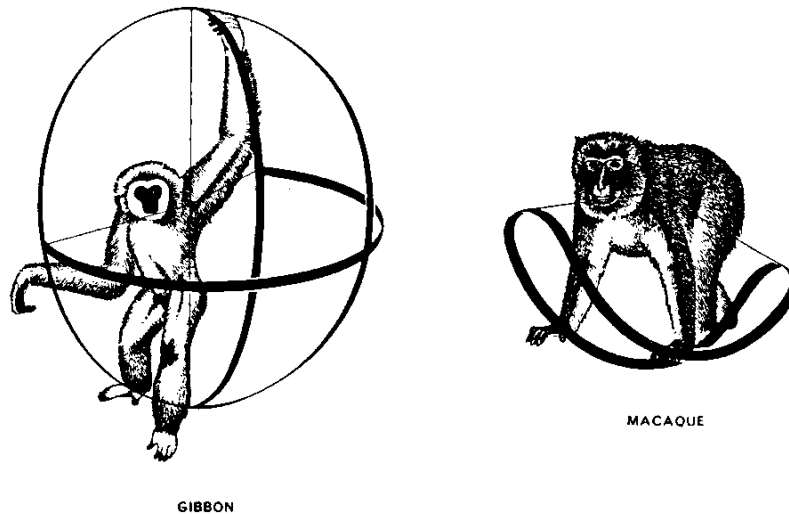
Figure 1.2: Limber forelimbs of apes. Left: gibbon (ape). Right: macaque (monkey). Apes have much greater flexibility of movement in their forelimbs than monkeys which makes difference in their form of locomotion. While monkeys are quadruped, apes can swing by their arms. Pictures taken from [18].

and going up and down stairs avoiding obstacles or recovering from unexpected slip or stumble at the same time. There were growing expectations in the 80's that such humans' dexterity could be achieved with the rapid progress in robotics and computer science and technology. However, the following was pointed out by Koditschek [36] in 1993, about seven years ago from now:

> While computers has been built that play chess better than almost every human being, we have yet to build a machine as capable as a toddler of walking up the stairs or grabbing a cup[1].

In fact, even now, we are still far from developing robots fully capable of achieving dynamically dexterous behaviors that humans easily do in the real world such as throw and catch, walk and run with the requirement of physical interaction with unactuated and unstructured environment. Much of the traditional literature in robot control has been centrally concerned with set point, tracking and force control problems, and typically tasks such as handling workpieces and assembly were executed by forcing the robot to track reference trajectories generated in some ways. In contrast, when considering dynamically dexterous tasks that involve unactuated degrees of freedom, there is no hope of controlling all the degrees of freedom independently or forcing the system to track arbitrary reference trajectories.

Under these circumstances, we are interested in exploring how such dynamically dexterous behaviors can be achieved by use of physical insight into the task and intrinsic dynamics of the system in its environment. Brachiation is an interesting form of locomotion which is in the larger category of dynamically dexterous behaviors such as a walk, run, hop and juggle. In this study, we consider a simplified two degrees of freedom brachiating robot depicted in Figure 1.3, which

---

[1]As we may recall, IBM's super computer "Deep Blue" beat World Champion Garry Kasparov in 1997.
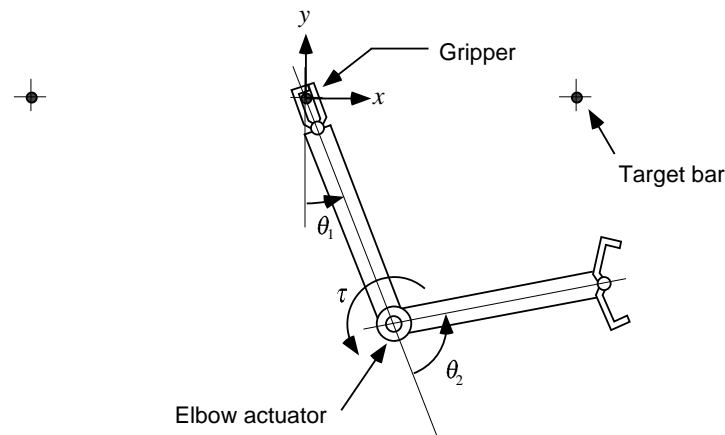
Figure 1.3: A two-link brachiating robot.

is an underactuated system having fewer actuators than its degrees of freedom. The dynamics of the system take the form of a planar double pendulum system with actuation at the second joint. In spite of its simple structure, analysis of its dynamics is very difficult since the differential equations of motion, which have strong nonlinear dynamical coupling, cannot be solved in terms of elementary functions, and general theory for nonlinear coupled oscillators is not available yet[2]. Furthermore, in general, nonlinear systems whose phase space dimension is equal or more than three are known to exhibit "chaos," which is defined as "aperiodic long-term behavior in a deterministic system that exhibits sensitive dependence on initial conditions" [75]. Thus, our system arising from revolute-revolute kinematic chains whose dynamics have four dimensional phase space are "chaotic" and can be expected to exhibit extremely complex orbits.

In the following, we first review the relationship of the robot brachiation problem domain to the overlapping areas of dexterous manipulation, legged locomotion and underactuated mechanisms. Then, we also briefly refer to the studies on nonholonomic systems and Lagrangian systems from a theoretic view of nonlinear control systems.

Dexterous Manipulation

Problems of dexterous manipulation have given rise to a growing literature concerned with explicit manipulation of an environment's kinetic as well as potential energy. Arguably, the first great success in this domain must be attributed to Andersson [2] whose ping pong playing robot developed a decade ago was capable of beating many humans. The control architecture employs a black board style rule-based AI decision process which relies on carefully crafted aerodynamics and impact dynamics of the ping pong ball and manipulator dynamics models.

Subsequently, Koditschek and his colleagues [14, 15, 16, 61] developed a family of juggling robots that exhibit increasingly sophisticated strategic as well as mechanical skills in various "games against nature" from a theoretical basis. They have introduced "mirror algorithms" based on what they call a "geometric robot programming" approach — "the desirability of translating

---

[2]Russian mathematician Arnold says in his textbook of classical mechanics [7], "Analyzing a general potential system with two degrees of freedom is beyond the capability of modern science."

Figure 1.4: The spatial juggler—the "Bühgler Arm"—developed by Koditcshek *et al.* which is capable of batting two balls simultaneously [59, 60]. This picture is taken from [8].

abstract user defined goals into phase space geometry for purpose of task encoding" [14]. In the mirror algorithm, the robot is forced to track the reference trajectory of the mirror image of the ball states servoing the mechanical energy of the ball around the desired level in order to achieve juggling with the specified height of the ball [15]. This strategy was generalized from the vertical one-juggle—prismatic-prismatic batting—into the planer two-juggle where the one degree of freedom revolute robot bats two balls simultaneously in a two dimensional plane [14]. Furthermore, they scaled it up to the spatial juggling where the three degrees of freedom robot juggles two balls simultaneously in a three dimensional space [59, 60] as depicted in Figure 1.4 with the generalization to dynamical obstacle avoidance problems as well [16].

Schaal and Atkeson have also investigated similar dexterous maneuvers such as batting and juggling using learning methods. They implemented a memory-based learning algorithm to achieve "devil sticking" which is a form of juggling where a stick is batted back and forth between two handsticks [67]. More recently, Lynch and Mason have studied the problem of dynamic nonprehensile manipulation from the control theoretic point of view [42]. Following a careful controllability analysis, they have designed open loop control laws for a one degree of freedom revolute robot which performs dynamic tasks such as snatching, rolling, throwing and catching as depicted in Figure 1.5. These maneuvers are achieved by numerically generated solutions to appropriate optimal trajectory planning problems with respect to the carefully modelled plant.

The present study is most reminiscent of the juggling work by Koditschek *et al.* since our approach entails feedback regulation rather than the optimal control theoretic approach generating open loop pre-planned trajectories developed by Lynch and Mason, the AI system developed by Andersson, or the learning approach by Schaal and Atkeson.
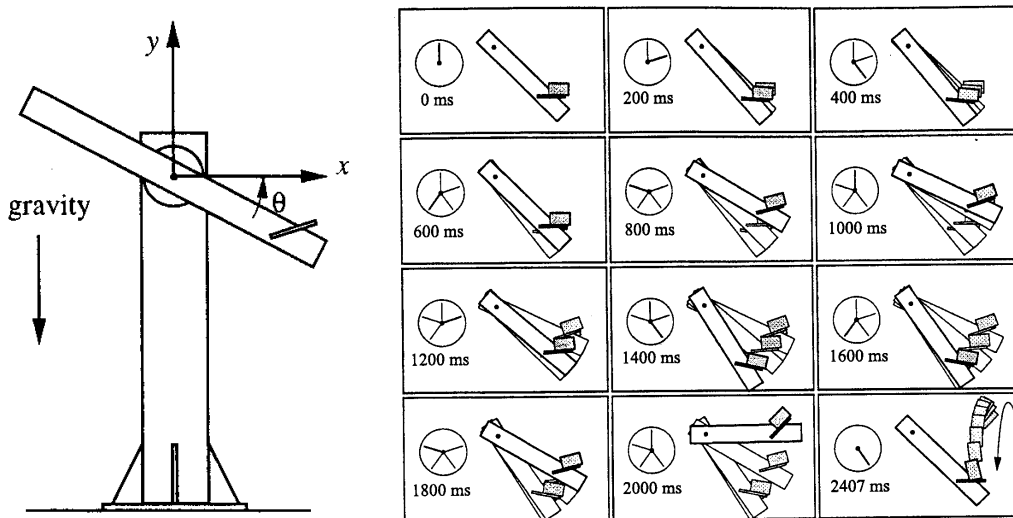
Figure 1.5: Dynamic nonprehensile manipulation by Lynch and Mason [42]. Left: One degree of freedom revolute robot (NSK direct-drive arm) built by them. Right: The robot performs a throw of a block. Pictures are taken from [42].

Legged Locomotion

Raibert's landmark success in legged locomotion [57] represents another important influence on the present work. He and his colleagues first studied the control a running machine with one leg in the plane. They introduced a simple feedback algorithm for a planar one-legged hopping machine in order to regulate its desired hopping height, body posture, and forward velocity based on their physical insight, which was extended to achieve running in three dimensions (see Figure 1.6). Furthermore, they generalized their one-leg algorithms for biped running and quadruped running [57]. They achieved gymnastic maneuvers such as a flip and a front aerial using their planar biped robot as well [28] (see Figure 1.7). Koditschek and his colleagues have pursued a number of analytical studies of simple hopping machines that are directly inspired by Raibert's work addressing such questions as regulation of hopping height [37], forward velocity [68] and duty factor [69]. They found the same underlying stability mechanisms in Raibert's hoppers as in their juggling algorithms [15, 37, 57]. Burdick and his colleagues have also investigated numerically the periodic motion of Raibert style hopping robots [46, 82].

The formulation of this brachiation problem in terms of a lower dimensional target dynamics owes much to Raibert's original notion that dynamical dexterity may be encoded in terms of desired energy and achieved with the help of the environment's intrinsic dynamics. Moreover, we have adapted his use of a reverse time symmetry and analysis of the mechanics of a flip to our problem setting.

Underactuated Systems

Amidst the large and growing controls literature on underactuated mechanisms, this work is closest in method to Spong and his colleagues' studies of the "Acrobot" [73]. They considered the problem of swinging up and stabilization to the vertical equilibrium position of an underactuated
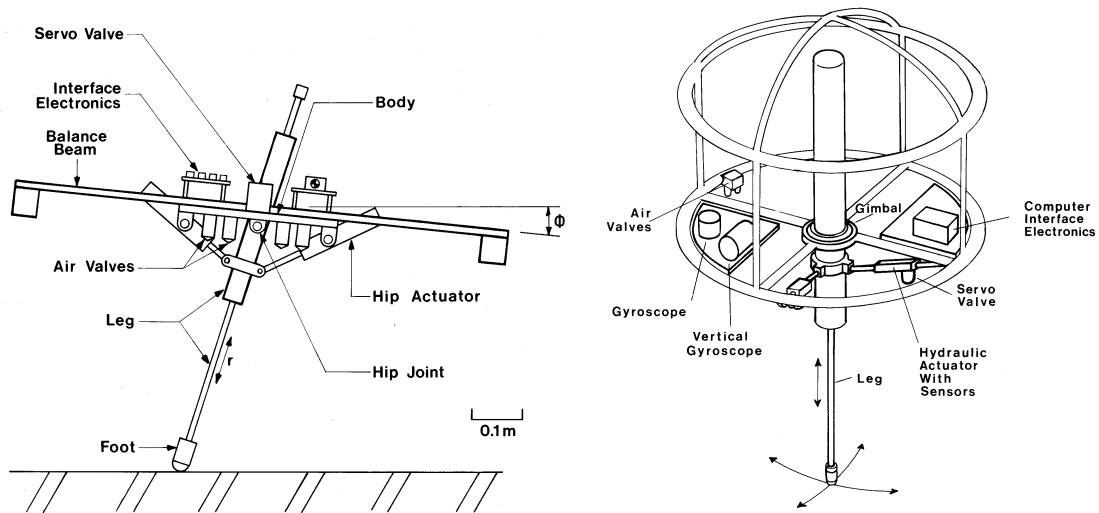
Figure 1.6: The planar and 3D one-legged hopping machines developed by Raibert *et al.* Pictures are taken from [57].

system, which is similar to the two-link brachiating robot we treat in this work. Their control algorithm pumps energy to the system in an instance of Spong's more general notion of partial feedback linearization [72] directed toward achieving a kind of target dynamics whose motions solve the swing up problem.

Recently, there has been much work on the joint position/tracking control of underactuated systems in a horizontal plane, which are not affected by the gravity. Oriolo and Nakamura treat unactuated portions of the dynamical equation of the system as second order nonholonomic constraints[3], which are generally nonintegrable [53]. A review of recent work on nonholonomic robotic systems is provided by Nakamura in [47]. From this point of view, he and his colleagues proposed a position control scheme for a two degree of freedom horizontal underactuated manipulator using time-periodic inputs to the first actuated joint [77]. Subsequently, Suzuki and Nakamura analyzed the behavior of such an underactuated system in response to periodic inputs using averaging method as well as a three degree of freedom planar manipulator whose first joint is actuated and the other two joints are unactuated [78]. For the same class of two degrees of freedom underactuated manipulators, Arai *et al.* proposed a path planning algorithm based on time-scaling of active joint trajectories and a bidirectional approach[4]. Their algorithm achieves simultaneous positioning of active and passive joints with only two swings [4], however existence of the desired path is not analytically shown. At the same time, Lynch studied the collision-free motion planning problem for a three degrees of freedom horizontal manipulator with a passive

---

[3]In classical mechanics [26], systems are defined to be "holonomic" whose constraints of the motion are expressed as algebraic equations with respect to the generalized coordinates, x, and the time, t, of the form $f(x, t) = 0$, and constraints which cannot be expressed in this fashion are called nonholonomic, e.g. $f(x, \dot{x}, \ddot{x}, t) = 0$ [47].

[4] The bidirectional approach in path planning of space robots proposed by Nakamura *et al.* [48] first considers asymptotic stabilization of the augmented system consisting of two of the original systems to the same manifold both from the initial state and the goal state simultaneously via state feedback based on Lyaponov's direct method. Then, the desired path from the initial state to the goal state is obtained by connecting the generated trajectories from the initial state to the manifold and from the goal state to the manifold traced back in time [47].
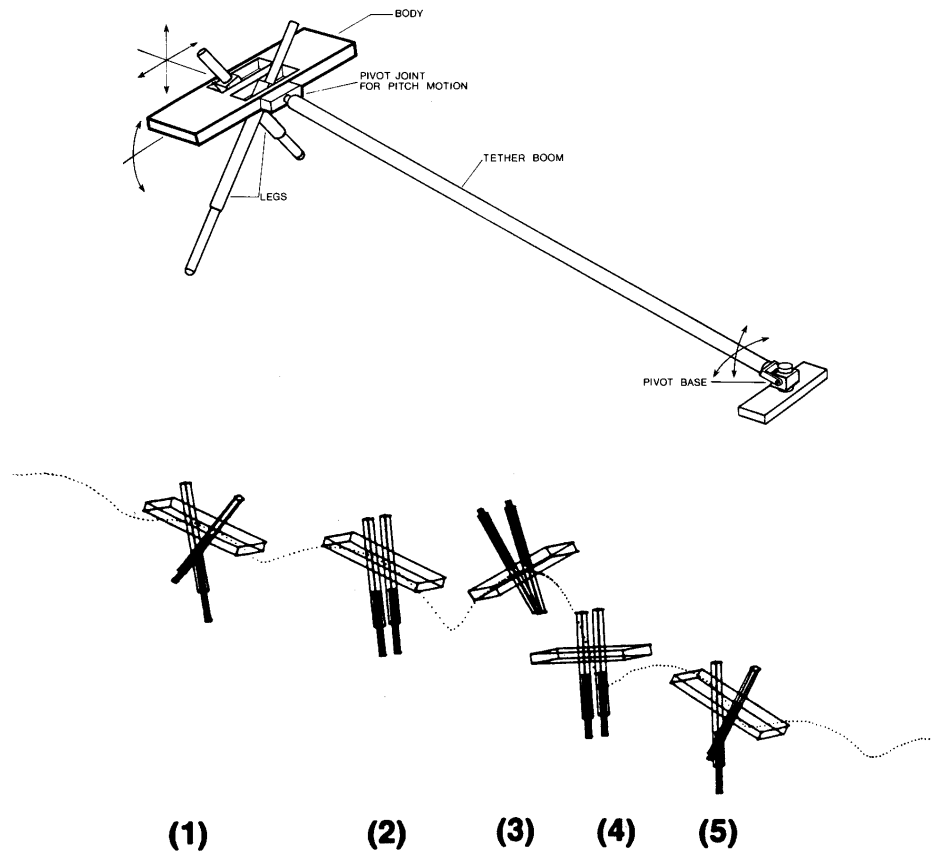
Figure 1.7: Top: the planar biped legged hopping machine developed by Raibert *et al.* Bottom: a flip maneuver of the planar biped. Pictures are taken from [57].

third joint in collaboration with Arai *et al.* [43]. Following a controllability analysis for the passive third link based on [3], they proposed an algorithm which generates collision-free fast trajectories between two states with zero velocity in the presence of obstacles. More recently, Kobayashi *et al.* investigated controllability of planar underactuated manipulators in collaboration with Imura and Yoshikawa [34]. Motivated by the bidirectional approach [48], they derived a necessary and sufficient controllability condition for a class of planar manipulator with n actuated joints and one unactuated joint. They concluded that such underactuated manipulators are controllable if and only if the first joint is actuated, i.e., there exists a control input which will transfer any initial state to any state in finite interval of time [34]. In their proof motivated by the bidirectional approach, they consider the configuration of the system where the whole arm is fully stretched out rotating at a constant angular velocity as an intermediate manifold to stabilize the system from the initial and the goal states.

In the control of underactuated systems under the influence of the gravity in addition to Spong's work, Mareczek *et al.* proposed a switching algorithm for joint position control for a 2 dof manipulator equipped with a brake at the unactuated second joint in a inclined plane [44].

Hauser and Murray studied the control of the Acrobot using an approximate linearization to force the system to track trajectories near inverted equilibrium manifold [27]. Berkemeier *et al.* also considered the tracking problem of a class of periodic joint trajectories of their interest for the Acrobot [9]. Furuta *et al.* have investigated the swing up control of single and double pendulum systems on a rotating arm [25, 52, 84] which can be also regarded as underactuated systems. In [25, 52], they designed a swing up controller for a single pendulum system with a bang-bang type control input whose sequence is determined using an optimal control. To stabilize at the inverted equilibrium position, the control is switched from the swing up controller to a stabilizing controller with a linear optimal regulator in the neighborhood of the upright position. Subsequently, for a double pendulum system they considered the control problem of transferring an equilibrium state to another among four equilibrium states, e.g. swinging up from the bottom state to the upright position [84]. The swing motion control in casting manipulation [6] and the control of gymnastic maneuvers on a high bar [79] also have relationship to our problem setting.

In conjunction with gymnastic robots, posture control problems of kinematic chains during free flight are also of our interest as we are concerned with a leaping maneuver arising from an ape's fast brachiation involving a component of free flight as well as swing locomotion. Once airborne, angular momentum of the system is conserved. In the biomechanics literature, Frohlich discusses basic physics of somersaulting and twisting that springboard divers and trampolinists perform [21, 22]. Kane and Scher studied mechanics of the "falling cat phenomenon" where falling cats turn over in midair and land on their feet even if they are released upside down[5] [30].

In robotics, Hodgins and Raibert explored aerial gymnastic maneuvers such as a flip and a front aerial [28] as briefly mentioned above. They proposed a control algorithm for a planar biped robot to perform such maneuvers based on their simplified analysis of the mechanics of a flip. They experimentally achieved such dynamic maneuvers using their biped robot as shown in Figure 1.7. Basically, their flight strategy is to synchronize foot contact with full body rotation by changing the leg length to adjust the pitch rate. In their analysis of the mechanics of a flip, they found that the equation of the conservation of angular momentum resulting from the robot dynamics can be integrated in a closed form if the legs are lengthened at a fixed rate. We will borrow this idea in our study of a leaping maneuver in robot brachiation. Nakano *et al.* studied the posture control problem of a simplified two-link planar free flying system with one joint [49]. They design the desired joint trajectory from an initial state to a goal state using a fourth order polynomial with an unknown coefficient. It is determined so that the integral arising from the conservation of angular momentum satisfies boundary conditions in which the integral is evaluated approximately by neglecting higher order terms. Subsequently, Kamon and Yoshida proposed a motion planning algorithm for free flying multi-link systems in a three dimensional space [29]. Their approach is based on an extension of an optimization algorithm called a "basis algorithm" originally proposed by Fernandes *et al.* [19], where the control input is expressed in Fourier series with finite terms and its coefficients are updated iteratively to minimize a cost function. These problems are also related to the control of space manipulators, e.g. [48], whose angular momentum is conserved.

The swing controller we introduce in this study bears many similarities to Spong's. However, the more extended problems of slow brachiation swinging up to an (unstabilizable) handhold

---

[5]Kawamura *et al.* developed a robot modelled on two cylinders with a universal joint and experimentally achieved this behavior [31].
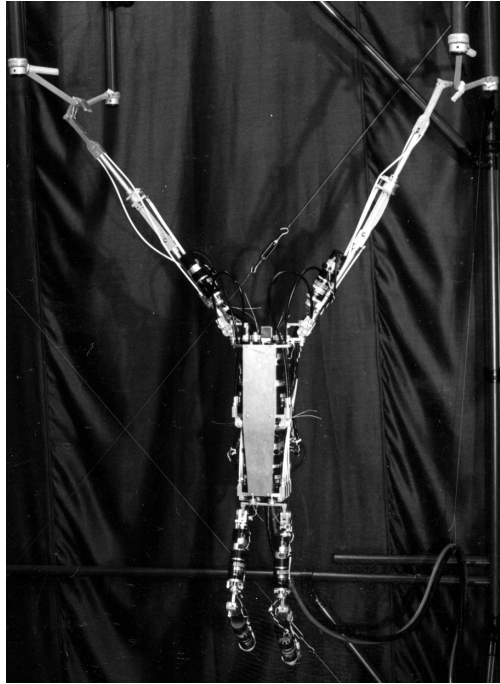
Figure 1.8: The brachiating robot with 12 degrees of freedom, "Brachiator III", modelled on a real siamang developed by Saito *et al.* [62] (Photo courtesy of Fukuda Lab, Nagoya University).

(refer to footnote 1 on page 30) require a rather different task specification than seen in the related literature mentioned above such as the stabilization and joint position/tracking control problems. In our problem, equilibrium motions (i.e. hybrid limit cycles) are the regulated goal sets rather than equilibrium points.

Robot Brachiation

Here, we would like to mention the pioneering work on the brachiation control problem by Saito in collaboration with Fukuda *et al.* [24, 62, 65, 66, 63, 64] following the preliminary studies of robot brachiation by Fukuda and his colleagues [23]. Their view of this problem explored how dynamic behaviors such as brachiation can be generated for robots in a manner analogous to the way humans and animals learn by heuristics. The advantage of their learning method is that dynamical parameters are not needed (known kinematics and measurements of joint angle/velocity are necessary). However, the method requires a long training period (about 200 experiments with the physical robot) to generate a feedforward torque signal for each configuration of the robot and given intervals between the branches. They built the physical two-link brachiating robot we use in this study and experimentally demonstrated the validity of the proposed control algorithm [63, 66]. Then, they considered the control of a higher degree of freedom robot, and developed the brachiating robot with 12 degree of freedom modelled on a real long armed ape as depicted in Figure 1.8. They succeeded as well in the basic experiment generating brachiation behavior based on a manually tuned control [62, 64].

In contrast, our approach presented in this dissertation using the notion of target dynamics

for a known model is quite different. As mentioned before, our view in this work explores how dynamically dexterous tasks can be achieved by physical insight into the task and the intrinsic dynamics of the system. Although our algorithm requires a calibrated dynamical model and kinematic parameters of the robot, the selection of one or two key parameters in the controller suffices in achieving the specific behavior of the robot.

Nonlinear Control Systems Theory

Difficulty in the control of underactuated systems lies in their nature that in general we cannot control all the degrees of freedom independently or force such systems to track arbitrary trajectories as mentioned above. In [11] it is shown by Bloch *et al.* that a class of systems under nonholonomic constraints cannot be asymptotically stabilized to a single equilibrium solution by a smooth state feedback according to Brockett's theorem [12]. From a viewpoint of nonlinear control systems theory (different from dynamically dexterous robotics point of view), controllability, stabilization and characterization of nonlinear systems under nonholonomic constraints and Lagrangian mechanical systems have been investigated. In [13], Brockett discusses controllability of nonlinear systems using Lie algebra and Frobenius' theorem. Murray and his colleagues have investigated controllability of Lagrangian mechanical systems introducing a notion of "equilibrium controllability," where the system can be driven between arbitrary two equilibrium states [38]. They derived sufficient conditions for equilibrium controllability based on Sussman's small-time local controllability condition [76]. In fact, Lynch *et al.* followed this kind of controllability analysis using Lie algebra in their work on nonprehensile manipulation and underactuated systems mentioned above. Murray *et al.* discussed certain properties of Lagrangian systems such as "differential flatness" and "configuration flatness" which simplify the analysis of those systems [58, 83]. Differential flatness is closely related with feedback linearizability of systems. Specifically, for single input systems, differential flatness is equivalent to feedback linearizability [83]. Bloch and colleagues studied stabilization problems of nonhononomic systems from theoretical framework using a nonlinear geometric control approach [11]. They showed that there is no smooth state feedback which can stabilize a class of nonholonomic systems as mentioned above. Under these circumstances, they proposed a piecewise state feedback control to stabilize such systems to an equilibrium state asymptotically. In their recent work [10], they studied feedback stabilization of an inverted pendulum by a method of "controlled Lagrangians". In their method, the kinetic energy is modified by state feedback to produce a new controlled Lagrangian so that the closed-loop dynamics behave in the desired manner.

However, these considerations may lie outside of the scope of this work since theoretical developments mentioned above do not seem directly applicable to our problem setup and our problem requires rather different task specifications. In this study, we are most concerned with solving designated tasks from Raibert's approach—by use of physical insight and intrinsic dynamics of the system and its environment—and demonstrating its effectiveness via laboratory experiments. In Section 1.3, we mention the role of "task encoding" to achieve dynamical dexterous tasks.

1.3 Encoding of Dynamically Dexterous Tasks

We view the robot's task to be one of solving an "environmental control problem" [15]. For example, in robot juggling a fully actuated robot controls the motion of a ball (which is the

unactuated environment) through intermittent interaction. In this case, interaction between the robot and environment only occurs at the ball-robot impact. In contrast, in robot brachiation, the robot and environment (respectively the actuated and unactuated joints) have continuous interaction during the motion. The difficulty in controlling a brachiating robot arises due to this continuous coupling. Hopping robots might be considered as lying in between since they have continuous interaction with the ground only in the stance phase.

Appropriate task encoding plays an important role in achieving robot dynamical dexterity in dynamical environment. We mention some previous instances of task encoding based on a good understanding of the intrinsic dynamics of a system and an environment.

The first example of task encoding is in the control of legged locomotion by Raibert [57]. He decomposes the control of legged locomotion into three parts and encodes as:

- Regulation of hopping height: control of the mechanical energy of the system through leg's thrust.

- Control of forward velocity: choice of foot placement at touchdown.

- Control of body posture: servoing the hip during stance.

He implements a simple feedback control law to achieve the desired locomotion according to this task encoding and successfully demonstrated the validity of his control strategy.

The second example is in the robot juggling achieved by Koditschek *et al.* [15]. Their idea is analogous to that of Raibert's. In order to achieve juggling with the specific apex height of a ball they introduce a "mirror algorithm" by means of which the robot is forced to track the nonlinear reflected mirror trajectory of a ball servoing its mechanical energy around a desired steady state energy level. In these examples, appropriate task encoding achieves such dynamically dexterous behaviors as hopping and juggling. From this point of view, we formally encode the brachiation task as the output of an appropriately chosen lower dimensional "target dynamical system" inspired by the pendulous motion of an ape's brachiation as we will introduce in Chapter 2.

We also would like to mention recent work on the "passive velocity field control" by Horowitz *et al.* [41], which can be viewed as a different notion of task specification. The control law mimics the behavior of a passive energy storage element such as a flywheel. Tasks are coded in terms of the desired velocity fields, which is suitable for contour following problems such as the control of smart exercise machines [39, 40].

1.4   Problem Statement

As described in Section 1.1, brachiation is a form locomotion swinging its arms unique to apes. In our reading of the biomechanics literature [18], we distinguish three variants of brachiation that we will refer to in this work as the

- Ladder and swing up problem
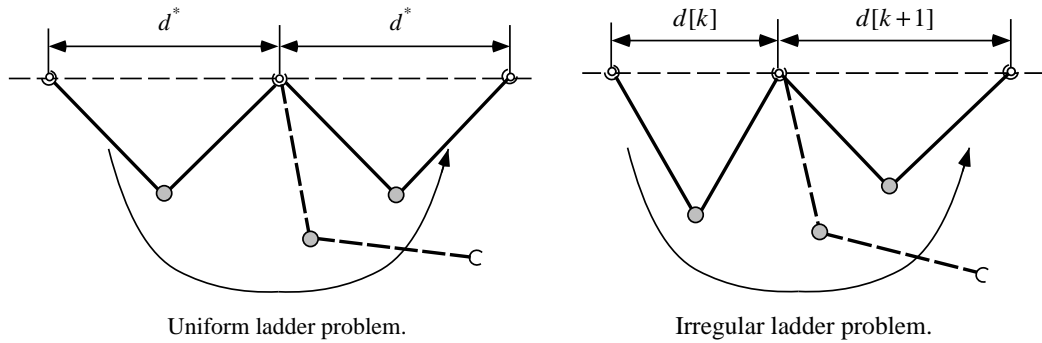
- Rope problem

- Leap problem

Figure 1.9: The ladder problems. The uniform ladder problem (left) considers brachiation on a set of evenly spaced bars at the same hight. The irregular ladder problem (right) considers brachiation on a set of irregularly spaced bars at the same hight.
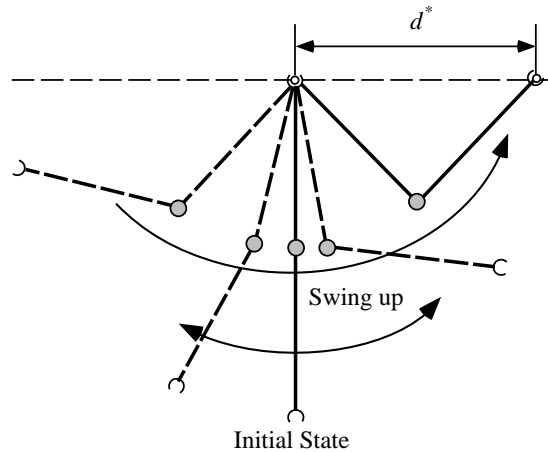

Figure 1.10: The swing up problem in which we consider the task of swinging up from a suspended posture with one hand grip to the target bar.

The first arises when an ape transfers from one branch to another and controlling the arm position at next capture represents the central task requirement. In the "uniform" ladder problem, we restrict our attention to brachiation on a ladder with evenly spaced bars at the same height as depicted in Figure 1.9 (left), which is the simplest problem setting. The "irregular" ladder problem considers much more natural problem of locomotion over irregularly spaced handholds at the same height as depicted in Figure 1.9 (right). The swing up problem entails pumping up from the suspended posture at rest and catching the next bar (see Figure 1.10). A robotics version of these problems has been previously introduced to the literature by Saito *et al.* [62, 66]. They presented the robot we consider here with a set of discrete evenly spaced bars and the requirement to swing up from rest, catch the next bar, and then swing from bar to bar by pumping up energy in a suitable fashion[6]. In our view, this problem seems as much akin to that of throwing and

---

[6]They experimentally implemented the learning algorithm on the physical two-link robot in the uniform ladder problem [63, 66]. However, experiments in the irregular ladder problem were not carried out because of the
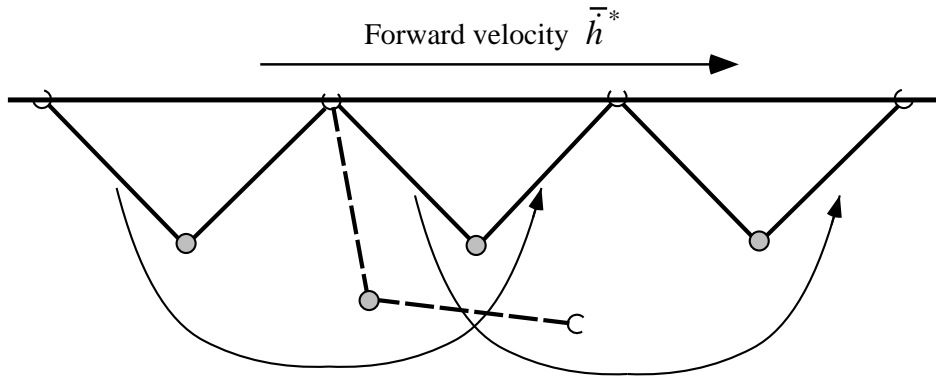
Figure 1.11: The rope problem considers brachiation along a continuum of handholds such as afforded by a branch or a rope. In this problem, we consider the regulation of horizontal velocity.

catching as to locomotion.

The second problem arises from brachiation along a continuum of handholds—a branch or a rope—that seems most closely analogous to human walking as depicted in Figure 1.11. Since grasps are afforded at will, the resulting freedom of placement can be exploited to achieve a specified forward rate of progress. This is not possible for a two degree of freedom machine on a ladder whose forward velocity is essentially determined by the distance between the bars and its own kinematics. To our knowledge, all previous work on robot brachiation has addressed only the ladder and swing up problems. We have found no studies concerned with the control of forward velocity. We find the results of the rope problem in Section 4.1 to be somewhat analogous to Schwind's study on the forward velocity control of simplified hopping robots [68].

The third problem arises in the context of fast brachiation where the next branch is far out of reach and the task cannot be accomplished without a large initial velocity and a significant component of free flight as shown in Figure 1.12. Roughly analogous to running quickly through a field of boulders, apes can apparently achieve this movement with great regularity and ease. Solving this problem involves not merely a swing phase but a nonholonomic flight as well where the angular momentum of the system is conserved. This maneuver seems analogous to a flip of a hopping robot [28] and the posture control of free flying systems [29, 49].

1.5   Organization of the Dissertation

This dissertation presents our studies of a new control strategy for a two-link brachiating robot. The material is organized as depicted in Figure 1.13.

In this chapter, we have introduced the background of this study. First, we described apes' brachiation from our reading of primatology and biomechanics literature. Then, we have reviewed the related work and discussed the role of task encoding to achieve dynamical dexterity. Finally, we defined the robot brachiation problems that we refer to by our reading of biomechanics

requirement of a large number of iterations for the learning process while they studied brachiation on bars with different distances and heights using learning and neural networks [65].
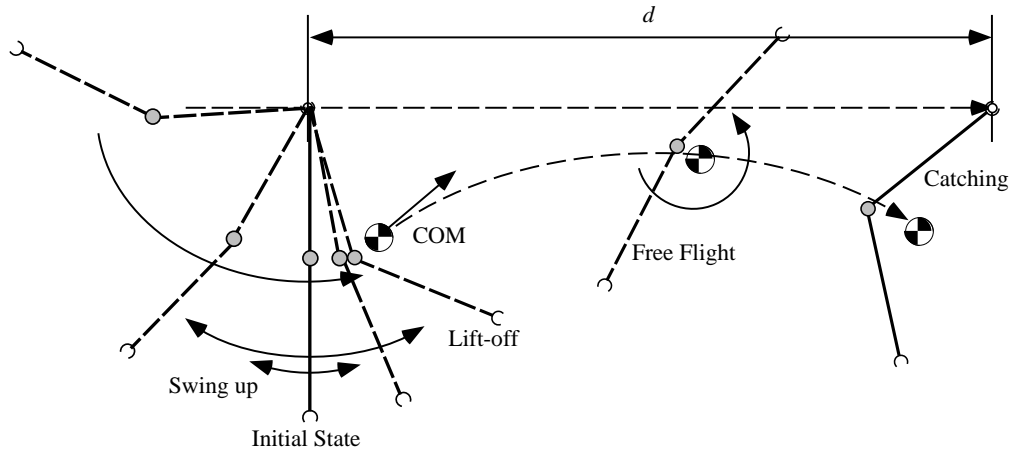
Figure 1.12: The leap problem considers the task of transferring from a handhold to the next which is far out of reach with a component of free flight arising from an ape's fast brachiation.

literature such as the "uniform/irregular ladder", "swing up", "rope" and "leap" problems.

In Chapter 2, we propose a control strategy for a two-link brachiating robot. Sections 2.1 and 2.2 describe the physical apparatus and the model of the robot which we use. In Sections 2.3 and 2.4, we introduce the notion of "target dynamics." Specifically, Preuschoft *et al.* [56] studied the mechanics of an ape's brachiation and identified a close correspondence between slow brachiation and the motion of a simplified pendulum. Accordingly, we choose formally to encode the problem of slow brachiation in terms of the output of a "target dynamical system." This task specification lends a slightly new twist to the traditional view of underactuated mechanisms, as we now discuss. In Section 2.5, we explore a generalized class of mechanical oscillators and discuss its feasibility as a target dynamical system.

In Chapter 3, the target dynamics method is first applied to the uniform ladder problem—brachiation on a horizontal ladder with evenly spaced rungs. We show how a symmetry property of an appropriately chosen target dynamics solves this problem. Then we consider the swing up problem—the task of swinging up from a suspended posture at rest and catching the next bar. The target dynamics is modified to introduce a stable limit cycle to achieve the desired swing up motion, which requires energy pumping with suitable magnitude and relative phase in state.

In Chapter 4, we first consider the forward velocity regulation using the target dynamics controller in the rope problem—brachiation along a continuum of handholds afforded by a branch or a rope. Then, we present a control strategy for the irregular ladder problem arising from brachiation on a ladder with irregularly spaced rungs placed at the same height. We extend the results in the uniform and rope problems to handle more natural problem of locomotion, which increases the behavioral repertoire of the robot.

Chapter 5 introduces a "hybrid" swing up controller, in which the original target dynamics swing up controller and a mechanical energy regulator are combined in a suitable fashion. The proposed hybrid controller achieves much better regulation of the desired behavior than the original target dynamics swing up controller by itself. Moreover, it guarantees the boundedness of the total energy of the system.

Chapter 6 presents our preliminary studies of the leap problem arising from an ape's fast

brachiation when the next branch is far out of reach with a component of free flight. We formulate a control strategy to achieve such a dynamic maneuver.

In Chapter 7, the proposed controller is experimentally implemented on the physical two-link brachiating robot in the uniform ladder, swing up, and irregular ladder problems in order to demonstrate the effectiveness of the proposed algorithm. Our experimental success encompasses a number of brachiation tasks starting from a variety of different initial hand positions. We have achieved swing locomotion in the uniform and irregular ladder problems, where both hands are initially on the ladder; various swing up behaviors from a suspended posture, where only one hand is initially on the ladder; and repeated locomotion over several rungs, where the robot starts with either one or both hands on the ladder. We also present preliminary results of the experimental implementation of the hybrid swing up controller to suggest its effectiveness.

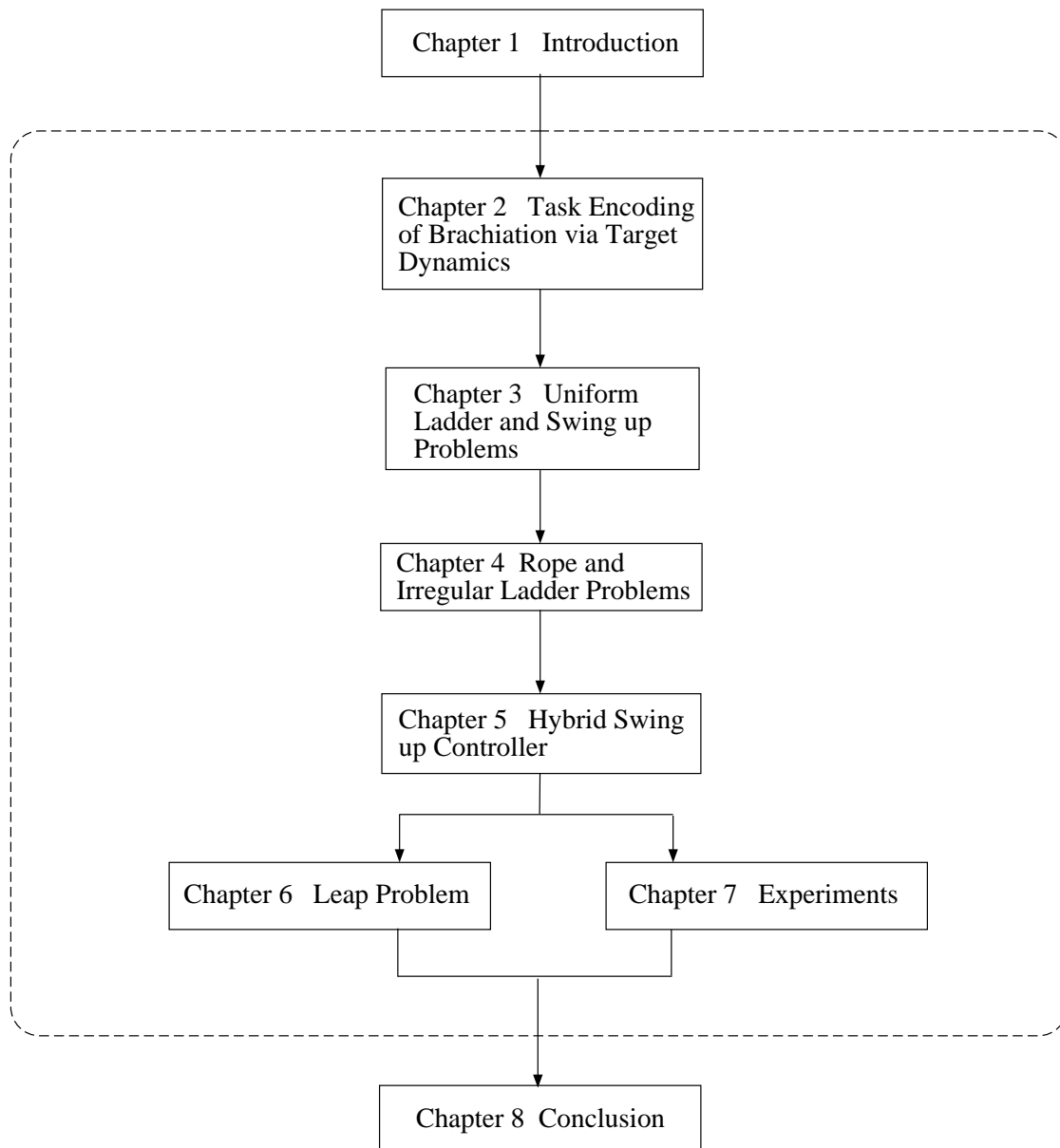Chapter 8 concludes this dissertation. Open problems and future work are addressed.

Figure 1.13: Organization of this dissertation.

Chapter 2

Task Encoding of Brachiation via Target Dynamics

This chapter presents our control strategy for a two-link brachiating robot. Appropriate task encoding plays an important role in achieving robot dynamical dexterity in dynamical environment as seen in the examples of the control of legged locomotion by Raibert and the study of robot juggling by Koditschek *et al.* mentioned in Section 1.3.

Sections 2.1 and 2.2 describe the physical apparatus and the model of the two-link brachiating robot. In Sections 2.3 and 2.4, we introduce the notion of "target dynamics" as a particular instance of input/output plant inversion. Specifically, brachiation is encoded as the output of a lower dimensional target dynamical system—a harmonic oscillator, that we must force the robot to mimic. Section 2.5 explores a class of mechanical oscillators in addition to a harmonic oscillator (1 dof lossless Lagrangian systems with a family of potentials) and its feasibility as a target dynamical system. As we have pointed out in Section 1.2, the handhold state we consider, cannot be made to be an equilibrium state under the influence of gravity. Thus, traditional set point stabilizing control schemes are not relevant in the present problem setting. Under these circumstances, we need to consider some "natural" orbit which achieves the designated task by combining physical insight into the task and the intrinsic dynamics of the system in its environment. We now introduce the notion of task encoding via target dynamics as a means of finding a family of such "natural orbits."

2.1 Physical Apparatus

Figure 2.1 depicts the configuration of our experimental setup. We use the two-link brachiating robot originally developed by Saito *et al.* [66]. The length of each arm is 0.5m and the total weight of the robot is about 4.8kg.

Controller Hardware   In Saito's original version of this experimental setup, a personal computer equipped with I/O devices was used to control the robot. We have replaced it with a VME bus board computer, MVME 167 (Motorola, CPU MC68040, 33MHz), with a real-time operating system, VxWorks 5.1 and VME bus based I/O devices. The control law is evaluated exactly at a rate of 500Hz, but we increase the rate up to 1250Hz in the experimental implementation of the
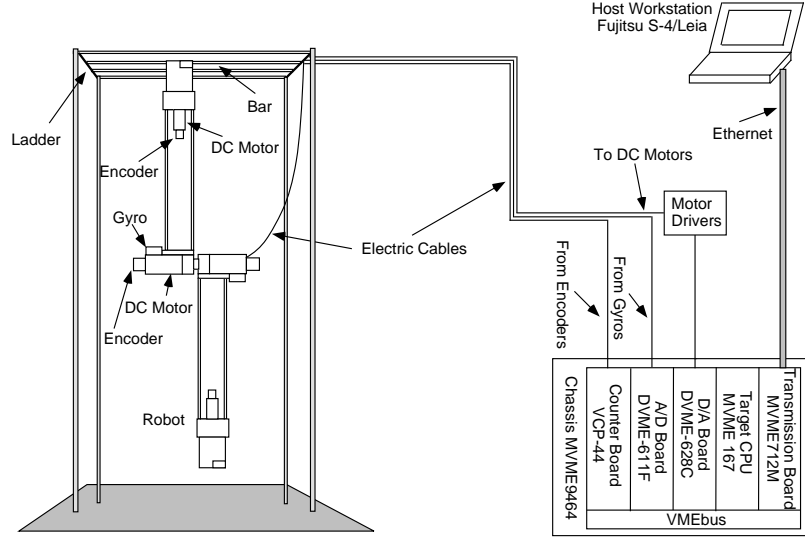
Figure 2.1: The experimental setup of the two-link brachiating robot.

hybrid controller presented in Section 7.5.

Elbow Joint   The elbow joint is actuated by two DC motors with harmonic gears (Harmonic Drive Systems, RH-14-6002) driven by a single motor driver circuit (Titiech Robot Driver). The stator of each motor is fixed to a link, and their rotor shafts are directly connected to each other. As a consequence, we can achieve a total rotational speed at the elbow which is two times faster than the case where there is only one motor. This was necessary since the rated rotational speed of these motors is 360 deg/sec, while we require that the rotational speed of the elbow joint be grater than 600 deg/sec. An additional benefit of the symmetrical structure of this design is better overall balance in the mechanism. Each gripper is equipped with a DC motor (Harmonic Drive Systems, RH-8-6006) which opens and closes it. The specifications of the motor, motor driver circuit can be found in Appendix D.

Sensors   The angle of the first joint is measured by integrating its angular velocity, which is in turn obtained through a gyro (Murata Manufacturing, ENV-05S) attached to the arm. The specifications of the gyro can be also found in Appendix D. The angle of the second joint and the opening angle of the gripper are measured using optical encoders.

2.2   Model

The equations used to model the swing dynamics of the robot take the form of a standard two-link planar manipulator as depicted in Figure 2.2.

$$\dot{T}q = \mathcal{L}(Tq, v_r) = \begin{bmatrix} \dot{q} \\ M(q)^{-1} \left(-V(q, \dot{q}) - k(q) - B\dot{q} - C\mathrm{sgn}(\dot{q}) + \begin{bmatrix} 0 \\ Kv_r \end{bmatrix} \right) \end{bmatrix} \qquad (2.1)$$
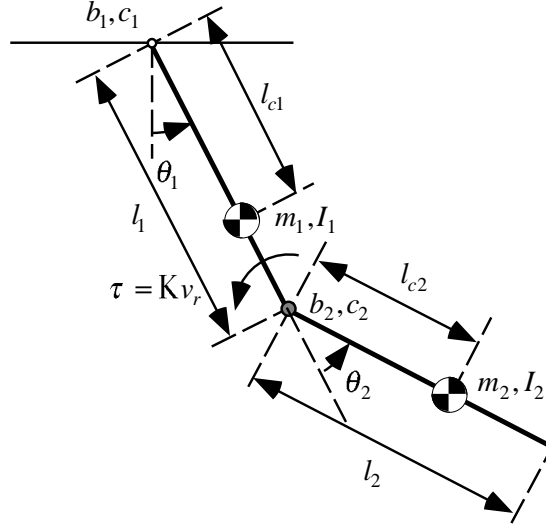
Figure 2.2: The mechanical model of the two-link brachiating robot.

where

$$q = \begin{bmatrix} \theta_1 \\ \theta_2 \end{bmatrix} \in \mathcal{Q}, \ Tq = \begin{bmatrix} q \\ \dot{q} \end{bmatrix} \in T\mathcal{Q} \ ^1, \ M = \begin{bmatrix} m_{11} \ m_{12} \\ m_{21} \ m_{22} \end{bmatrix}$$

$$m_{11} = m_1 l_{c1}^2 + I_1 + m_2(l_1^2 + 2l_1 l_{c2} \cos \theta_2 + l_{c2}^2) + I_2$$
$$m_{12} = m_{21} = m_2(l_{c2}^2 + l_1 l_{c2} \cos \theta_2) + I_2$$
$$m_{22} = m_2 l_{c2}^2 + I_2$$

$$V(q,\dot{q}) = \begin{bmatrix} V_1 \\ V_2 \end{bmatrix} = -m_2 l_1 l_{c2} \sin \theta_2 \begin{bmatrix} 2\dot{\theta}_1 \dot{\theta}_2 + \dot{\theta}_2^2 \\ -\dot{\theta}_1^2 \end{bmatrix}$$

$$k(q) = \begin{bmatrix} k_1 \\ k_2 \end{bmatrix} = \begin{bmatrix} m_1 g l_{c1} \sin \theta_1 + m_2 g(l_1 \sin \theta_1 + l_{c2} \sin(\theta_1 + \theta_2)) \\ m_2 g l_{c2} \sin(\theta_1 + \theta_2) \end{bmatrix}$$

$$B = \operatorname{diag}\{b_i\}, \quad C = \operatorname{diag}\{c_i\}.$$

M is the inertia matrix, V is the Coriolis/centrifugal vector, k is the gravity vector. B and C denote the viscous and coulomb friction coefficient matrices respectively. m_i and I_i are the mass and the moment of inertia of each link respectively, and l_i is the link length. The center of mass of each link is located on the center line which passes through adjacent joints at a distance l_{ci}. c_i and b_i are the coulomb and viscous friction coefficients respectively. We assume that the elbow actuator produces torque proportional to a voltage command, v_r, sent to a driver as $\tau = Kv_r$, where K is a positive constant. In this work, we assume that the length of each link is the same, $l_1 = l_2 = l$.

---

[1]Throughout the dissertation, we shall use the tangent notation of Abraham and Marsden [1]. If $\mathcal{X}$ is a manifold, then $T_x\mathcal{X}$ denotes the tangent vector space at some $x \in \mathcal{X}$ and $T\mathcal{X} = \bigcup_{x \in \mathcal{X}} T_x\mathcal{X}$ denotes the tangent bundle. Moreover Tx will denote some point in $T_x\mathcal{X}$ and $h : \mathcal{X} \to \mathcal{Y} \Rightarrow Th : T\mathcal{X} \to T\mathcal{Y}$ is the derived "tangent map," in coordinates, $Th = (h(x), Dh(x)\dot{x})$ where D denotes the Jacobian.

It is generally known that DC motors with harmonic gear mechanisms bear complicated nonlinear characteristics, which are difficult to model [81]. However, for simplicity, we model the dynamics using only viscous and coulomb friction as well as rotor inertia. As the results of parameter identification presented in Appendix B suggest, the model we offer in Table 2.1 fits the dynamics of the physical system fairly well. In the dissertation, we use a lossless version of the model ($B, C \to 0$ in (2.1)) for the development of the controller and its analysis, but introduce the losses in simulation.

Description		i=1	i=2
Mass	$m_i(\text{kg})$	3.499	1.232
Moment of inertia	$I_i(\text{kgm}^2)$	0.090	0.033
Link length	$l_i(\text{m})$	0.50	0.50
Location of CG	$l_{ci}(\text{m})$	0.414	0.333
Viscous friction	$b_i(\text{Nm/s})$	0.02	0.14
Coulomb friction	$c_i(\text{Nm})$	0.02	0.45
Torque constant	$K(\text{Nm/V})$	1.752	

Table 2.1: The dynamical parameters of the robot obtained by the procedure described in Appendix B.

2.3   Input/Output Linearization and Target Dynamics

The notion of target dynamics represents a slight variant on standard techniques of plant inversion. A system is inverted then forced to have the characteristic of a chosen target dynamics. Thus, instead of tracking an exogenously designed reference trajectory, we force the system to generate and track its own reference motion.

Suppose a plant

$$\dot{w} = F(w, v) \tag{2.2}$$

$$y = H(w) \tag{2.3}$$

is input/output linearizable. That is, given

$$L_F H(w, v) = DH \cdot F(w, v) \tag{2.4}$$

if there can be found an implicit function such that for every $u \in \mathcal{U}$ and $w \in \mathcal{W}$, then

$$v = L_F H^{-1}(w, u) \tag{2.5}$$

implies

$$L_F H(w, v) = u. \tag{2.6}$$

$L_F H$ denotes the Lie derivative of H with respect to F [33]. One calls (2.5) an input/output linearizing inverse controller in the sense that $\dot{y} = u$.

It is traditional in the underactuated robot control literature to use the linearizing feedback (2.5) to force y to track some reference trajectory $r_d(t)$. In the present article, we find it more useful to mimic a target dynamical system,

$$\dot{y} = f(y). \tag{2.7}$$

This behavior obtains by substituting f for u in (2.5), yielding the feedback law,

$$v = L_F H^{-1}(w, f(y)) = L_F H^{-1}(w, f \circ H(w)). \tag{2.8}$$

2.4 A Target Dynamics and Its Associated Controller

According to the biomechanics literature [56], slow brachiation of apes resembles the motion of a pendulum. Although the ape's moment of inertia varies during the swing according its change of posture, the motion of a simplified pendulum gives a fairly good approximation. Motivated by this pendulous motion , we encode the robot brachiation task in terms of the harmonic oscillator

$$y = Tx = \begin{bmatrix} x \\ \dot{x} \end{bmatrix}, \quad f_\omega(Tx) = \begin{bmatrix} 0 & 1 \\ -\omega^2 & 0 \end{bmatrix} Tx, \tag{2.9}$$

where ω, the natural frequency of the virtual pendulum, will play the role of the task level control parameter in the sequel. Supporting this role, the function, f_ω (2.9), serves as the target dynamical system (2.7) for all the empirical work reported in this dissertation.

The choice of output map (2.3) seems to be much more critical, since it prescribes the combination of states that will be forced to exhibit the selected target dynamics (2.14). In Figure 2.3 we illustrate the local change of coordinates from joint space to polar coordinates on $I\!R^2$,

$$\begin{bmatrix} r \\ \theta \end{bmatrix} = \bar{q} = \bar{g}(q) = \begin{bmatrix} l\sqrt{2(1 + \cos\theta_2)} \\ \theta_1 + \frac{1}{2}\theta_2 \end{bmatrix}. \tag{2.10}$$

Intuitively, pursuing the analogy arising from biomechanical observation [56], the simplest pendulum to be found in the underlying RR kinematic chain obtains from its polar coordinate "angle," θ, motivating the choice,

$$x = h(q) := \theta = [0, 1]\, \bar{g}(q) = \theta_1 + \frac{1}{2}\theta_2. \tag{2.11}$$

With these choices in place, the controller synthesis is formally complete. In summary, the virtual pendulum angle, θ, is forced to follow the target dynamics, $\ddot{\theta} + \omega^2\theta = 0$. Namely, identify $w = Tq = [\, q^T, \, \dot{q}^T \,]^T$, $v = \tau$, $F = \mathcal{L}$ in (2.2) and $H = Th$, and apply the control law formulated in (2.8) with respect to the target (2.9):

$$\begin{aligned}
\tau = \tau_\omega &:= L_F H^{-1}(Tq, f_\omega \circ Th(Tq)) \\
&= \left(D_q h \begin{bmatrix} n_{12} \\ n_{22} \end{bmatrix} \right)^{-1} \left[-\omega^2\theta - (D_q \dot{h})\dot{q} + D_q h M^{-1}(V + k) \right] \\
&= \frac{1}{n_{12} + \frac{1}{2}n_{22}} \left[-\omega^2(\theta_1 + \frac{1}{2}\theta_2) + (n_{11} + \frac{1}{2}n_{21})(V_1 + k_1) \right] + V_2 + k_2. \tag{2.12}
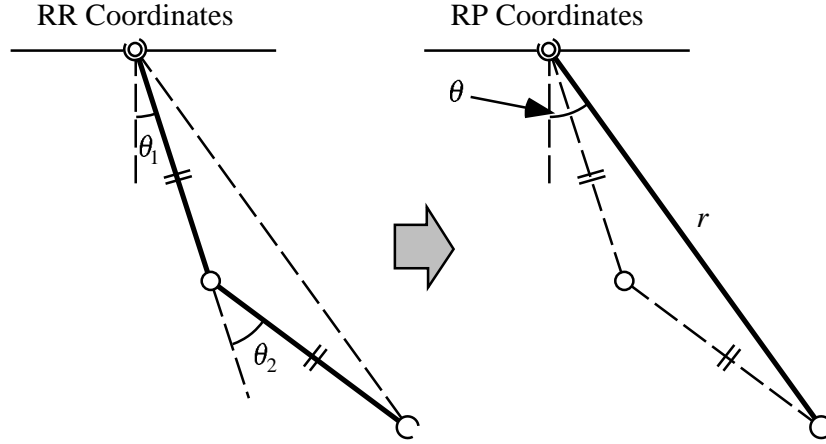\end{aligned}$$

Figure 2.3: Change of coordinates from RR to RP. We control θ to follow the dynamics $\ddot{\theta}+\omega^2\theta = 0$ using a target dynamics controller.

where

$$M^{-1} = \begin{bmatrix} n_{11} & n_{12} \\ n_{21} & n_{22} \end{bmatrix}.$$

Notice that

$$D_q h \begin{bmatrix} n_{12} \\ n_{22} \end{bmatrix} = n_{12} + \frac{1}{2}n_{22} = \frac{m_1 l_{c1}^2 + m_2(l_1{}^2 - l_{c2}{}^2) + I_1 - I_2}{2\det(M)} \neq 0 \qquad (2.13)$$

i.e., the invertibility condition of $L_F H$ is satisfied in the particular setting with the parameter values shown in Table 2.1.

2.5   A Class of Target Dynamics

In the lab, we use a harmonic oscillator to encode the brachiation task motivated by the pendulous motion of an ape's brachiation as mentioned above. Here, we explore a class of mechanical oscillators (1 dof lossless Lagrangian systems with a family of potentials) and its feasibility as a target dynamical system. We find it preferable to use a harmonic oscillator whose potential is a Hooke's law spring for the reasons now we discuss.

Consider a class of lossless mechanical oscillator of the form for the target system (2.7),

$$y = Tx = \begin{bmatrix} x \\ \dot{x} \end{bmatrix}, \ \ f_\omega(Tx) = \begin{bmatrix} \dot{x} \\ -\omega^2 DU(x) \end{bmatrix}. \qquad (2.14)$$

Simulations suggest that any lossless mechanical oscillator (2.14) can encode brachiation when $U(x)$, an "artificial potential" function, is even and convex in the region of operation. For future reference, let $\bar{E}$ be the "pseudo" mechanical energy defined by this oscillator,

$$\bar{E} := \frac{1}{2}\dot{x}^2 + \omega^2 U(x). \qquad (2.15)$$

The control law with respect to the target (2.14) with the output map, $x = h(q)$, is formulated as

$$\tau = \tau_\omega := L_F H^{-1} \left(Tq, f_\omega \circ Th(Tq) \right)$$

$$= \left(D_q h \begin{bmatrix} n_{12} \\ n_{22} \end{bmatrix} \right)^{-1} \left[-\omega^2 D_x U \circ h(q) - (\dot{D_q h})\dot{q} + D_q h M^{-1}(V+k) \right]$$

$$= \frac{1}{n_{12} + \frac{1}{2}n_{22}} \left[-\omega^2 D_x U \circ h(q) + (n_{11} + \frac{1}{2}n_{21})(V_1 + k_1) \right] + V_2 + k_2, \qquad (2.16)$$

In Chapter 3.1.1 we make the formal observation (Proposition 3.3) that any even potential together with an appropriately "odd" choice of output map (2.3) will support the Raibert-style reverse time symmetry [57] essential to the efficacy of our task encoding. Indeed, in our numerical investigations in Sections 3.1.4, 3.2.2 and 4.1.4, we have had good experience with many choices for the artificial potential function. In our empirical work, we have found it particularly convenient to adopt the specific Hooke's Law potential, $U(x) = \frac{1}{2}x^2$, (2.9), for two reasons.

First, the elliptic integral

$$T_N = 4 \int_0^{x_0} \frac{dx}{\sqrt{2(\bar{E}_0 - \omega^2 U(x))}} = \frac{4}{\omega} \int_0^{x_0} \frac{dx}{\sqrt{2(U(x_0) - U(x))}} \qquad (2.17)$$

is solvable in closed form using elementary functions for a Hooke's law spring. This closed form expression significantly simplifies the computational effort incurred by the root finding procedure of (3.18) required to tune the "natural frequency," ω, in the ladder and rope problems.

Second, numerical study addressing the swing up problem in Section 3.2.2 reveals that the "stiffness" (the second derivative of the potential, U) plays an important role for reasons we do not yet understand well. Specifically, we require not only positive stiffness (i.e., convex potentials, U), but find that some "stiffness margin" profile is key to effective swing up behavior. We plot in Figures 2.4 and 2.5 some examples of the potential and its associated stiffness of several spring laws. Generally speaking, "hard" spring laws such as $U(x) = \frac{1}{4}x^4$ or $U(x) = \frac{1}{2}x^2 + \frac{1}{4}x^4$ work very nicely. In contrast, consider the effective torsional spring potential introduced by a gravity loaded simple pendulum, $U(x) = 1 - \cos x$, whose stiffness becomes zero at the boundary of the domain of operation, and a spring law, $U(x) = \frac{1}{2}x^2 - \frac{1}{24}x^4$, whose stiffness becomes negative over the domain of operation. Such "soft" springs (i.e., potentials whose second derivative stiffness functions are not bounded away from zero over the domain of operation) characteristically result in "out of phase" swingups that fail the task. While "hard" springs work nicely in simulation, they typically incur unavailably large torques. The Hooke's Law potential enjoys benefits of positive stiffness and realistic torque requirements.

2.6   Summary

This chapter is summarized as follows:

- We have presented the control strategy for the two-link brachiating robot. Motivated by the pendulous motion of an ape's brachiation, the task is encoded as the output of a lower dimensional target dynamical system, and the robot is forced to follow the target dynamics using Input/Output linearization.
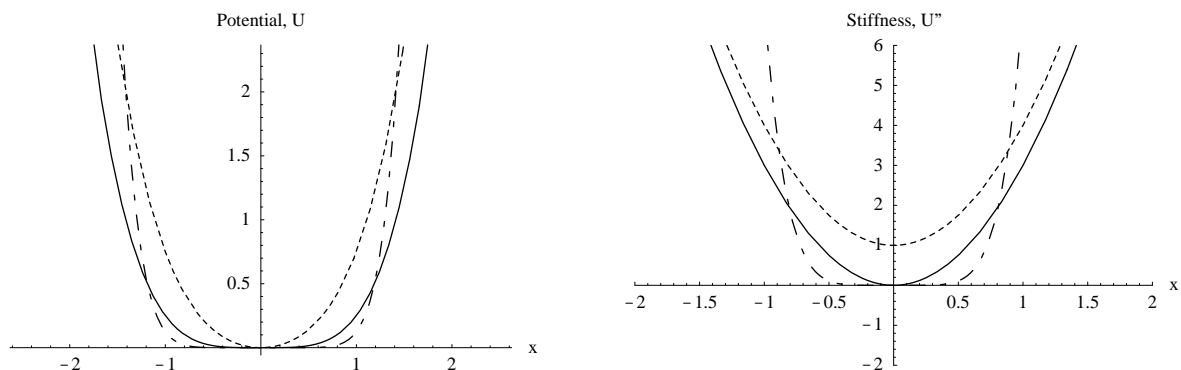
Figure 2.4: Some examples of the potential and its associated stiffness of "hard" spring laws. Solid: $U(x) = \frac{1}{4}x^4$, dashed: $U(x) = \frac{1}{2}x^2 + \frac{1}{4}x^4$, and dot-dashed: $U(x) = \frac{1}{8}x^8$.
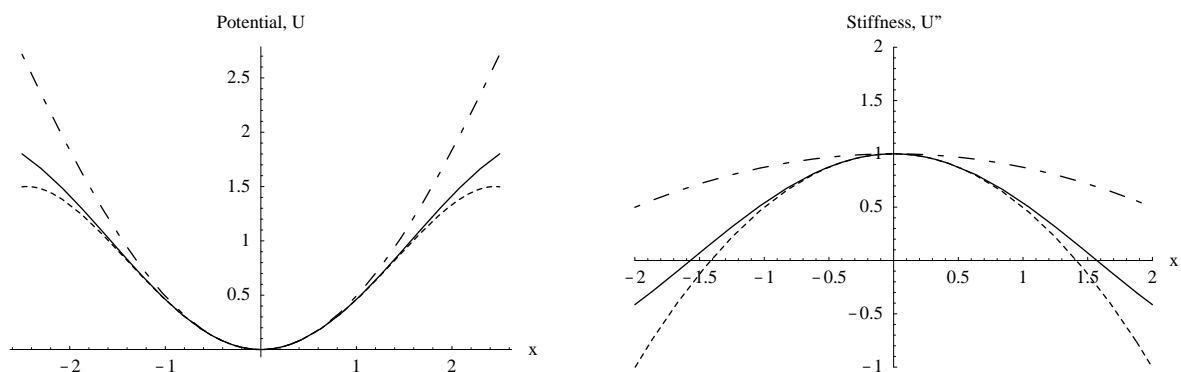

Figure 2.5: Some examples of the potential and its associated stiffness of "soft" spring laws. Solid: $U(x) = 1 - \cos x$, dashed : $U(x) = \frac{1}{2}x^2 - \frac{1}{24}x^4$, and dot-dashed: $U(x) = \frac{1}{2}x^2 - \frac{1}{96}x^4$.

- We have also explored a class of mechanical oscillators and its feasibility as a target dynamical systems. We have found that any even potential with an appropriately "odd" choice of output map supporting the reverse time symmetry would suffice the task encoding of brachiation. However, for two reasons, we have concluded that it is particularly preferable to adopt a harmonic oscillator for the target dynamics.

Chapter 3

Uniform Ladder and Swing up Problems

We now move on to the specific problems of robot brachiation. In this chapter, we first apply the target dynamics method to the uniform ladder problem. Then we consider the swing up problem. Analysis on the reverse time symmetry that is concerned with the choice of the lower dimensional target dynamics, and numerical simulations are provided to suggest the effectiveness of the proposed algorithms. Furthermore, we will also show the experimental results in Chapter 7 to demonstrate the validity of our strategy. In this chapter, we use the lossless model for the following analysis, but introduce the losses in simulation.

3.1   Uniform Ladder Problem

As we have pointed out, the ladder problem arises when an ape transfers from one branch to another and the control of arm position at the next capture represents the control task requirement. Here, we restrict our attention to brachiation on a set of evenly spaced bars at the same height. The target dynamics method is applied to the uniform ladder problem. We show how a symmetry property of an appropriately chosen target system— (2.14) in the present case—can solve this problem.

3.1.1   Neutral Orbits, $\mathcal{N}$

This section follows closely the ideas originally developed in [68, 69]. We discuss a reverse time symmetry inherent in the brachiating robot's dynamics. Here, we are interested in orbits whose forward time motions from the bottom states are a horizontal reflection of their backward time motion from the same initial condition.

First, we show that the natural dynamics of the two-link brachiating robot admit this reverse time symmetry, S. Then, we give a condition under which feedback laws result in closed loops that still admit S. Lastly, following Raibert [57], we introduce the notion of the neutral orbits of the symmetry, and show how they may be used to solve the ladder problem. In the sequel, we will denote the integral curve of a vector field f by the notation f^t.

Definition 3.1 $f : \mathcal{X} \rightarrow T\mathcal{X}$ *admits a reverse time symmetry* $S : \mathcal{X} \rightarrow \mathcal{X}$ *if and only if* $S \circ f^t = f^{-t} \circ S$.

Note that when S is linear, after taking time derivatives, this definition might be equivalently stated as $S \circ f = -f \circ S$. In this paper, we are concerned specifically with the symmetry operator

$$S = \begin{bmatrix} -I_{2\times 2} & 0 \\ 0 & I_{2\times 2} \end{bmatrix}. \tag{3.1}$$

(where $I_{2\times 2}$ denotes the 2×2 identity matrix.) When f admits S in (3.1), there exist orbits integrated forward in time from some initial conditions which are reflections of orbits backward in time from the same initial conditions odd in angles and even in velocities, i.e., $q(-t) = -q(t)$ and $\dot{q}(-t) = \dot{q}(t)$.

Now, supposing we have chosen a feedback law, $\tau(q, \dot{q})$, denote the closed loop dynamics of the robot as

$$\dot{Tq} = \mathcal{L}_\tau(Tq) = \mathcal{L}(Tq, \tau(Tq)). \tag{3.2}$$

Say that τ "admits S" if and only if $\mathcal{L}_\tau$ admits S.

Proposition 3.2 *The closed loop dynamics* $\mathcal{L}_\tau$ *admits* S *as in (3.1), i.e.,* $S \circ \mathcal{L}_\tau(Tq) = -\mathcal{L}_\tau \circ S(Tq)$ *if and only if* $\tau(q, \dot{q})$ *has the property* $\tau(-q, \dot{q}) = -\tau(q, \dot{q})$.

Proof:

$$\mathcal{L}_\tau \circ S(Tq) = \begin{bmatrix} \dot{q} \\ M(-q)^{-1} \left(-V(-q, \dot{q}) - k(-q) + \begin{bmatrix} 0 \\ \tau(-q, \dot{q}) \end{bmatrix} \right) \end{bmatrix}$$

$$= \begin{bmatrix} \dot{q} \\ M(q)^{-1} \left(V(q, \dot{q}) + k(q) + \begin{bmatrix} 0 \\ \tau(-q, \dot{q}) \end{bmatrix} \right) \end{bmatrix} \tag{3.3}$$

since $M(-q) = M(q), V(-q, \dot{q}) = -V(q, \dot{q}), k(-q) = -k(q)$. On the other hand,

$$S \circ \mathcal{L}_\tau(Tq) = \begin{bmatrix} -\dot{q} \\ M(q)^{-1} \left(-V(q, \dot{q}) - k(q) + \begin{bmatrix} 0 \\ \tau(q, \dot{q}) \end{bmatrix} \right) \end{bmatrix} \tag{3.4}$$

From (3.3) and (3.4) we see that if $\tau(-q, \dot{q}) = -\tau(q, \dot{q})$, then $S \circ \mathcal{L}_\tau(Tq) = -\mathcal{L}_\tau \circ S(Tq)$. On the other hand, if $S \circ \mathcal{L}_\tau(Tq) = -\mathcal{L}_\tau \circ S(Tq)$, $\tau(q, \dot{q})$ has to satisfy the property $\tau(-q, \dot{q}) = -\tau(q, \dot{q})$. ∎

Proposition 3.3 *If the artificial potential function* $U(x)$ *in (2.14) is even,* $U(-x) = U(x)$, *and if* $x = h(q)$, *i.e a smooth scalar valued function, has the property* $h(-q) = -h(q)$, *then the feedback law (2.16),* τ_ω, *admits* S.

Proof:

$$\tau(-q, \dot{q}) = \left(D_q h(-q) \begin{bmatrix} n_{12} \\ n_{22} \end{bmatrix} \right)^{-1} \left\{ -\omega^2 D_x U \circ h(-q) - \frac{d}{dt} [D_q h(-q)] \dot{q} \right.$$
$$\left. + D_q h(-q) M(-q)^{-1} \left[V(-q, \dot{q}) + k(-q) \right] \right\}$$
$$= \left(D_q h(q) \begin{bmatrix} n_{12} \\ n_{22} \end{bmatrix} \right)^{-1} \left\{ \omega^2 D_x U \circ h(q) + \frac{d}{dt} [D_q h(q)] \dot{q} \right.$$
$$\left. + D_q h(q) M(q)^{-1} \left[-V(q, \dot{q}) - k(q) \right] \right\}$$
$$= -\tau(q, \dot{q}), \tag{3.5}$$

since

$$M(-q)^{-1} = M(q)^{-1}, V(-q, \dot{q}) = -V(q, \dot{q}), k(-q) = -k(q),$$

and

$$D_x U \circ h(-q) = D_x U \circ (-h(q)) = -D_x U \circ h(q)$$

because $h(-q) = -h(q)$ and $D_x U(-x) = -D_x U(x)$ (the derivative of an even function is an odd function). Furthermore, recalling h is a scalar valued function,

$$\frac{d}{dt}(D_q h) = D_q(D_q h)\frac{d}{dt}q = D_q{}^2 h \dot{q},$$

$$\frac{d}{dt}[D_q h(-q)]\dot{q} = [D_q{}^2 h(-q)]\dot{q}^2 = -[D_q{}^2 h(q)]\dot{q}^2 = -\frac{d}{dt}[D_q h(q)]\dot{q}$$

because $D_q h(-q) = D_q h(q)$ and $D_q{}^2 h(-q) = -D_q{}^2 h(q)$. Since $\tau(-q, \dot{q}) = -\tau(q, \dot{q})$, Proposition 3.2 applies. ∎

Define the fixed points of the symmetry S to be

$$\text{Fix}S := \{ Tq \in TQ \,|\, S(Tq) = Tq \}. \tag{3.6}$$

In the present case, i.e., for S in (3.1) note that

$$\text{Fix}S = \{ (q, \dot{q}) \in TQ | q = 0 \}.$$

Define the set of "neutral orbits" to be the integral curves which go through the fixed point set,

$$\mathcal{N} := \bigcup_{t \in \mathbb{R}} \mathcal{L}^t(\text{Fix}S), \tag{3.7}$$

where $\mathcal{L}^t(\text{Fix}S)$ denotes the integral curve which goes through a point in $\text{Fix}S$. We use this notation in the following for convenience. Note that a neutral orbit has a symmetry property about its fixed point—namely, if $Tq_0 \in \text{Fix}S$, then

$$S \circ \mathcal{L}^t(Tq_0) = \mathcal{L}^{-t} \circ S(Tq_0) = \mathcal{L}^{-t}(Tq_0)$$
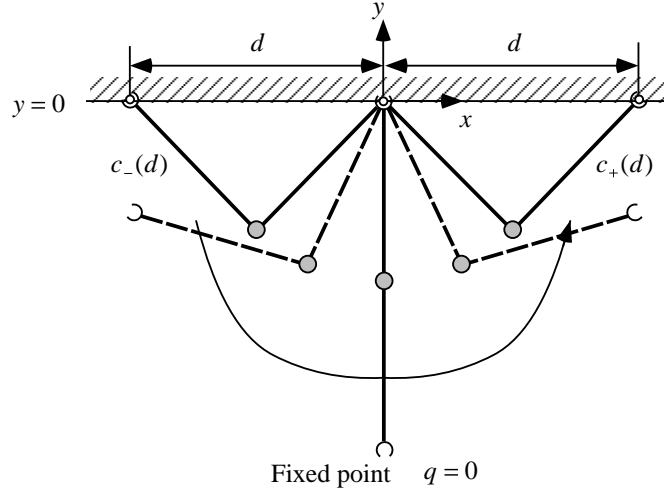
Figure 3.1: A ceiling configuration. The ceiling is parametrized by the distance between the grippers d. A left branch $c_-(d)$ and right branch $c_+(d)$ are defined in this manner.

3.1.2   The Ceiling, $\mathcal{C}$, and Its Neutral Orbits

Define the "ceiling"

$$\mathcal{C} = \{q \in \mathcal{Q} | \cos\theta_1 + \cos(\theta_1 + \theta_2) = 0\} . \tag{3.8}$$

to be those configurations where the hand of the robot reaches the height $y = 0$ as depicted in Figure 3.1 [1].

In general, arms which drop from the ceiling, whether under active torque control or not, will not pass through a bottom state — they will not trace out a neutral orbit. Our problem now is to find a virtual frequency, ω, matched to the desired distance, d, that renders this ceiling state neutral.

The ceiling, $\mathcal{C}$, can be parameterized by two branches,

$$\mathcal{C} = \operatorname{Im} c_- \cup \operatorname{Im} c_+, \tag{3.9}$$

of the maps, $c_\pm : [0, 2l] \to \mathcal{C}$,

$$c_\pm(d) = \begin{bmatrix} \pm \arcsin\left(\frac{d}{2l}\right) \\ \pm \left[\pi - 2\arcsin\left(\frac{d}{2l}\right)\right] \end{bmatrix} . \tag{3.10}$$

In the sequel, we will be particularly interested in initial conditions of (3.2) originating in the zero velocity sections of the ceiling that we denote $T\mathcal{C}_0$. Now note that $S(T\mathcal{C}_0) \subseteq T\mathcal{C}_0$ since

$$S \begin{bmatrix} c_-(d) \\ 0 \\ 0 \end{bmatrix} = \begin{bmatrix} c_+(d) \\ 0 \\ 0 \end{bmatrix} . \tag{3.11}$$

---

[1]Notice that this handhold state,"ceiling," cannot be made to be an equilibrium state under the influence of the gravity since we cannot find τ such that $\mathcal{L}(Tq, \tau) \equiv 0$ in (2.1) when $k(q) \neq 0$.

Proposition 3.4 *If a feedback law, τ, admits S and if* $\begin{bmatrix} c_-(d) \\ 0 \\ 0 \end{bmatrix} \in \mathcal{N} \cap T\mathcal{C}_0$, *then there can be found a time* $t_N \in \mathbb{R}$ *such that for* $\nu = \frac{t_N}{4}$ *we have*

$$\mathcal{L}_\tau^{2\nu}\left(\begin{bmatrix} c_-(d) \\ 0 \\ 0 \end{bmatrix}\right) = \begin{bmatrix} c_+(d) \\ 0 \\ 0 \end{bmatrix} \tag{3.12}$$

i.e., a time at which the left branch at zero velocity in the ceiling reaches the right branch in the ceiling also at zero velocity.

Proof: By the definition of $\mathcal{N}$, there can be found a time $\nu \in \mathbb{R}$ at which

$$\mathcal{L}_\tau^{\nu}\left(\begin{bmatrix} c_-(d) \\ 0 \\ 0 \end{bmatrix}\right) := Tq^* \in \operatorname{Fix}S \tag{3.13}$$

Therefore,

$$\mathcal{L}_\tau^{-\nu}(Tq^*) = \begin{bmatrix} c_-(d) \\ 0 \\ 0 \end{bmatrix}. \tag{3.14}$$

Applying the symmetry S, we have

$$\begin{bmatrix} c_+(d) \\ 0 \\ 0 \end{bmatrix} = S\begin{bmatrix} c_-(d) \\ 0 \\ 0 \end{bmatrix} \qquad \text{(from (3.11)).} \tag{3.15}$$

But

$$S\begin{bmatrix} c_-(d) \\ 0 \\ 0 \end{bmatrix} = S \circ \mathcal{L}_\tau^{-\nu}(Tq^*) \qquad \text{(from (3.14)),} \tag{3.16}$$

hence,

$$\begin{bmatrix} c_+(d) \\ 0 \\ 0 \end{bmatrix} = S \circ \mathcal{L}_\tau^{-\nu}(Tq^*) = \mathcal{L}_\tau^{\nu} \circ S(Tq^*)$$

$$= \mathcal{L}_\tau^{\nu}(Tq^*) = \mathcal{L}_\tau^{\nu} \circ \mathcal{L}_\tau^{\nu}\left(\begin{bmatrix} c_-(d) \\ 0 \\ 0 \end{bmatrix}\right)$$

$$= \mathcal{L}_\tau^{2\nu}\left(\begin{bmatrix} c_-(d) \\ 0 \\ 0 \end{bmatrix}\right) \tag{3.17}$$

∎

Thus, we conclude that any feedback law, τ, which admits S, solves the ladder problem, assuming we can find a d such that $[\, c_-(d)^T, \, 0, \, 0\,]^T \in \mathcal{N}$. Note that finding such a ceiling point requires solving the equation

$$\Phi(d, t_N) = \left[\, I_{2\times 2} \,,\, 0_{2\times 2}\,\right] \mathcal{L}_\tau^\nu \left(\begin{bmatrix} c_-(d) \\ 0 \\ 0 \end{bmatrix} \right) = \begin{bmatrix} 0 \\ 0 \end{bmatrix}, \tag{3.18}$$

for d and t_N simultaneously, where $\nu = \frac{t_N}{4}$, $I_{2\times 2}$ denotes a 2×2 identity matrix and $O_{2\times 2}$ denotes a 2×2 zero matrix. Of course solving this equation is quite difficult: it requires a two dimensional "root finding" procedure for a function whose evaluation entails integrating the dynamics (2.1).

3.1.3   Application of Target Dynamics

The feedback law τ_ω (2.16) arising from the target (2.9) and output map (2.11) admits S since Proposition 3.3 applies. The special target, the harmonic oscillator in (2.9), enjoys a very nice property relative to the difficult root finding problem (3.18). Namely, using this control algorithm, t_N is given by

$$t_N(\tau_\omega) = 4 \int_0^{\frac{\pi}{2}} \frac{d\theta}{\sqrt{2(\bar{E}_0 - \frac{1}{2}\omega^2\theta^2)}} = \frac{2\pi}{\omega}. \tag{3.19}$$

By this assignment, then we have reduced the dimension of the tuning parameter space by half: we need merely solve (3.18) for d. More formally, we seek an implicit function $d^* = \lambda^{-1}(\omega)$ such that $\Phi\left(\lambda^{-1}(\omega), \frac{2\pi}{\omega}\right) = 0$. Of course, we are more likely in practice to take an interest in tuning ω as a function of a desired d^*. Thus, we are most interested in determining

$$\omega = \lambda(d^*). \tag{3.20}$$

In general, we can expect no closed form expression for λ or λ^{-1}, and we compute an estimate, $\hat{\lambda}$, using a standard numerical scalar root finding method (i.e. the "false position" method or "secant" method) whose convergence properties are well known [74].

We plot in Figure 3.2 a particular instance of $\hat{\lambda}$ for the case where the robot parameters are shown in Table 2.1. ω is tuned according to this mapping. We will use these parameter values in the sequel for the sake of comparison between this and subsequent figures.

3.1.4   Simulation

Simulation with a Hooke's Law Potential for Target Dynamics

Consider the case $d^* = 0.6$ for this parameter set above. The initial condition of the robot is $Tq_0 = [\, c_-(d^*)^T, \, 0, \, 0\,]^T$. From the numerical solution depicted in Figure 3.2, $\omega = \hat{\lambda}(0.6) = 3.36$ with the choice of the Hooke's spring law, $U(x) = \frac{1}{2}x^2$. In this simulation, the lossy model (2.1) is used and friction terms are added in the inverse dynamics controller (2.16) as follows:

$$\begin{aligned}
\tau =: \tau_\omega &= L_F H^{-1}\left(Tq, f_\omega \circ Th(Tq)\right) \\
&= \left(D_q h \begin{bmatrix} n_{12} \\ n_{22} \end{bmatrix} \right)^{-1} \left[-\omega^2\theta - (D_q\dot{h})\dot{q} + D_q h M^{-1}\left(V + k + B\dot{q} + C\mathrm{sgn}(\dot{q})\right) \right]
\end{aligned}$$

$$\tag{3.21}$$

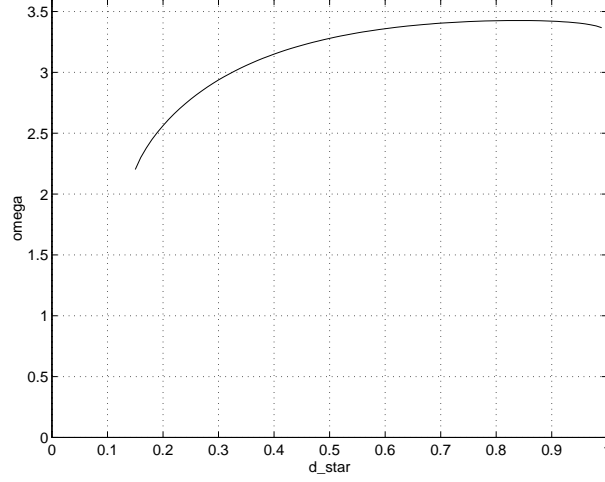**Figure 3.2**: Numerical approximation $\omega = \hat{\lambda}(d^*)$ with $U(x) = \frac{1}{2}x^2$ for target dynamics. Target dynamics controller, τ_ω, is tuned according to this mapping, $\hat{\lambda}$, that is designed to locate neutral orbits originating in the ceiling.
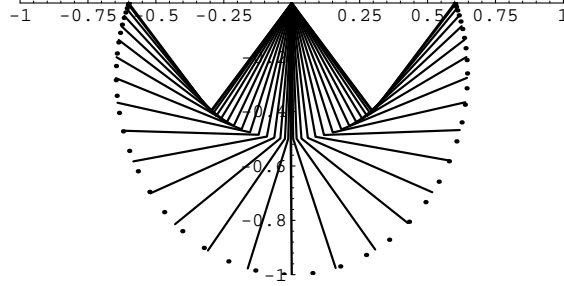

Figure 3.3: Movement of the robot (simulation) with $U(x) = \frac{1}{2}x^2$ in the target dynamics. The symmetry properties of the neutral orbit from the ceiling solves the uniform ladder problem.

where $v_r = \frac{1}{K}\tau$. Figure 3.3 shows the resulting movement of the robot. The joint trajectories and the voltage command to the motor driver are shown in Figure 3.4.

Note that the closed loop dynamics of the system does not strictly admit a reverse time symmetry discussed above, since the uncancelled friction terms of the first joint enter the dynamics of the unactuated degree of freedom. However, under these circumstances, the numerical simulation shown in Figures 3.3 and 3.4 suggests that the desired brachiation can be achieved. In practice, we have found that model mismatch seems to affect behavior of the physical robot rather considerably as discussed in Appendix C.

Simulation using Various Artificial Potential Functions for Target Dynamics

In this section, we present numerical studies on the ladder problem using various choices of the artificial potential, $U(x)$. Consider even artificial potential functions such as, $U(x) = \frac{1}{4}x^4$, $U(x) = \frac{1}{2}x^2 + \frac{1}{4}x^4$ and $U(x) = \frac{1}{8}x^4$, which are in the family of "hard" springs, and $U(x) = 1 - \cos x$
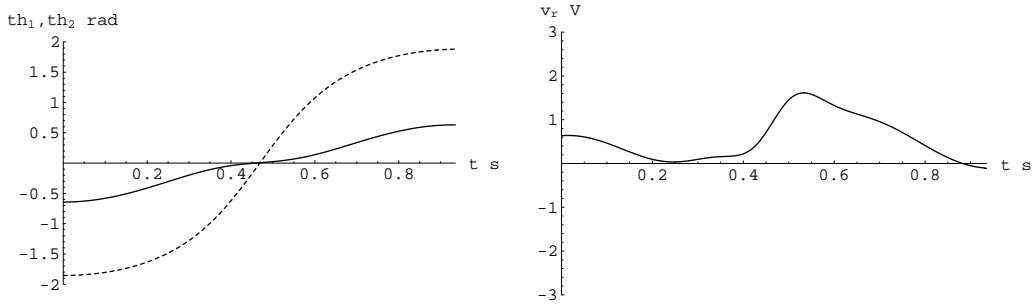
Figure 3.4: Simulation results of the uniform ladder problem with $U(x) = \frac{1}{2}x^2$ for the target dynamics. Left: Joint trajectories (θ_1: solid, θ_2: dashed). Right: Voltage command to the motor driver.

and $U(x) = \frac{1}{2}x^2 - \frac{1}{24}x^4$, which are in the family of "soft" springs. In these simulations, the interval between the bars is $d = 0.6$.

As the following simulation results depicted in Figures from 3.5 to 3.9 suggest, all of these spring potentials work nicely in the ladder problem. Notice that a higher order "hard" spring such as $U(x) = \frac{1}{8}x^8$ calls for a large torque as shown in Figure 3.7.
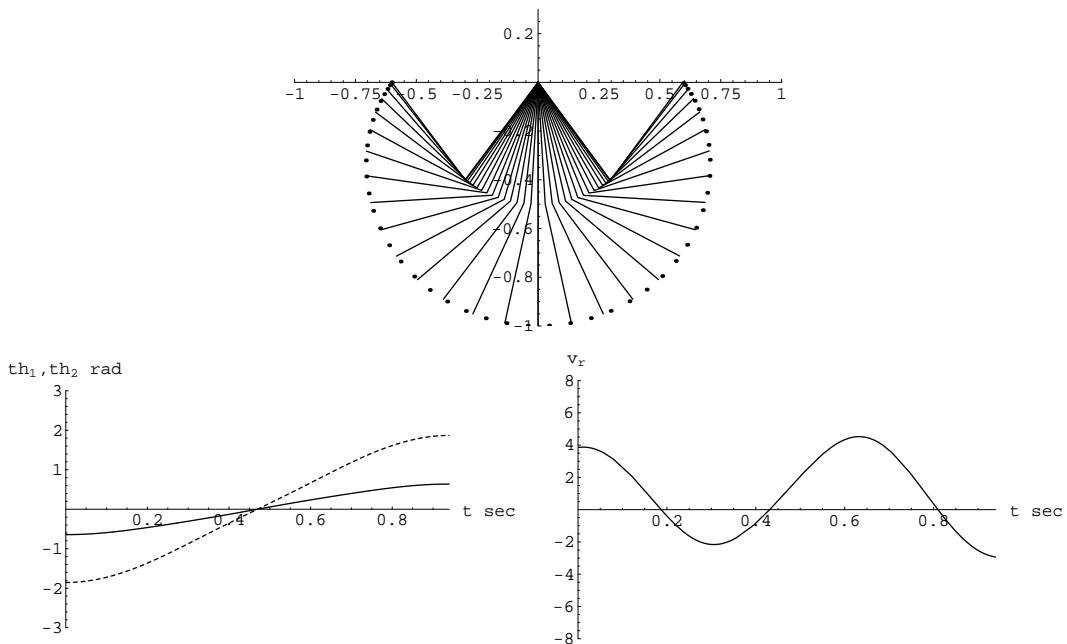

Figure 3.5: Simulation results of the ladder problem with a "hard" spring, $U(x) = \frac{1}{4}x^4$, in the target dynamics ($\omega = 2.513$). Top: Movement of the robot. Left: Joint trajectories (θ_1: solid, θ_2: dashed). Right: Voltage command to the motor driver.
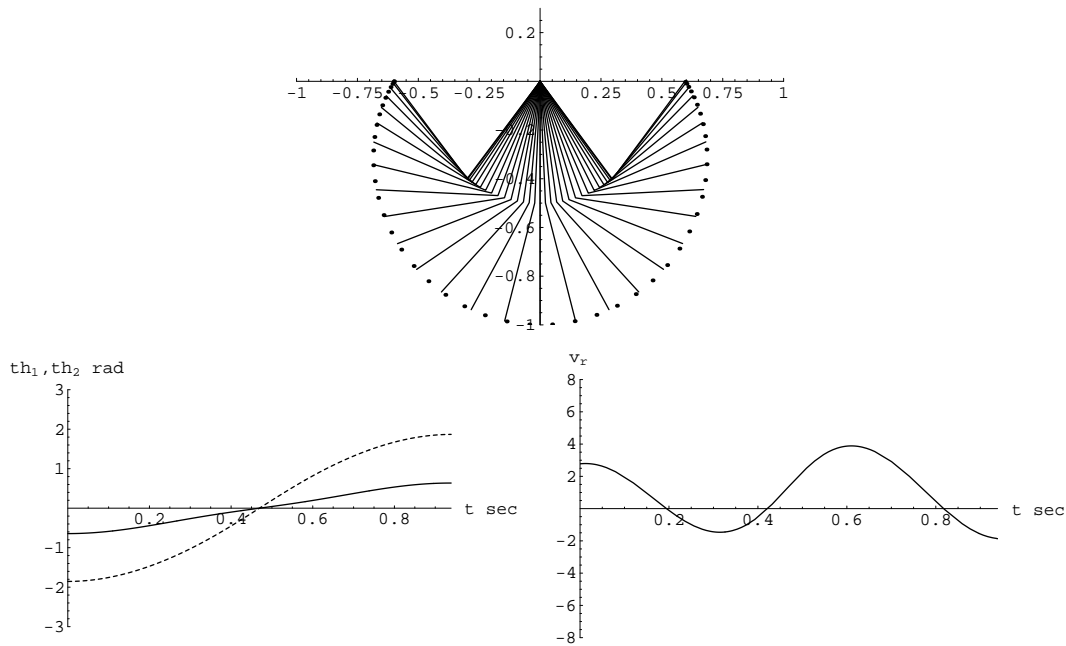
Figure 3.6: Simulation results of the ladder problem with a "hard" spring, $U(x) = \frac{1}{2}x^2 + \frac{1}{4}x^4$, in the target dynamics ($\omega = 2.00$). Top: Movement of the robot. Left: Joint trajectories (θ_1: solid, θ_2: dashed). Right: Voltage command to the motor driver.

3.2 Swing up Problem

The swing up problem entails pumping up from the suspended posture at rest and catching the next bar. In order to achieve this task it is necessary not only to add energy in a suitable fashion but also to control the arm position at the capture of the next target bar. This suggests that we need to introduce a stable limit cycle to the system with suitable magnitude and relative phase in state. The idea we present here is a simple modification of the foregoing target dynamics. We define the "pseudo energy" with respect to the target variable and add a compensation term to the target dynamics in order to introduce the desired limit cycle.

3.2.1 Swing up Controller

As we have mentioned, swing up requires energy pumping in a suitable fashion. To achieve this we modify the target dynamics (2.14) as

$$\dot{Tx} = \begin{bmatrix} \dot{x} \\ -K_e(\bar{E} - \bar{E}^*)\dot{x} - \omega^2 DU(x) \end{bmatrix} := f_{\bar{E}^*}(Tx) \tag{3.22}$$

where, $x = h(q) = \theta = \theta_1 + \frac{1}{2}\theta_2$ as defined in (2.11)
$\qquad K_e$: a positive constant
$\qquad \bar{E}$: "pseudo energy" as defined in (2.15)
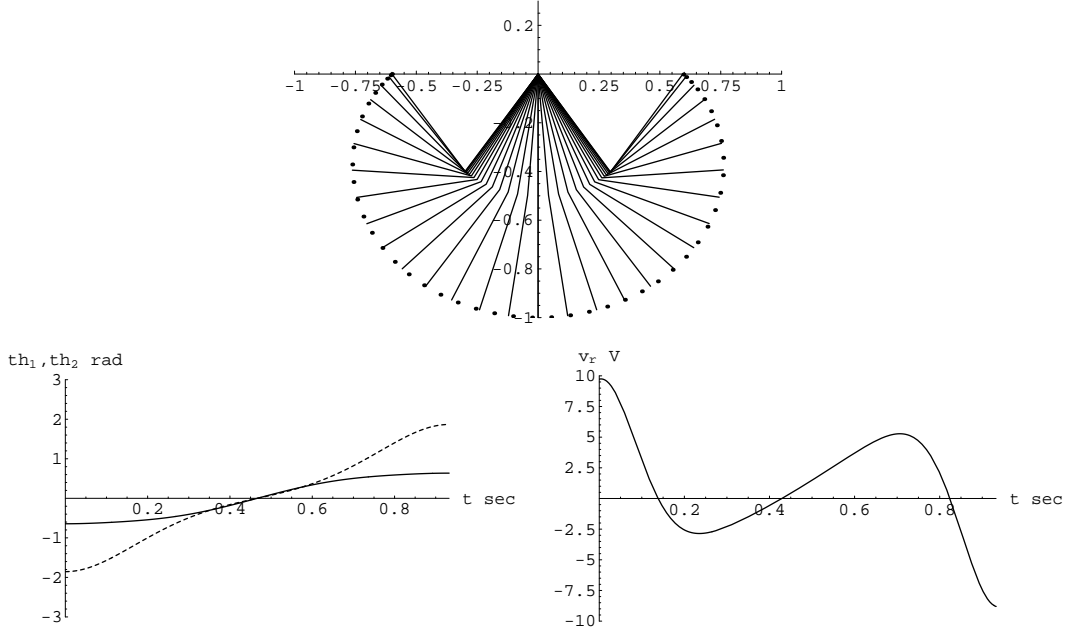$\qquad \bar{E}^*$: the desired pseudo energy level

Figure 3.7: Simulation results of the ladder problem with a "hard" spring, $U(x) = \frac{1}{8}x^8$, in the target dynamics ($\omega = 1.288$). Top: Movement of the robot. Left: Joint trajectories (θ_1: solid, θ_2: dashed). Right: Voltage command to the motor driver. This potential achieves the task, but calls for a large torque.

To achieve this target dynamics, the control law is formulated as

$$
\begin{aligned}
\tau_{\bar{E}^*} &= L_F H^{-1}\left(Tq, f_{\bar{E}^*} \circ Th(Tq)\right) \\
&= \left(D_q h \begin{bmatrix} n_{12} \\ n_{22} \end{bmatrix}\right)^{-1} \left[-\omega^2 DU(x) \circ h(q) - K_e(\bar{E} - \bar{E}^*)\dot{x} - (\dot{D_q h})\dot{q} + D_q h M^{-1}(V + k)\right] \\
&= \frac{1}{n_{12} + \frac{1}{2}n_{22}}\left[-\omega^2 DU(x) \circ h(q) - K_e(\bar{E} - \bar{E}^*)\dot{x} + (n_{11} + \frac{1}{2}n_{21})(V_1 + k_1)\right] \\
&\quad + V_2 + k_2
\end{aligned}
\tag{3.23}
$$

Now consider the time derivative of $\bar{E}$ along the motion

$$
\dot{\bar{E}} = -K_e(\bar{E} - \bar{E}^*)\dot{x}^2.
\tag{3.24}
$$

If $\bar{E} > \bar{E}^*$ then the pseudo energy $\bar{E}$ decreases, and if $\bar{E} < \bar{E}^*$ then $\bar{E}$ increases. Therefore, $\bar{E}$ will converge to the desired level $\bar{E}^*$ eventually. This implies that the target dynamics has a stable limit cycle whose trajectory is characterized by $\frac{1}{2}\dot{x}^2 + \omega^2 U(x) = \bar{E}^*$ on the phase plane of $(x, \dot{x})$.

Although the system's motion projected onto the target subspace must exhibit the desired limit cycle, the swing up task still requires a coordination of the full four dimensional robot trajectory in order to guarantee the arm extension is correct at the moment the "virtual pendulum" angle reaches the ceiling. But for this task, in contrast to the ladder problem, we can make no assumption regarding the robot's initial conditions – the arm might start out in any configuration
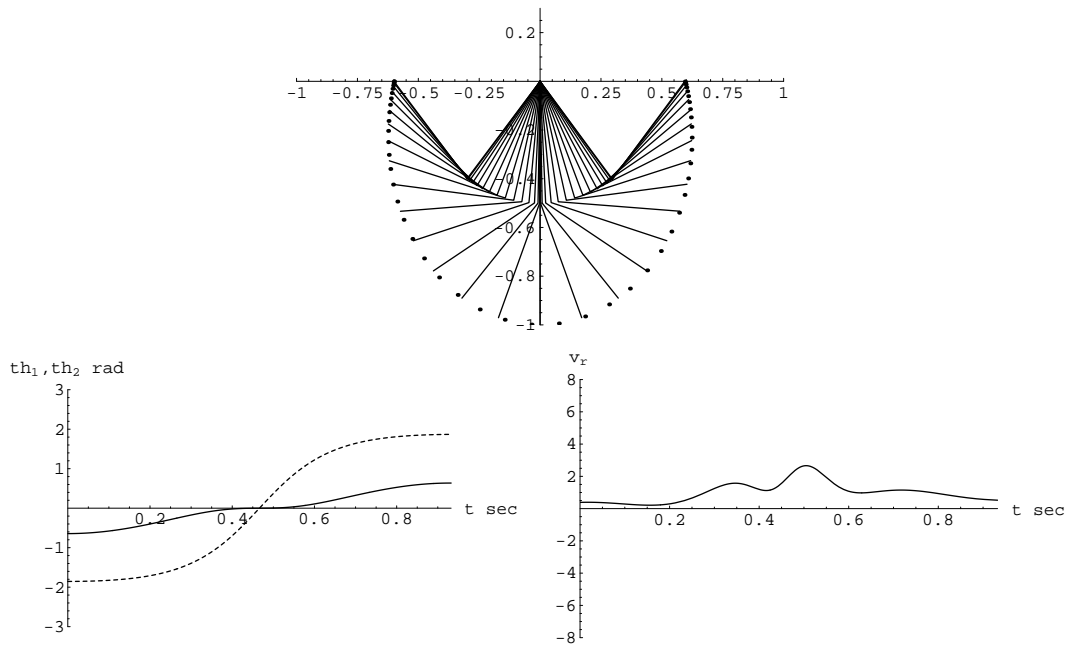
Figure 3.8: Simulation results of the ladder problem with a "soft" spring, $U(x) = 1 - \cos x$, in the target dynamics ($\omega = 3.977$). Top: Movement of the robot. Left: Joint trajectories (θ_1: solid, θ_2: dashed). Right: Voltage command to the motor driver.

(typically, at small velocity) near the bottom state following a small "kick" of torque administered to break out of that passively stable equilibrium state. In particular, there is no comparable means of appeal to a tuned symmetry as before. Unfortunately, no general method is presently known to stabilize a highly nonlinear underactuated mechanical system around a specific (necessarily non-equilibrium) orbit. Hence, we are reduced to empirical tuning of the pumping gain, K_e in order to find task worthy values.

The effect of K_e on the target system is quite straightforward—equation (3.24) shows that it sets the time constant for convergence to the specified lower dimensional target limit cycle, hence, higher gains must result in quicker approach to the "virtual" steady state behavior. In contrast, the four dimensional closed loop system can be expected to exhibit extremely complex (revolute-revolute kinematic chains are "chaotic") orbits as depicted in Figure 3.11. Certainly, there is no reason to expect limit cycles from the true four dimensional system as its orbits accumulate toward the three dimensional limit set. Empirically, however, we find there are favorable regimes for small K_e wherein the system's motion tends toward "near-neutral" orbits resulting very slow swing up — that is, a relative phasing between the virtual angle and extension that brings the gripper to the next handhold at an acceptably small velocity. Fortunately, a numerical one parameter search is quite simple to implement. We have found it relatively straightforward to achieve effective swing up controllers both in simulation as well as in the lab by simply incrementing the value of this pseudo-energy pumping gain (starting from very small values), recording the favorable values as they recur, and then running with a favorable value whose associated pseudo-energy convergence rate is fast enough to yield a viable handhold over three or four swings. Under these
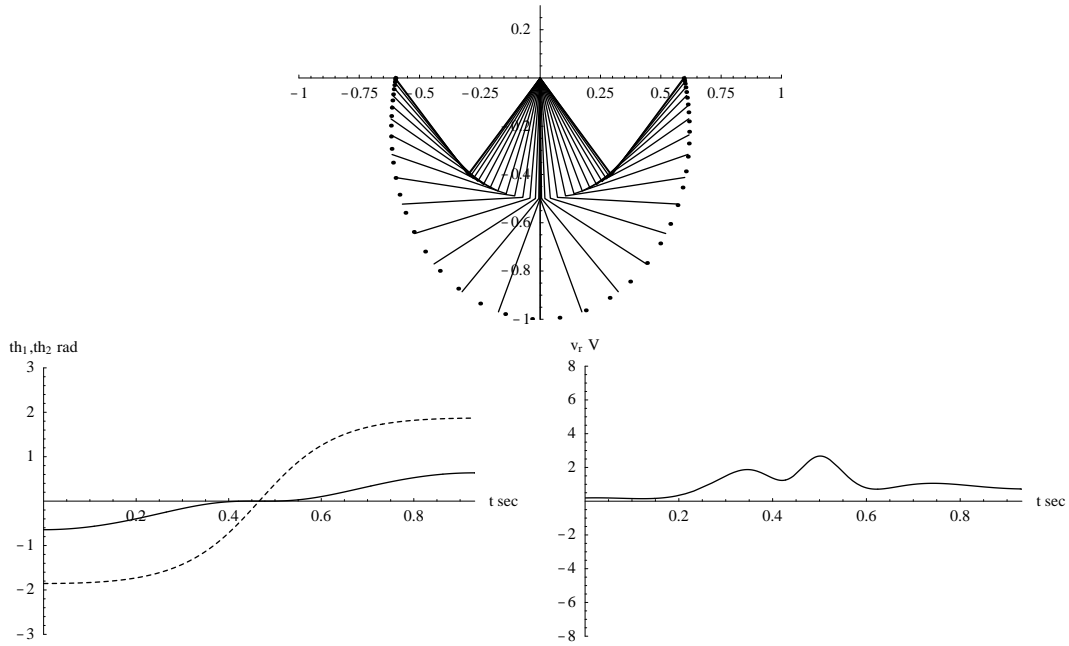
Figure 3.9: Simulation results of the ladder problem with a "soft" spring, $U(x) = \frac{1}{2}x^2 - \frac{1}{24}x^4$, in the target dynamics ($\omega = 3.499$). Top: Movement of the robot. Left: Joint trajectories (θ_1: solid, θ_2: dashed). Right: Voltage command to the motor driver.

circumstances, in Chapter 5 we introduce a hybrid swing up controller in which the original target dynamics swing up controller discussed in this chapter and a mechanical regulator are combined to achieve better regulation of the desired swing behavior.

3.2.2   Simulation

Simulation with a Hooke's Law Potential for Target Dynamics

What follows here is a presentation of different swing up behaviors resulting from changes in the rate of energy pumping as characterized by K_e using a Hooke's law potential, $U(x) = \frac{1}{2}x^2$, for target dynamics. The next bar is located at the distance $d^* = 0.6$, and we choose $\omega = \lambda(0.6) = 3.36$ according to the mapping depicted in Figure 3.2. Since the bottom condition with zero velocity is an equilibrium state of the closed loop dynamics, we give small initial velocity to the second joint to initiate the swing motion in the desired direction[2].

In the following simulations, we assume that the robot can catch the bar when it comes very close to the desired handhold.

Very Slow Swing up ($K_e = 0.05$)   Figure 3.10 shows the joint trajectories and the voltage command to the motor driver. The robot catches the bar at $t = 19.2$ seconds. A near neutral orbit is achieved with small choice of K_e.

---

[2]Here, we give a small "kick" velocity, $\dot{\theta}_{20} = \pm 0.2$, to the second joint in these simulations.

A Typical "Chaotic" Swing Behavior   Figure 3.11 shows a typical "chaotic" swing motion of the system in the "virtual" steady state behavior with large choice of $K_e = 0.18$ as mentioned in Section 3.2.

Slow Swing up ($K_e = 0.20$)   Figure 3.12 shows the joint trajectories and the voltage command to the motor driver. The robot catches the bar at $t = 7.23$ seconds.

Fast Swing up ($K_e = 0.228$)   Figure 3.13 shows the joint trajectories and the voltage command to the motor driver. The robot catches the bar at $t = 3.55$ seconds.

Faster Swing up ($K_e = 0.328$)   Figure 3.14 shows the joint trajectories and the voltage command to the motor driver. The robot catches the bar at $t = 2.78$ seconds.

Simulation using Various Artificial Potential Functions for Target Dynamics

In this section, we present numerical studies addressing the swing up problem using various choices of the artificial potential, $U(x)$. We consider artificial potential functions such as, $U(x) = \frac{1}{4}x^4$, $U(x) = \frac{1}{2}x^2 + \frac{1}{4}x^4$, and $U(x) = \frac{1}{8}x^8$, which are in the family of "hard" springs, and $U(x) = 1 - \cos x$, $U(x) = \frac{1}{2}x^2 - \frac{1}{24}x^4$, and $U(x) = \frac{1}{2}x^2 - \frac{1}{96}x^4$, which are in the family of "soft" springs.

Figures from 3.15 to 3.20 show the simulation results of the swing up problem using these spring potential functions. "Hard" spring laws such as $U(x) = \frac{1}{4}x^4$, $U(x) = \frac{1}{2}x^2 + \frac{1}{4}x^4$ and $U(x) = \frac{1}{8}x^8$ work nicely and achieve a near neutral orbit as shown in Figures from 3.15 to 3.17. However, as observed in Figures 3.15 and 3.17, notice that potential functions with zero stiffness around the origin results in oscillation with a long period when the amplitude of the swing is small.

In contrast, "soft" spring laws without "stiffness margin" profile such as $U(x) = 1 - \cos x$, $U(x) = \frac{1}{2}x^2 - \frac{1}{24}x^4$ fail the swing up task as shown in Figures 3.18 and 3.19. However, a "soft" spring law with some "stiffness margin" profile bounded away from zero (see Figure 2.5) achieves a near neutral orbit as shown in Figure 3.20.

As discussed in Section 2.5, these simulation results suggest that the stiffness profile plays an important role in achieving effective swing up behavior, while all of these work nicely in the ladder problem. Further investigation is necessary to gain full understanding of this matter.

3.3   Summary

This chapter is summarized as follows:

- This chapter was concerned with the uniform ladder and swing up problems. First, we applied the target dynamics to the uniform ladder problem and showed how a symmetry property of neutral orbits can solve this problem.

- Then, we considered the swing up problem, which requires not only to pump up the energy but also to control the arm position at the capture of the next target bar to achieve the task. We presented an idea to modify the target dynamics to introduce the stable limit cycle to the system by adding the compensation term of the pseudo energy.
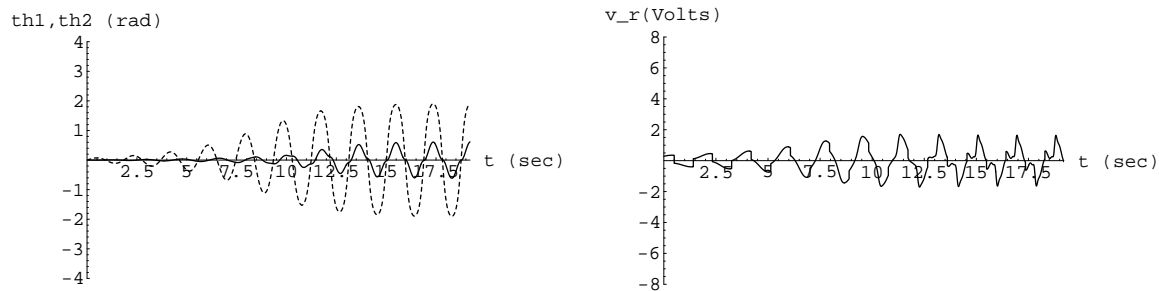
Figure 3.10: Simulation results of very slow swing up behavior ($K_e = 0.05$) using $U(x) = \frac{1}{2}x^2$. Left: Joint trajectories (θ_1: solid, θ_2: dashed). Right: Voltage command to the motor driver. The robot captures the bar at $t = 19.2$ seconds. Small choice of K_e achieves a near neutral orbit in the long time swing behavior.
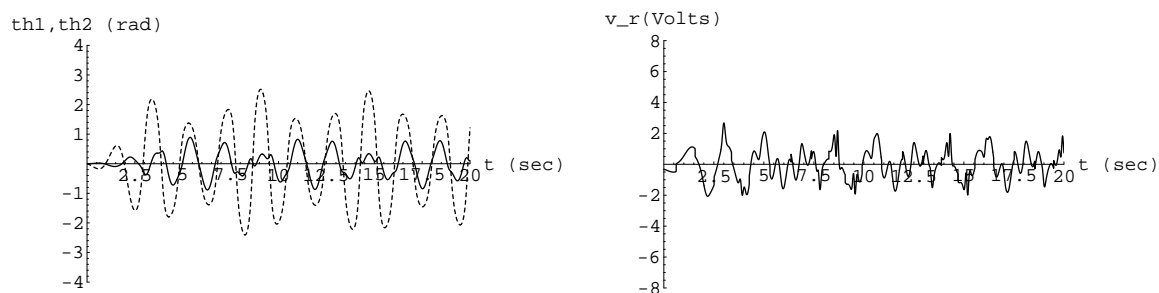

Figure 3.11: Simulation results of "chaotic" swing behavior ($K_e = 0.18$) using $U(x) = \frac{1}{2}x^2$. Left: Joint trajectories (θ_1: solid, θ_2: dashed). Right: Voltage command to the motor driver. "Chaotic" swing motion is observed when we let the robot keep swinging with large choice of K_e.
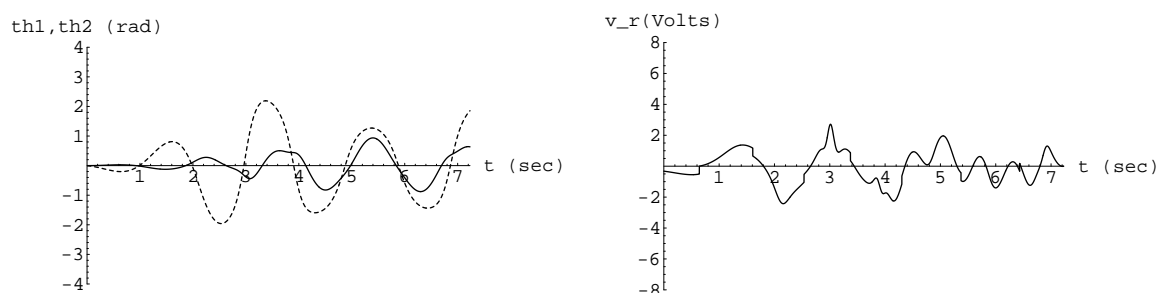

Figure 3.12: Simulation results of slow swing up behavior ($K_e = 0.20$) using $U(x) = \frac{1}{2}x^2$. Left: Joint trajectories (θ_1: solid, θ_2: dashed). Right: Voltage command to the motor driver. The robot captures the bar at $t = 7.23$ seconds.

Figure 3.13: Simulation results of fast swing up behavior ($K_e = 0.228$) using $U(x) = \frac{1}{2}x^2$. Left: Joint trajectories (θ_1: solid, θ_2: dashed). Right: Voltage command to the motor driver. The robot captures the bar at $t = 3.55$ seconds.
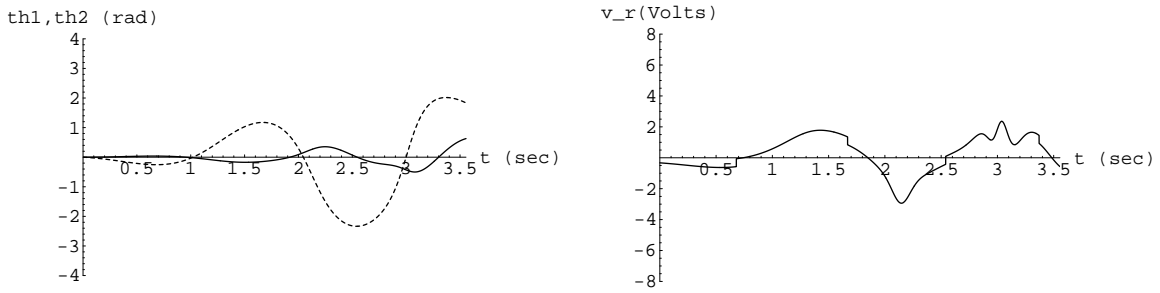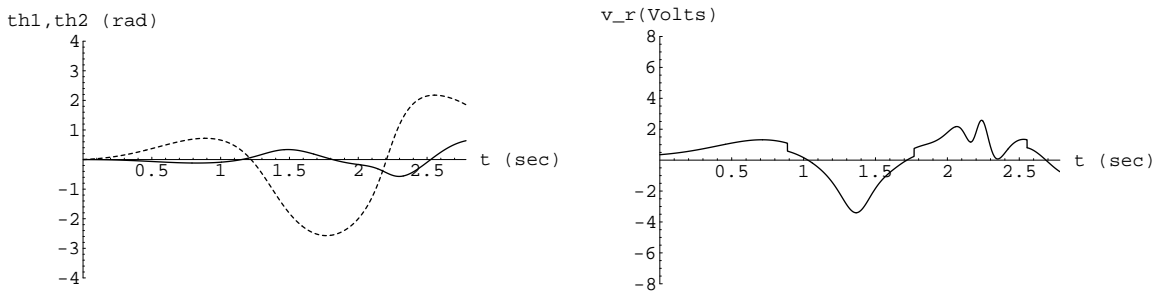

Figure 3.14: Simulation results of faster swing up behavior ($K_e = 0.328$) using $U(x) = \frac{1}{2}x^2$. Left: Joint trajectories (θ_1: solid, θ_2: dashed). Right: Voltage command to the motor driver. The robot captures the bar at $t = 2.78$ seconds.

- The results of numerical simulation suggest the effectiveness of the proposed control algorithm. In these problems, we have explored a number of choice of the artificial potential, $U(x)$, for the target dynamics. In our numerical investigations, we found that all of these spring potentials work nicely in the uniform ladder problem, but some "stiffness margin" profile is key to effective swing up behavior.
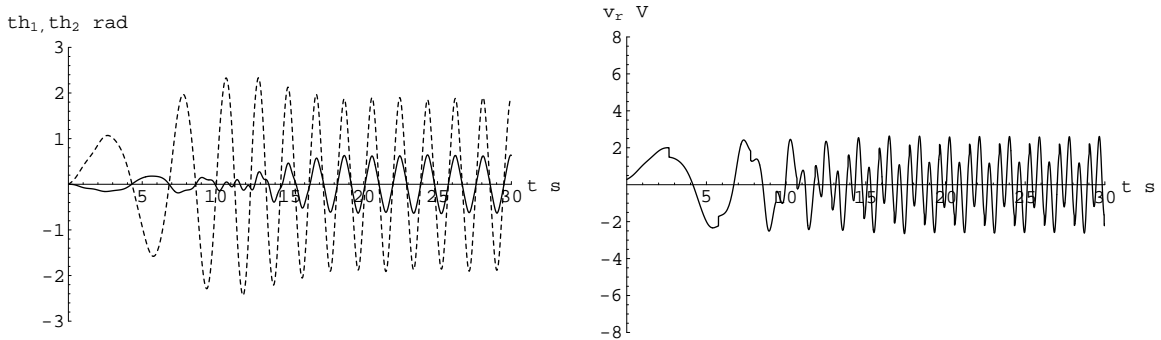
Figure 3.15: Simulation results of the swing up problem with $U(x) = \frac{1}{4}x^4$ for the target dynamics ($K_e = 0.05$). Left: Joint trajectories (θ_1: solid, θ_2: dashed). Right: Voltage command to the motor driver. This spring law achieves a near neutral orbit. Notice that the period of swing is long when the amplitude of oscillation is small.

Figure 3.16: Simulation results of the swing up problem with $U(x) = \frac{1}{2}x^2 + \frac{1}{4}x^4$ for the target dynamics ($K_e = 0.05$). Left: Joint trajectories (θ_1: solid, θ_2: dashed). Right: Voltage command to the motor driver. This spring law achieves a near neutral orbit.

Figure 3.17: Simulation results of the swing up problem with $U(x) = \frac{1}{8}x^8$ for the target dynamics ($K_e = 0.05$). Left: Joint trajectories (θ_1: solid, θ_2: dashed). Right: Voltage command to the motor driver. This spring law achieves a near neutral orbit. Notice that the period of swing is long when the amplitude of oscillation is small.
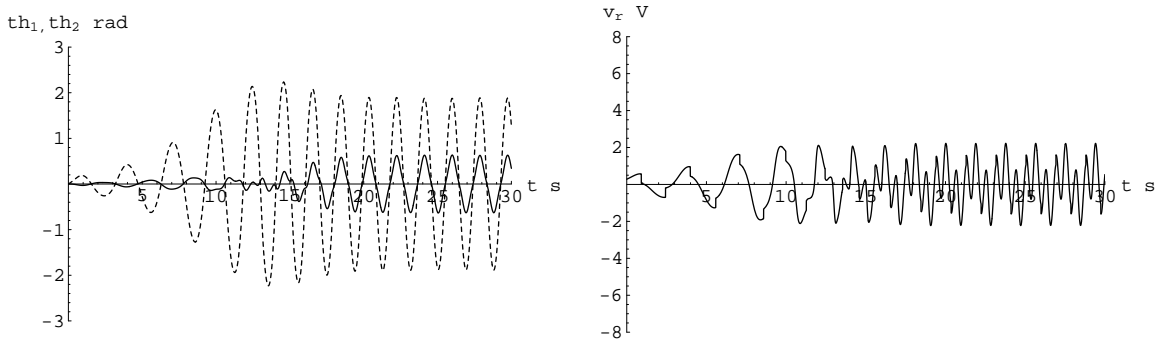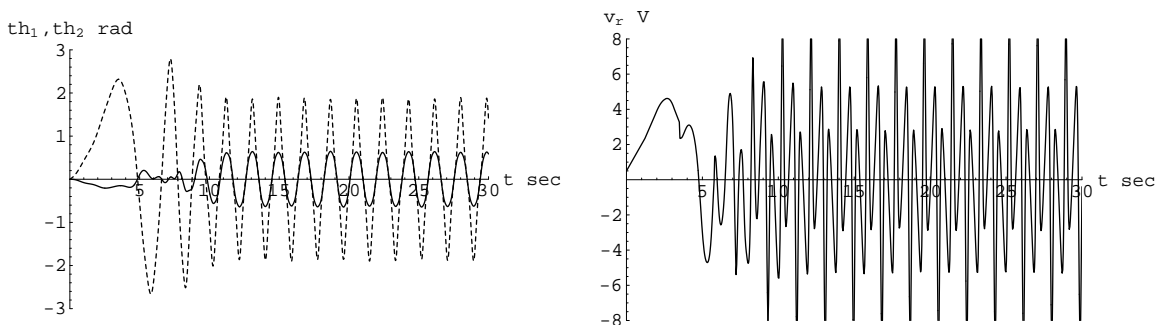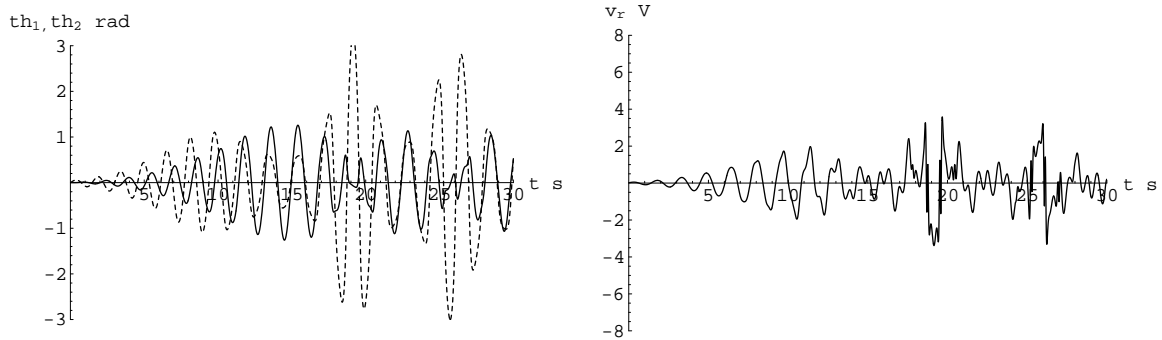
Figure 3.18: Simulation results of the swing up problem with $U(x) = 1 - \cos x$ for the target dynamics ($K_e = 0.05$). Left: Joint trajectories (θ_1: solid, θ_2: dashed). Right: Voltage command to the motor driver. This spring law fails the effective swing up task.

Figure 3.19: Simulation results of the swing up problem with $U(x) = \frac{1}{2} - \frac{1}{24}x^4$ for the target dynamics ($K_e = 0.05$). Left: Joint trajectories (θ_1: solid, θ_2: dashed). Right: Voltage command to the motor driver. This spring law results in a "out of phase" swing up which fails the task.
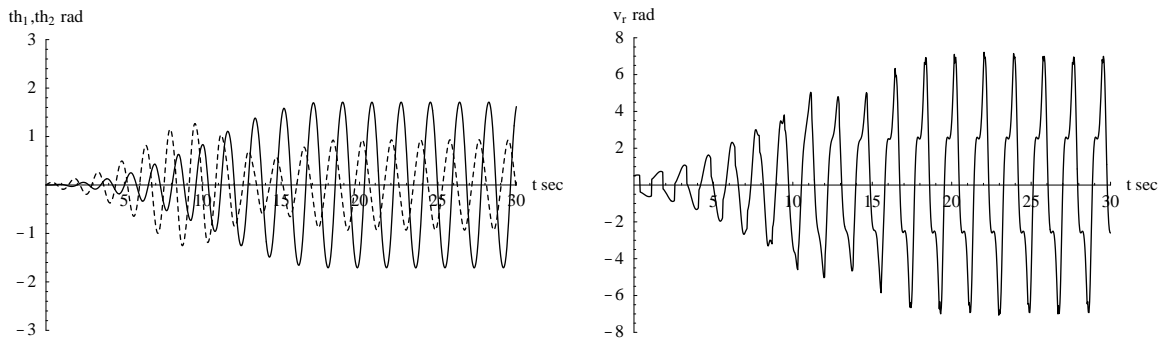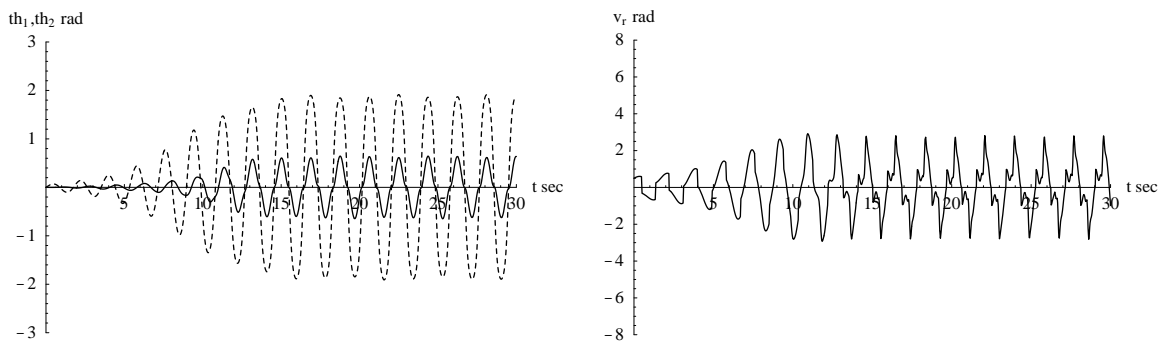

Figure 3.20: Simulation results of the swing up problem with $U(x) = \frac{1}{2} - \frac{1}{96}x^4$ for the target dynamics ($K_e = 0.05$). Left: Joint trajectories (θ_1: solid, θ_2: dashed). Right: Voltage command to the motor driver. With some "stiffness margin," this spring law achieves a near neutral orbit.

Chapter 4

Rope and Irregular Ladder Problems

In this chapter, we first address the rope problem—brachiation along a continuum of handholds such as afforded by a branch or a rope. We use the freedom of placement of grasps to achieve a specified forward velocity. Then, we consider the irregular ladder problem—brachiation on a ladder with irregularly spaced bars. We propose a control strategy extending the results on the rope problem seeking the tuning rule for ω which locates the desired asymmetric orbit to achieve the task. Numerical simulations and experiments presented in Chapter 7 suggests its effectiveness.

4.1 Rope Problem

In this section, the average horizontal velocity is first characterized as a result of the application of the target dynamics controller, τ_ω, introduced in Chapter 2. Then, we consider the regulation of horizontal velocity using this controller. An associated numerical "swing map" suggests that we indeed can achieve good local regulation of the forward velocity through the target dynamics method.

4.1.1 The Iterated Ladder Trajectory Induces a Horizontal Velocity

Supposing that the robot starts in the ceiling with zero velocity, then it must end in the ceiling under the target dynamics controller since θ follows the dynamics $\ddot{\theta} + \omega^2\theta = 0$. However, if d and ω are not "matched" as $\omega = \lambda(d)$, then the trajectory ends in the tangent of the right branch of the ceiling, $Tq \in T\mathcal{C}_+$, with $\dot{\theta} = 0$ but $r \neq d$ and $\dot{r} \neq 0$. Shortly, we will present numerical evidence suggesting that when $d = d^* + \delta$ for small δ, then $\dot{r}$ at $Tq \in T\mathcal{C}_+$ is also small. Assuming that any such small nonzero velocity is "killed" in the ceiling, brachiation may be iterated by opening and closing the grippers at left and right ends in the appropriately coordinated manner. Namely, imagine that the robot concludes the swing by grasping firmly with its gripper the next handhold in the ceiling and thereby damps out the remaining kinetic energy. Imagine at the same instant that it releases the gripper clutching the previous handhold and thereby begins the next swing. We will call such a maneuver the Iterated Ladder Trajectory ("ILT").

It is natural to inquire as to how quickly horizontal progress can be made along the ladder in so doing. Notice in Figure 4.1 that when a gripper moves a distance $2d^*$ in the course of the ladder trajectory, and if the trajectory is immediately repeated, as described above, then the
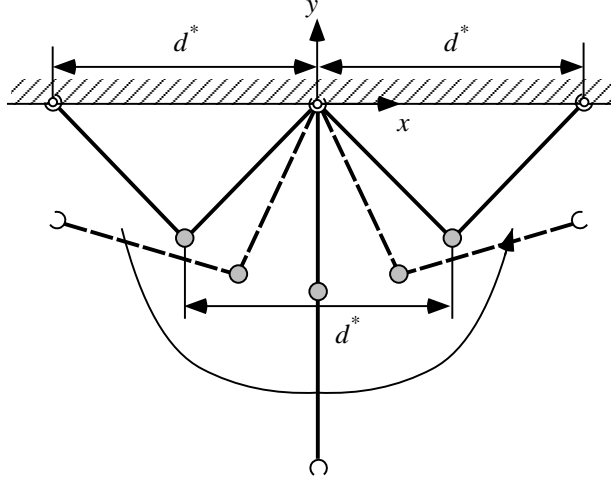
Figure 4.1: Progress of the robot per swing. The robot's body proceeds d^* per swing while a gripper moves $2d^*$.

body will also move a distance of d^* each swing. Hence, its average horizontal velocity will be

$$\bar{h} = \frac{d^* \omega}{\pi} = \frac{d^* \lambda(d^*)}{\pi} := \tilde{V}(d^*) \tag{4.1}$$

according to the discussion in Chapter 3. In Figure 4.2, we now plot the ceiling-to-velocity map $\bar{h} = \tilde{V}(d^*)$ for the choice of $U(x) = \frac{1}{2}x^2$ in target dynamics and the robot parameters in Table 2.1, where $\tilde{V}$ is computed using the numerical approximation, $\hat{\lambda}$ discussed in Section 3.1.3.

4.1.2   Inverting the Ceiling-to-Velocity Map

Consider now the task of obtaining the desired forward velocity $\bar{h}^*$ of brachiation. If $\tilde{V}$ is invertible, then $d^* = \tilde{V}^{-1}(\bar{h}^*)$ and we can tune ω in the target dynamics as

$$\omega = \lambda \circ \tilde{V}^{-1}(\bar{h}^*) \tag{4.2}$$

to achieve a desired $\bar{h}^*$ where λ is again the mapping (3.20).

4.1.3   Horizontal Velocity Regulation

Consider the ceiling condition with zero velocity

$$T\mathcal{C}_{0\pm} = \left\{ \begin{bmatrix} c_\pm(d) \\ 0 \\ 0 \end{bmatrix} \in T\mathcal{C} \mid d \in [0, 2l] \right\} \tag{4.3}$$

Define the maps, $C_\pm$, and their inverses, $C_\pm^{-1}$, as

$$C_\pm : [0, 2l] \rightarrow T\mathcal{C}_{0\pm} : d \mapsto \begin{bmatrix} c_\pm(d) \\ 0 \\ 0 \end{bmatrix}, \tag{4.4}$$
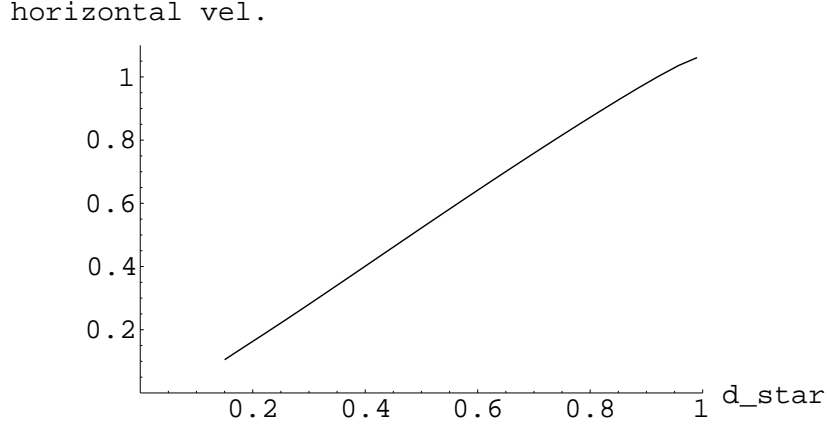
Figure 4.2: The ceiling-to-velocity map, $\tilde{V}$ using $U(x) = \frac{1}{2}x^2$. This mapping is inverted to obtain the desired forward velocity $\bar{\bar{h}}^*$.

$$C_{\pm}^{-1} : TC_{0\pm} \to [0, 2l] : \begin{bmatrix} c_{\pm}(d) \\ 0 \\ 0 \end{bmatrix} \mapsto d. \tag{4.5}$$

A target dynamics controller (2.9) gives

$$\mathcal{L}_{\tau_\omega}^{2\nu} \circ C_-(d) \in TC_+ \text{ , where } \nu = \frac{\pi}{2\omega} \tag{4.6}$$

since θ follows the dynamics $\ddot{\theta} = -\omega^2\theta$. Now, if $\omega = \lambda(d)$, then

$$\mathcal{L}_{\tau_\omega}^{2\nu} \circ C_-(d) = C_+(d) = \begin{bmatrix} c_+(d) \\ 0 \\ 0 \end{bmatrix} \in TC_{0+} \text{ , where } \nu = \frac{\pi}{2\omega} \tag{4.7}$$

because of the symmetry properties of the neutral orbits, demonstrated in Proposition 3.4.

Define a projection Π, from the ceiling's tangents into the zero velocity section,

$$\Pi : TC_{\pm} \mapsto TC_{0\pm}. \tag{4.8}$$

In other words, Π is a map that "kills" any velocity in the ceiling. We introduce this projection to model the ILT maneuver in cases when $\dot{r} \neq 0$ for $Tq \in TC$ since the robot is constrained by its own kinematics when both of the grippers grasp the bars firmly. We plot the approaching velocity in the right branch of the ceiling, $\dot{r}$, for $d \in [0, 2l]$ where $d^* = 0.6496, \omega = 3.385$ in Figure 4.3.

To gain an intuitive feeling for the magnitude of "leftover energy" that must be "killed" before the next swing begins, we will compare it to the energy of the steady state swing. In the worst case, the kinetic energy in the ceiling TC_+ resulting from the initial condition $Tq_0 = C_-(0.02)$ is $K(TC_+) = 1.432$ J. The maximum kinetic energy during a swing when $d = d^*$ is $K_{d^* \max} = 10.209$ J. The ratio $\frac{K(TC_+)}{K_{d^* \max}} = 0.1402$ seems to be acceptably small. Consider instead, more favorable range, where $d = d^* + \delta$ and $\delta = -0.2$. Now the kinetic energy killed in the ceiling is
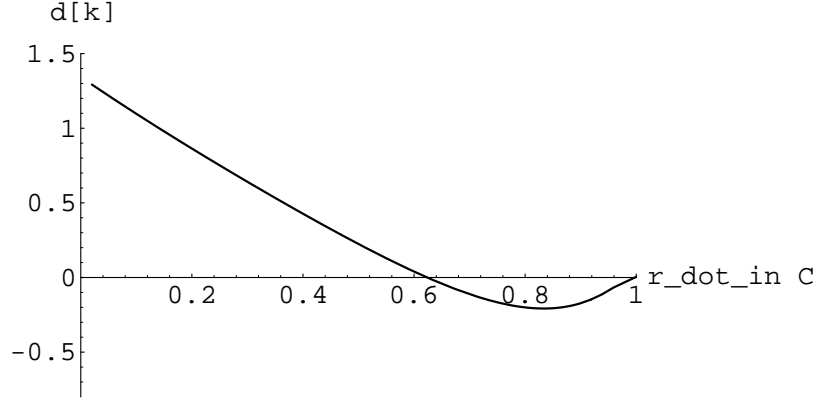
Figure 4.3: Approaching horizontal velocity of the robot gripper for the case $d^* = 0.6496, \omega^* = 3.385$ where $\omega^* = \hat{\lambda}(d^*)$ using $U(x) = \frac{1}{2}x^2$ and the robot parameters specified in Table 2.1. When the error in the initial condition from d^* is small, the resulting approaching velocity in the ceiling is also small.

$K(T\mathcal{C}_+) = 0.2574$ J, and the ratio $\frac{K(T\mathcal{C}_+)}{K_{d^*} \max} = 9.593 \times 10^{-3}$ in this case is very small despite fairly large error (31 %) in the initial condition. This suggests that the idea of killing any approaching horizontal velocity in the ceiling may be physically reasonable.

We now have from (4.6)

$$\Pi \circ \mathcal{L}_{\tau_\omega}^{2\nu} \circ C_-(d) \in T\mathcal{C}_{0+} \quad , \text{ where } \quad \nu = \frac{\pi}{2\omega} \tag{4.9}$$

hence we may define a "swing map", σ_ω, as a transformation of $[0, 2l]$ into itself,

$$\sigma_\omega(d) := C_+^{-1} \circ \Pi \circ \mathcal{L}_{\tau_\omega}^{2\nu} \circ C_-(d) : [0, 2l] \to [0, 2l] \tag{4.10}$$

Note that if $\omega = \omega^* = \lambda(d^*)$, then

$$\sigma_\omega(d^*) = d^* \tag{4.11}$$

that is, d^* is a fixed point of the appropriately tuned swing map.

It is now clear that the dynamics of the ILT maneuver can be modelled by the iterates of this swing map, σ_ω. Physically, suppose we iterate by setting the next initial condition in the ceiling to be

$$Tq_0[k+1] = C_- \circ \sigma_\omega(d[k]). \tag{4.12}$$

This yields a discrete dynamical system governed by the iterates of σ_ω,

$$d[k+1] = \sigma_\omega(d[k]). \tag{4.13}$$

Numerical evidence suggests that the iterated dynamics converges, $\lim_{k\to\infty} \sigma_{\omega^*}^k(d) = d^*$, when d is in the neighborhood of d^* as depicted in Figure 4.4 (local asymptotic stability of the fixed point d^*). We plot the swing map calculated numerically for the case where $U(x) = \frac{1}{2}x^2$ for target dynamics, $\bar{h} = 0.7, d^* = 0.6496, \omega = 3.385$ and the robot parameters in Table 2.1 are used (see Figure 4.4).
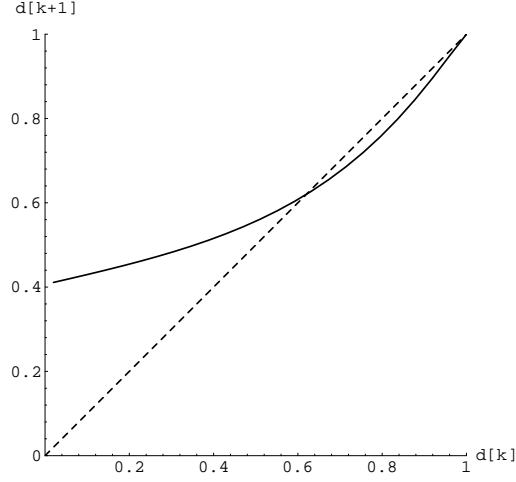
Figure 4.4: Swing map, σ_ω, (solid) and identity (dashed) for the case $\bar{h} = 0.7, d^* = 0.6496, \omega^* = 3.385$ using $U(x) = \frac{1}{2}x^2$ for the target dynamics where $\omega^* = \hat{\lambda}(d^*)$, and the robot parameters specified in Table 2.1 are used. This swing map has an attracting fixed point at d^*.

4.1.4 Simulation

Simulation with a Hooke's Law Potential for Target Dynamics

Suppose we would like to achieve the desired horizontal velocity, $\bar{h}^* = 0.7$. The parameters shown in Table 2.1 and $U(x) = \frac{1}{2}x^2$ for target dynamics are used. For this case, ω is obtained as $\omega = \hat{\lambda}(0.6496) = 3.385$.

First, consider ILT with the proper initial condition

$$Tq_0^* = \begin{bmatrix} c_-(d^*) \\ 0 \\ 0 \end{bmatrix} \tag{4.14}$$

which is proper in the sense $\bar{h}^* = \tilde{V}(d^*)$. The simulation result in this case is shown in Figure 4.5—a faithfully executed ILT at d^*.

Suppose, instead, that we select $\omega = \lambda(d^*)$ but the initial d_0 is wrong. We present the simulation result with the initial condition

$$Tq_0 = \begin{bmatrix} c_-(d^* + \delta) \\ 0 \\ 0 \end{bmatrix}, \text{where } \delta = -0.2 \tag{4.15}$$

in Figure 4.6. As the numerical swing map of (4.4) suggests, we nevertheless achieve asymptotically the desired locomotion, i.e., $d \to d^*$.

With the assumption that any velocity in the ceiling is killed, the size of the domain of attraction to d^* under σ_{ω^*} is fairly large according to the numerical evidence shown in Figure 4.4.
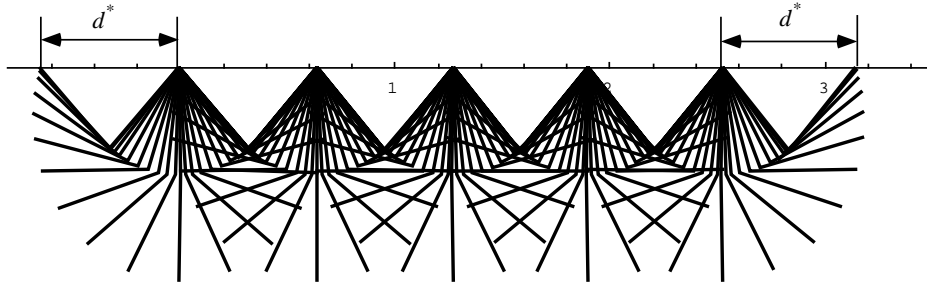
Figure 4.5: Brachiation along the bar with the initial condition (4.14) with $U(x) = \frac{1}{2}x^2$ for the target dynamics. ILT locomotion at the fixed point d^* yields the desired average horizontal velocity, $\bar{\dot{h}}^*$.
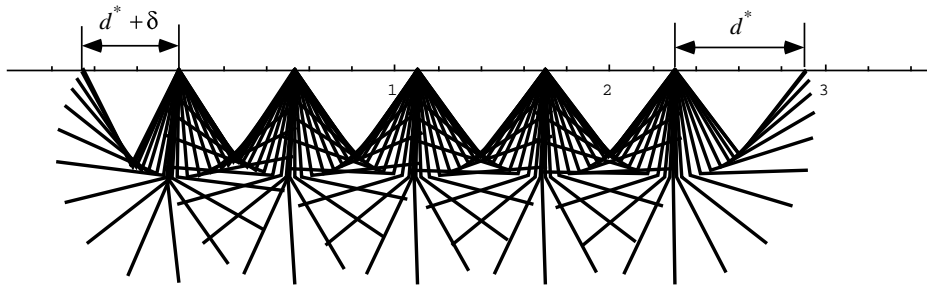

Figure 4.6: Brachiation along the bar with the initial condition (4.15) with $U(x) = \frac{1}{2}x^2$ for the target dynamics. Convergence of $d \to d^*$ is illustrated as the numerical swing map (Figure 4.4) indicates, and this yields convergence to the desired average velocity, $\bar{\dot{h}}^*$.

Simulation with Various Spring Potential Functions for Target Dynamics

In this section, we consider several spring potential laws for target dynamics addressing the rope problem. Consider the potential functions such as $U(x) = \frac{1}{4}x^4$, $U(x) = \frac{1}{2}x^2 + \frac{1}{4}x^4$ and $U(x) = 1 - \cos x$. We plot in Figure 4.7 the swing map for the case $\bar{\dot{h}} = 0.7$. Figures from 4.8 to 4.10 show the simulation results with the initial condition (4.15).

As the numerical swing maps in Figure 4.7 suggest, we nevertheless achieve asymptotically the desired locomotion, i.e., $d \to d^*$. These swing map and simulation results suggest that both "hard" and "soft" spring potential laws work nicely in the rope problem as well as in the ladder problem.

4.2   Irregular Ladder Problem

In the previous chapters, we have developed a brachiation controller that allows a two degrees of freedom robot to swing from handhold to handhold on a horizontal ladder with evenly space rungs as well as swing up from a suspended posture using a "target dynamics" controller. The question remains whether this approach is likely to yield a flexible enough repertoire of behaviors to motivate its further analytical and experimental exploration. In this section, we take a modest
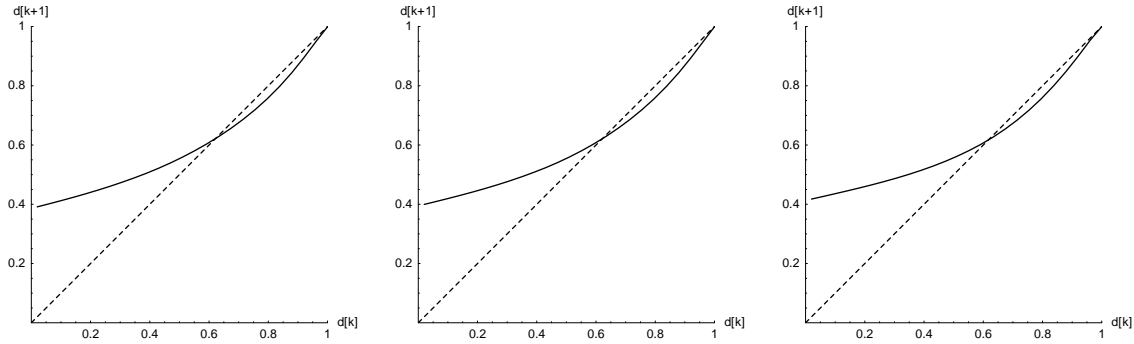
Figure 4.7: Swing map, σ_ω, (solid) and identity (dashed). Left: $U(x) = \frac{1}{4}x^4$, $\bar{h} = 0.7$, $d^* = 0.6522$, $\omega^* = 2.534$. Center: $U(x) = \frac{1}{2}x^2 + \frac{1}{4}x^4$, $\bar{h} = 0.7$, $d^* = 0.6520$, $\omega^* = 2.016$ Right: $U(x) = 1 - \cos x$, $\bar{h} = 0.7$, $d^* = 0.6479$, $\omega^* = 4.0066$. These swing maps has an attracting fixed point at each d^* respectively.
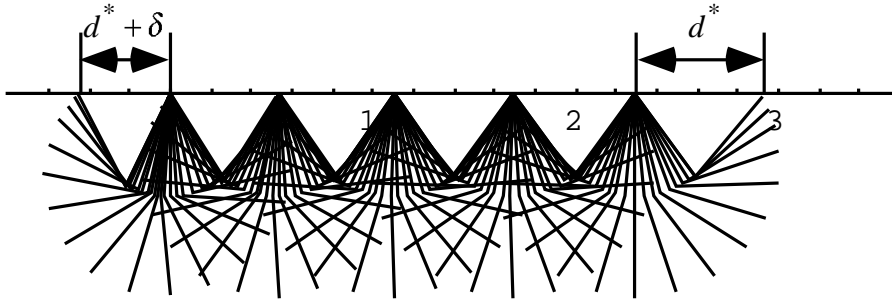

Figure 4.8: Brachiation along the bar with the initial condition (4.15) with $U(x) = \frac{1}{4}x^4$ for the target dynamics where $d^* = 0.6522$, $\omega = 2.534$. Convergence of $d \to d^*$ is illustrated as the numerical swing map (Figure 4.7) indicates, and this yields convergence to the desired average velocity, $\bar{h}^*$.

step of increasing the behavioral repertoire to include the "irregular ladder problem" — brachiation on a ladder with irregularly spaced rungs placed at the same height. This addition seems to be essential, if only from the point of view of our initial biomechanics motivation, since very few unstructured environments confront an ape with equally spaced branches. The original robot brachiation studies by Saito *et al.* [24, 62, 65, 66] considered brachiation on bars with different distances and heights using heuristic learning and neural networks [65]. However, experimental implementation of their control algorithms were not carried out in the irregular ladder problem because of the enormous experimental burden and parametric iterations required of the physical robot[1]. Here, we propose a control strategy to solve the irregular ladder problem by extending the results in our previous studies. Numerical simulation as well as experimental results presented in Chapter 7 illustrate the effectiveness of our approach.

---

[1]They did implement the learning algorithm on the physical two-link robot in the uniform ladder problem [66].
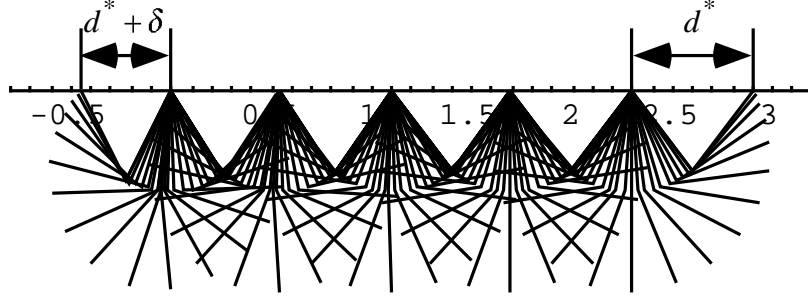
Figure 4.9: Brachiation along the bar with the initial condition (4.15) with $U(x) = \frac{1}{2}x^2 + \frac{1}{4}x^4$ for the target dynamics where $d^* = 0.6520$, $\omega = 2.016$. Convergence of $d \to d^*$ is illustrated as the numerical swing map (Figure 4.7) indicates, and this yields convergence to the desired average velocity, $\bar{h}^*$.
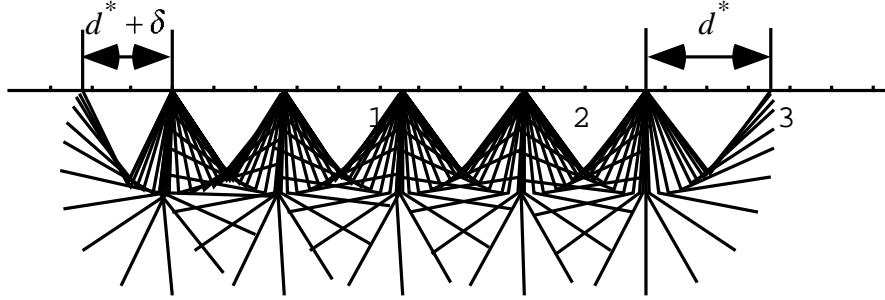
Figure 4.10: Brachiation along the bar with the initial condition (4.15) with $U(x) = 1 - \cos x$ for the target dynamics where $d^* = 0.6479$, $\omega = 4.0066$. Convergence of $d \to d^*$ is illustrated as the numerical swing map (Figure 4.7) indicates, and this yields convergence to the desired average velocity, $\bar{h}^*$.

4.2.1   A Control Strategy for Irregular Ladder Problem

This section presents a control strategy for the irregular ladder problem which extends the ideas discussed in the previous chapters. Here, we consider brachiation on a ladder with irregularly spaced rungs placed at the same height as depicted in Figure 4.11. Using the target dynamics, a single task level parameter, ω, in the controller characterizes the full range of the swing motion of the robot. Now, we seek the tuning rule for ω which locates the desired orbit from $C_-(d[k])$ to $C_+(d[k+1])$.

Define a new function

$$\tilde{\lambda} : [0, 2l] \times [0, 2l] \to I\!R \tag{4.16}$$

to solve the implicit function in ω by (4.13):

$$\tilde{\lambda}(d_1, d_2) := \text{solve}_{\omega \in I\!R}[d_2 - \sigma_\omega(d_1) = 0], \tag{4.17}$$

where d_1 and d_2 are the intervals between the bars of the left branch and the right branch respectively. This function is computed numerically and involves integrating the Lagrangian
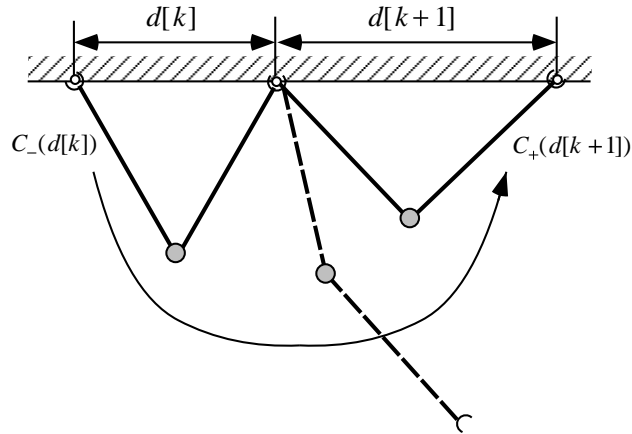
Figure 4.11: The irregular ladder problem. The robot moves from the left branch to the right branch with the intervals $d[k]$ and $d[k+1]$.

dynamics as in (4.12). In practice, we find that $\tilde{\lambda}$ is well defined only on a subset $\mathcal{D} \subseteq [0, 2l]$ whose extent depends upon the dynamical parameters of the robot as

$$\omega = \tilde{\lambda}(d[k], d[k+1]) : \mathcal{D} \times \mathcal{D} \to I\!\!R, \tag{4.18}$$

where $\mathcal{D} \subseteq [0, 2l]$. We plot in Figure 4.12 a particular instance of $\tilde{\lambda}$ for the case where the robot parameters are as specified in Table 2.1. The target dynamics controller is tuned according to this mapping to locate the orbit which achieves the desired gait of locomotion. Note that the mapping, $\omega = \lambda(d^*)$, in (3.20) is the intersection of the surface, $\tilde{\lambda}$, and the plane $d[k] - d[k+1] = 0$.
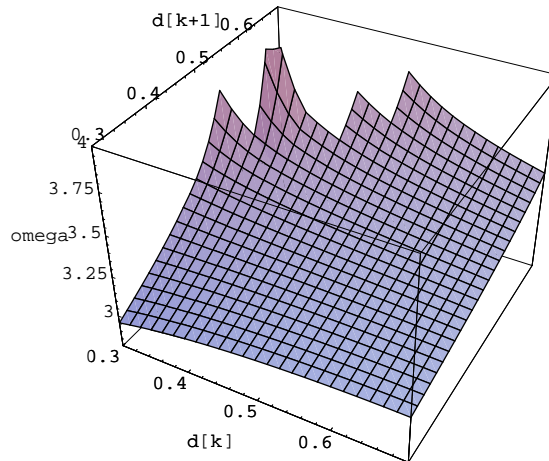
Figure 4.12: Numerical approximation of $\omega = \tilde{\lambda}(d[k], d[k+1])$. Target dynamics controller, τ_ω, is tuned according to this mapping, $\tilde{\lambda}$, that is designed to locate the desired orbit.

Figure 4.13: The simulation results ($d[k] = 0.4, d[k + 1] = 0.6$). Top: Movement of the robot. Left: Joint trajectories (solid: θ_1, dashed: θ_2) , Right: Voltage command to the motor driver.

4.2.2   Simulation

Consider the following three cases of the intervals between the bars as specified in Table 4.1. The initial condition of the robot is $Tq_0 = [c_-(d[k])^T, 0, 0]$. From the numerical solution to the mapping (4.18) depicted in Figure 4.12, ω is tuned for each case as shown in Table 4.1.

Case	$d[k]$	$d[k + 1]$	ω
1	0.4	0.6	3.66
2	0.5	0.6	3.47
3	0.6	0.5	3.255

Table 4.1: Intervals between the bars and ω considered in numerical simulation and experiments.

In the following simulations, we use the lossy model with the dynamical parameter as specified in Table 2.1. Note that discontinuity of the voltage command observed in Figures 4.13 and 4.14 results from the coulomb friction terms added in the controller. These simulation results suggest the effectiveness of the proposed strategy.

Case 1: $d[k] = 0.4, d[k + 1] = 0.6$ Figure 4.13 shows the movement of the robot, the joint trajectories and the voltage command to the motor driver.

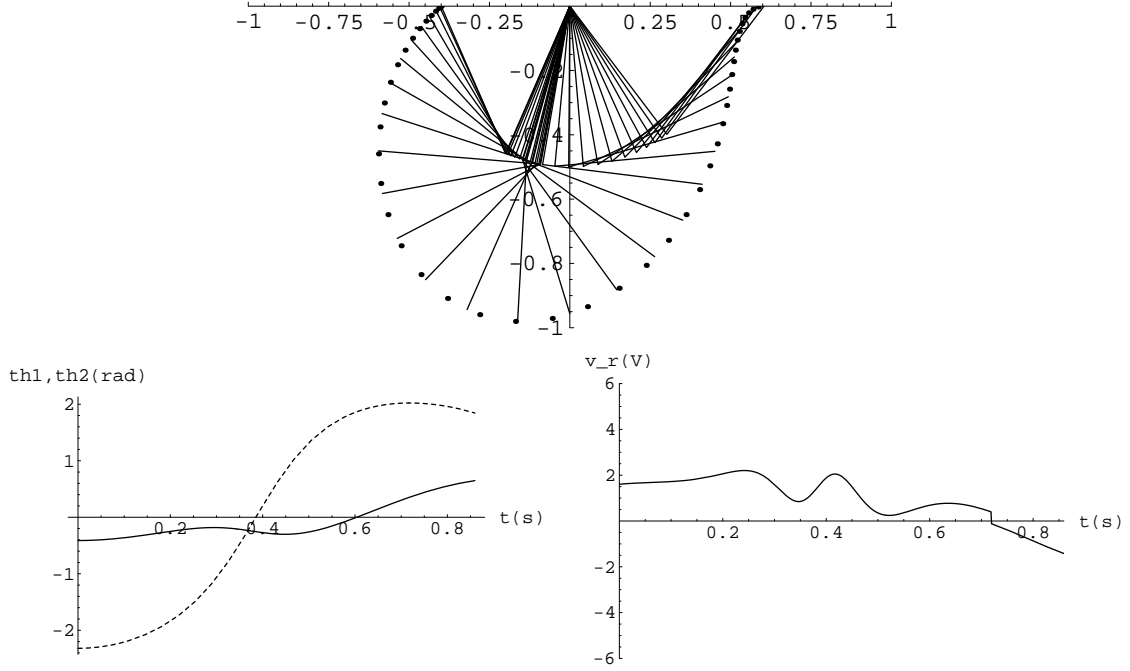**Figure 4.14**: The simulation results $(d[k] = 0.5, d[k + 1] = 0.6)$. Top: Movement of the robot. Left: Joint trajectories, (solid: θ_1, dashed: θ_2), Right: Voltage command to the motor driver.

Case 2: $d[k] = 0.5, d[k + 1] = 0.6$ Figure 4.14 shows the movement of the robot, the joint trajectories and the voltage command to the motor driver.

Case 3: $d[k] = 0.6, d[k + 1] = 0.5$ Figure 4.15 shows the movement of the robot, the joint trajectories and the voltage command to the motor driver.

4.3 Summary

This chapter is summarized as follows:

- This chapter first discussed the rope problem: brachiation along a continuum of handholds— a rope or a branch. We considered the regulation of horizontal velocity using the target dynamics method. An associated numerical "swing map" indicates that we can achieve good local regulation of forward velocity through this method.

- Then, we addressed the irregular ladder problem considering the task of brachiation on a ladder with irregular intervals. We proposed a control strategy extending the results on the rope problem seeking the tuning rule for ω which locates the desired asymmetric orbit to achieve the task.
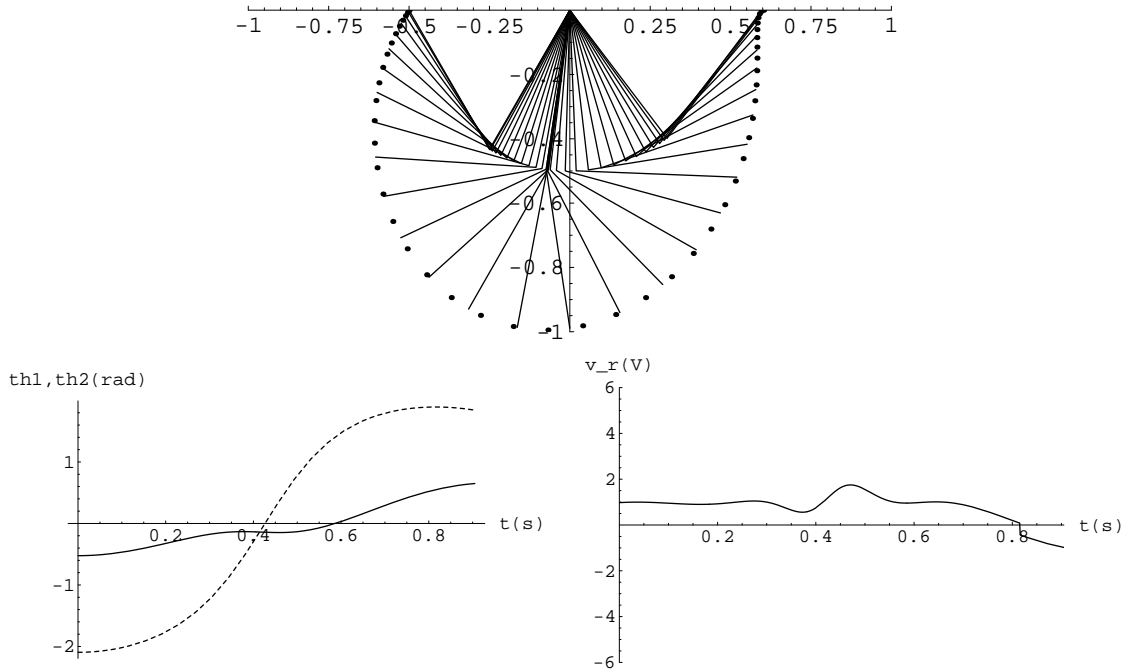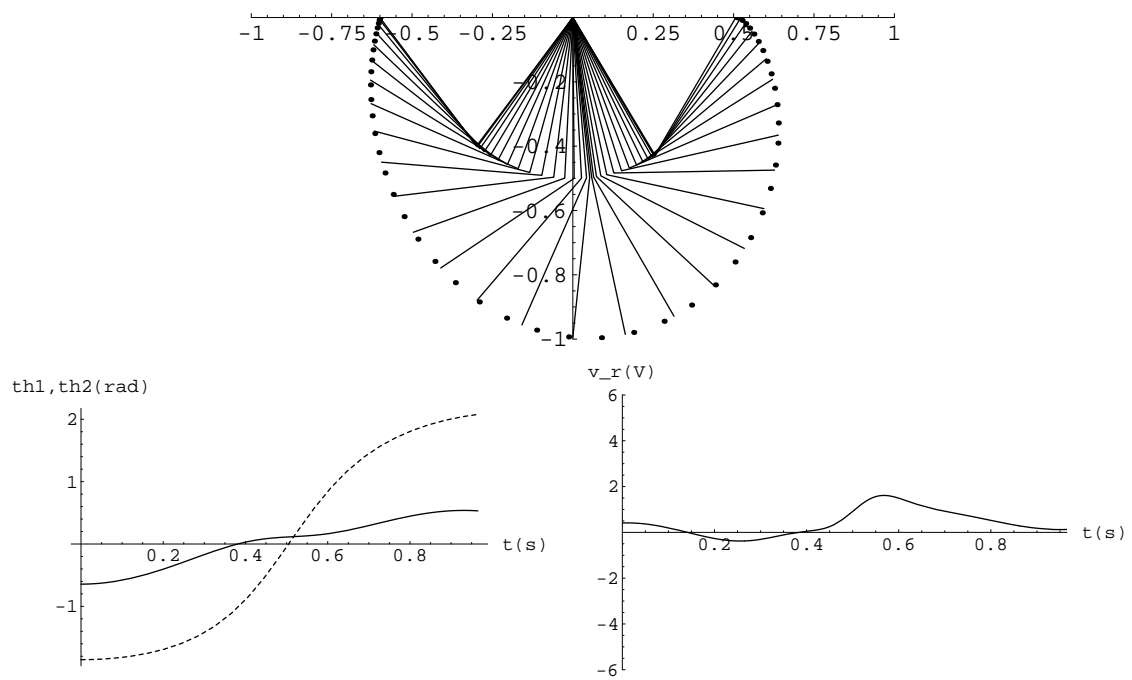
Figure 4.15: The simulation results ($d[k] = 0.6, d[k + 1] = 0.5$). Top: Movement of the robot. Left: Joint trajectories, (solid: θ_1, dashed: θ_2), Right: Voltage command to the motor driver.

Chapter 5

Hybrid Swing up Controller

In Section 3.2, we have proposed a control algorithm to achieve swing up from a suspended posture with one hand grip to the target bar with two hand grip based on the target dynamics method. However, a number of formal questions remain to be addressed, such as stability of the system and sensitivity to initial conditions in the swing up problem. In this chapter, we address certain issues that the previous controller design did not consider. We introduce a "hybrid" controller for the swing up problem, in which the target dynamics controller and a mechanical energy regulator are combined in a suitable fashion.

The proposed hybrid controller achieves good regulation of the desired behavior even from various initial conditions while the original target dynamics controller is quite sensitive to initial states. It also guarantees total energy boundedness, which implies that the mechanical energy of the system will not grow beyond a certain level. We consider that these features—good regulation of swing motion and mechanical energy, and a safety net—to be essential for our further investigation of robot brachiation such as the "leap" problem which we will explore in Chapter 6. Numerical studies as well as the experimental results presented in Section 7.5 suggest that the proposed strategy successfully improve the performance of the swing up behavior of the robot.

5.1   A Hybrid Controller

The swing up task can be achieved by the modified target dynamics (3.22), introducing the desired limit cycle to the target variable, θ, as discussed in Section 3.2. To accomplish this task, we need not only to pump up the energy, but also to control the position of the arm at the capture of the next bar.

As we have discussed in Section 3.2, the procedure for choosing the pseudo energy gain, K_e, defined in (3.22) is somewhat ad hoc. Some experience is helpful in determining the proper choice of K_e for a given initial condition. Since we have found that large K_e yields "chaotic" motion, we prefer to choose K_e small, which achieves the desired neutral orbit but with relatively slow energy pumping. Numerical studies suggest that some particular choices of larger K_e may result in robot trajectories which go through the next bar's position after a few of swings. Such motion allows for faster swing up times, as long as the robot catches the bar when the gripper's position coincides with that of the target bar. However, numerical simulations show that fast swing up behavior is quite sensitive to initial conditions.

Typically, in the fast swing up "chaotic" motion in the swing behavior is observed even after the pseudo energy converges to the desired level if we let the robot keep swinging without grasping the bar at that time. We also observe that the mechanical energy of the system behaves in an undesirable manner when "chaotic" motion stimulated by an overly large choice of K_e or wrong choice of ω even while the pseudo energy is well regulated. Thus, we find it useful to consider not only the pseudo energy (which has the nice property of being constant during the desired motion with respect to the target variable, θ) but also the mechanical energy which regulates the unactuated portion of the system.

In this section, we introduce a "hybrid" controller based on a new idea of combining the target dynamics and mechanical energy control in a suitable fashion. We successfully improve the performance of the swing up controller respecting insensitivity to initial conditions and mechanical energy boundedness. Numerical simulations suggest that good regulation of the desired swing motion can be achieved even when the robot starts from various initial conditions under the proposed hybrid controller. The proposed controller ensures the boundedness of the total energy. We suspect but not have yet proven that the desired orbit is also asymptotically stable—simulations to date bear out that suspicion.

5.1.1   Energy Regulation of Lagrangian Systems

The total mechanical energy of Lagrangian mechanical systems in the form

$$M(q)\ddot{q} + B(q,\dot{q}) + k(q) = \tau \tag{5.1}$$

is given by

$$E = \frac{1}{2}\dot{q}^T M(q)\dot{q} + U_g(q) \tag{5.2}$$

where $U_g(q)$ denotes the gravitational potential. The time derivative of the mechanical energy along the motion is calculated as

$$\dot{E} = \dot{q}^T \tau \tag{5.3}$$

using the skew-symmetric property in the Coriolis term [35].

For the particular example of our two-link brachiating robot, this relationship reduces to

$$\dot{E} = \dot{\theta}_2 \tau. \tag{5.4}$$

Supposing we choose the control law,

$$\tau := \tau_{E^*} = -K_{e2}(E - E^*)\dot{\theta}_2 \tag{5.5}$$

where K_{e2} is a positive constant and E^* is the desired mechanical energy level, then we have

$$\dot{E} = -K_{e2}(E - E^*)\dot{\theta}_2{}^2, \tag{5.6}$$

which implies that the energy regulation around the desired level can be achieved by this control law.

5.1.2   Hybrid Target Dynamics Controller

Consider the hybrid controller in which the original target dynamics swing up controller and the mechanical energy regulator are combined in the following way:

$$
\tau = \begin{cases}
\tau_{\bar{E}^*}(q, \dot{q}) & \text{if } E < E^* \\
\tau_{\bar{E}^*}(q, \dot{q}) + \tau_{E^*}(q, \dot{q}) & \text{if } E^* \le E < E_{max1} \\
(1-\rho)[\tau_{\bar{E}^*}(q, \dot{q}) + \tau_{E^*}(q, \dot{q})] - \rho K_{e3}\dot{\theta}_2 & \text{if } E_{max1} \le E < E_{max2} \\
-K_{e3}\dot{\theta}_2 & \text{if } E_{max2} \le E
\end{cases}
\tag{5.7}
$$

where

$$
\rho(E) = \frac{E - E_{max1}}{E_{max2} - E_{max1}},
\tag{5.8}
$$

$\tau_{\bar{E}^*}(q, \dot{q})$ is the original swing up controller (3.23) with the choice of the virtual spring potential in the target dynamics, $U(x) = \frac{1}{2}x^2$, τ_{E^*} is the mechanical energy regulator defined in (5.5) around the desired energy level, E^*. K_{e2} and K_{e3} are some positive gains, and E is the mechanical energy of the system defined in (5.2). This switching law is introduced based on our physical intuition that regulating the mechanical energy of the system as well as the pseudo energy in a suitable fashion may be useful for controlling the unactuated portion of the system.

The first equation regulates the swing motion of the robot through the original target dynamics controller. However, if the mechanical energy of the system exceeds the desired level, E^*, then it is refined during the swing motion according to the second equation. The third equation is introduced to obtain a continuous switching from the energy refinement controller to the energy regulator interpolating between them. The fourth equation acts as a "safety net." Consider the time derivative of the mechanical energy along the motion under this controller,

$$
\dot{E} = -K_{e3}\dot{\theta}_2{}^2.
\tag{5.9}
$$

This implies that the total energy is bounded. Note that the overall switching scheme in (5.7) is not smooth, but does not introduce discontinuity in the torque command.

5.2   Simulation

In this section, we present numerical simulations to suggest the effectiveness of the hybrid controller. As we have pointed out, the original swing up controller is quite sensitive to initial conditions when the robot swings up from the bottom state. Small deviation may result in undesirable orbit particularly when the pseudo energy gain is large. Under these circumstances, we first demonstrate insensitivity to initial conditions of the hybrid controller to achieve the desired orbit. Then, we show the energy boundedness feature of the hybrid controller. Lastly, we present simulations in achieving the desired neutral orbits with small amplitude taking the actuator's limitation into account for the experimental implementation of the hybrid controller on the physical robot presented in Section 7.5.

Numerical simulations illustrate the effectiveness of the proposed controller in comparison to the original swing up controller. In the following simulations, we use the lossless model of the robot with the dynamical parameters specified in Table 2.1 where $b_i, c_i \to 0$.
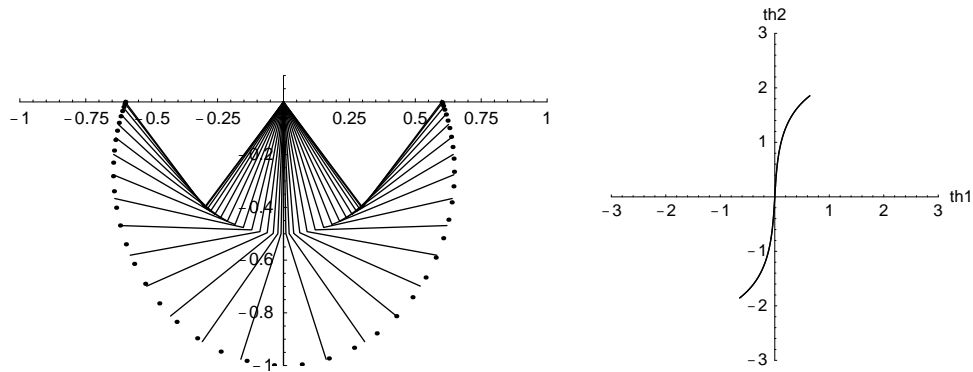
Figure 5.1: Left: Motion of the robot in the ladder problem achieving a neutral orbit, where $d = 0.6, \omega = 3.3649$. Right: The corresponding trajectorie of the motion of the robot on the (θ_1, θ_2) plane.
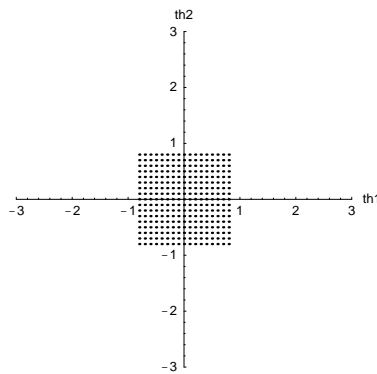
Figure 5.2: Initial conditions projected on the (θ_1, θ_2) plane. We take $17 \times 17 \times 3 \times 3 = 2601$ initial conditions on a grid in the hyper rectangular neighborhood of the origin from -0.8 to 0.8 rad in the joint angles and from -0.1 to 0.1 rad/s in the angular velocities with the interval of 0.1 respectively.

5.2.1 Insensitivity to Initial Conditions

In this section, we present a numerical study suggesting that hybrid controller can indeed achieve the task of swinging up to the ceiling and catching the target bar from variety of initial conditions. Consider the task of achieving the desired neutral orbit depicted in Figure 5.1 swinging up from various initial conditions near bottom state such that the robot reaches the target bar located at the distance of $d^* = 0.6$ in the ceiling. For this setting, the virtual frequency, ω, is chosen as $\omega = 3.3649$ which locates the desired neutral orbit in the ladder problem for the lossless model of the robot. The desired pseudo energy, $\bar{E}^*$, is chosen as $\bar{E}^* = \frac{1}{2}\omega^2 \left(\frac{\pi}{2}\right)^2$ so that the gripper reaches the height of the bar. The pseudo energy gain, K_e, is chosen empirically in our numerical experience as $K_e = 0.7$. These parameters are common to both the original target dynamics and the hybrid controller. The additional parameters for the hybrid controller are chosen as follows: The desired mechanical energy, E^*, is set to be $E^* = U_g \circ c(d^*) = -12.9254$, where $U_g(q)$ is the potential energy of the system and $c(d)$ denotes the "ceiling" parameterized by the distance between the grippers, d, as defined in (3.10). The energy gains, K_{e2} in (5.5) and K_{e3} in (5.7), are chosen empirically in our numerical experience as $K_{e2} = 2.3$ and $K_{e3} = 2.0$ respectively. The values for E_{max1} and E_{max2} introducing the upper bound of the total mechanical energy are chosen as $E_{max1} = E^* + 5.0$ and $E_{max2} = E^* + 10.0$.

In order to evaluate sensitivity to initial conditions, we consider time sampled trajectories originating from various initial conditions. In the following numerical simulation, we take $17 \times 17 \times 3 \times 3 = 2601$ initial conditions on a grid in the hyper rectangular neighborhood of the origin from -0.8 to 0.8 rad in the joint angles and from -0.1 to 0.1 rad/s in the angular velocities with the interval of 0.1 respectively as depicted in Figure 5.2.

Figure 5.3 depicts the evolution of the trajectories under the hybrid controller from the specified initial conditions above. This result suggests asymptotic convergence to the desired neutral orbit which achieves the desired locomotion shown in Figure 5.1. In contrast, Figure 5.4 depicts the growth of the trajectories under the original swing up controller starting from the same initial conditions, which shows divergence from the initial conditions. In Figures 5.5 and 5.6, we show the typical movement of the robot and joint trajectories of the corresponding simulations shown above respectively. The task can be successfully achieved under the hybrid controller. As the numerical simulations illustrate, we achieve good regulation of the swing motion of the robot, which suggests the desired orbit itself is also asymptotically stable (although we have yet to show this mathematically). Notwithstanding the favorable numerical results, it is not still clear how to choose suitable gains for the controller. Further mathematical analysis will be required to truly understand the properties of the hybrid controller.

5.2.2 Total Energy Boundedness

We have observed that the large ω calls for unrealistically high torque and the motion of the robot sometimes becomes "wild." In this section, we illustrate the energy boundedness feature of the proposed hybrid controller.

Figures 5.7 and 5.8 show the motion of the robot and its mechanical energy when $\omega = 4.5$ instead of the correct value, $\omega^* = 3.3649$. $K_e = 0.7$ is chosen for both controllers. For the hybrid controller, the additional parameters, $K_{e2} = 2.5$, $K_{e3} = 2.0$, $E_{max1} = E^* + 5.0 = -7.9254$ and $E_{max2} = E^* + 10.0 = -2.9254$ are chosen to introduce the upper bound of the system's total energy. The results show that the original controller yields very "wild" motion with large
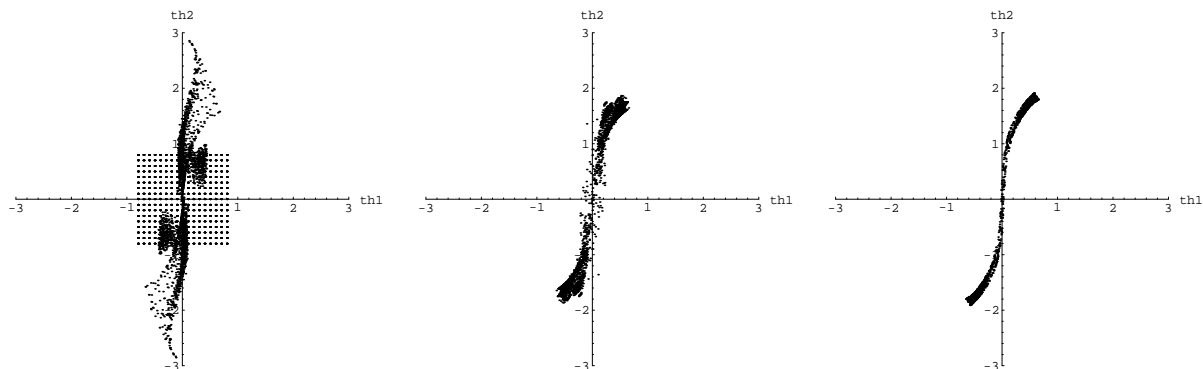
Figure 5.3: Time sampled trajectories in the (θ_1, θ_2) plane under the hybrid controller. Left: at $t = 0$ and $t = 4$, middle: at $t = 9$, right: at $t = 23$. These points show the evolution of the 2601 initial conditions along the motion of the system. This numerical evidence suggests convergence to a near-neutral orbit shown in Figure 5.1.
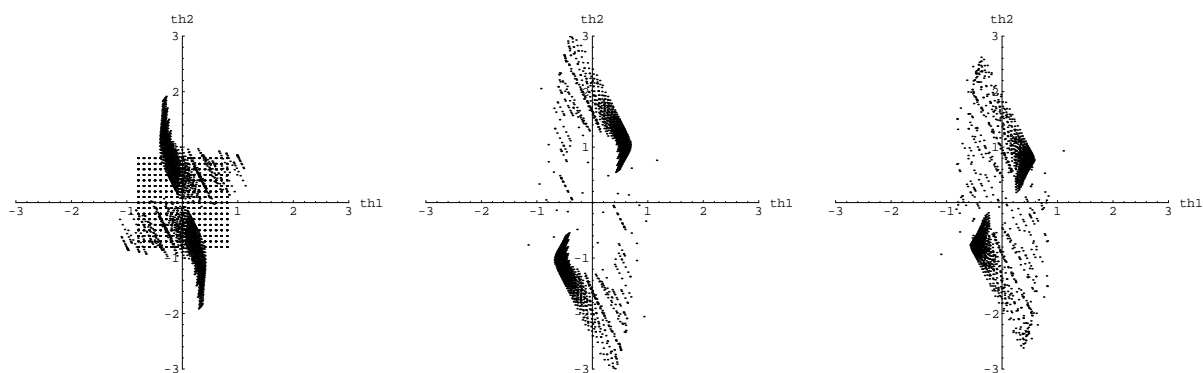
Figure 5.4: Time sampled trajectories in the (θ_1, θ_2) plane under the original swing up controller. Left: at $t = 0$ and $t = 4$, middle: at $t = 8$, right: $t = 21$. These points show the evolution of the 2601 initial conditions along the motion of the system. These results show that the trajectories do not converge to the desired neutral orbit.
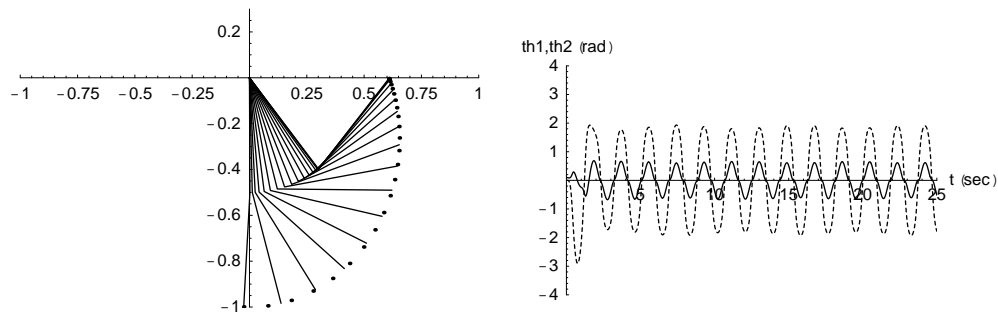
Figure 5.5: Typical movement of the well regulated swing motion under the hybrid controller, where initial condition is $Tq_0 = [0.1, 0, 0, 0]^T$. Left: motion of the robot at the capture of the bar at $d^* = 0.6$, when $t = 20 \sim 20.5$. Right: Joint trajectories (solid: θ_1, dashed: θ_2).

Figure 5.6: Typical "chaotic" motion under the original controller, where initial condition is $Tq_0 = [0.1, 0, 0, 0]^T$. Left: motion of the robot, when $t = 10 \sim 15$. Right: Joint trajectories (solid: θ_1, dashed: θ_2).

mechanical energy as shown in Figure 5.7, however, the hybrid controller indeed bounds the total energy of the system as depicted in Figure 5.8.

Figure 5.7: Top: Joint trajectories (solid: θ_1, dashed: θ_2), Bottom: pseudo energy (dashed), and mechanical energy (solid) under the original swing up controller with the "wrong" choice of $\omega = 4.5$. Note that "wild" motion is observed driven by unrealistically high torque in this case.
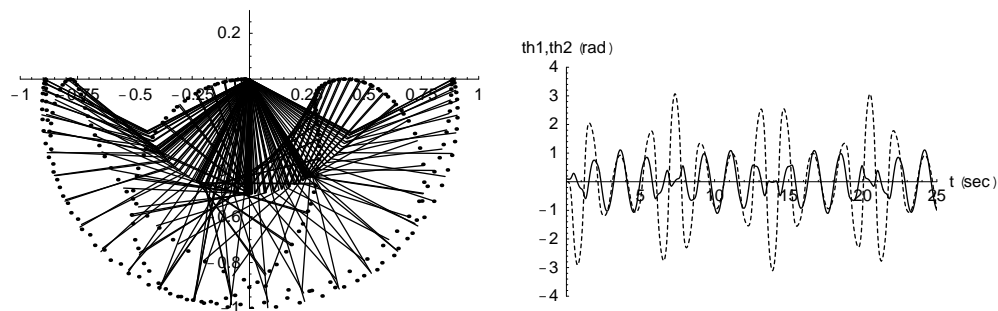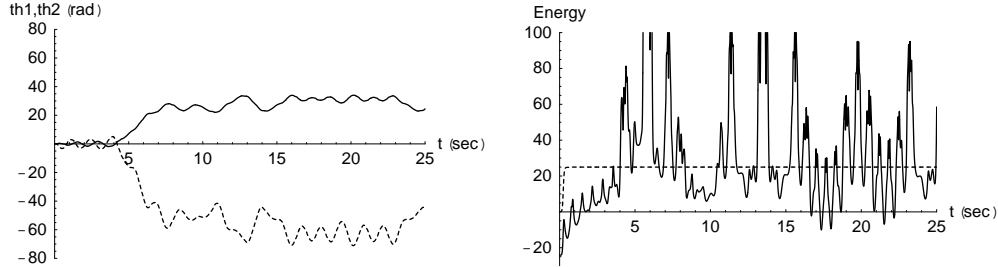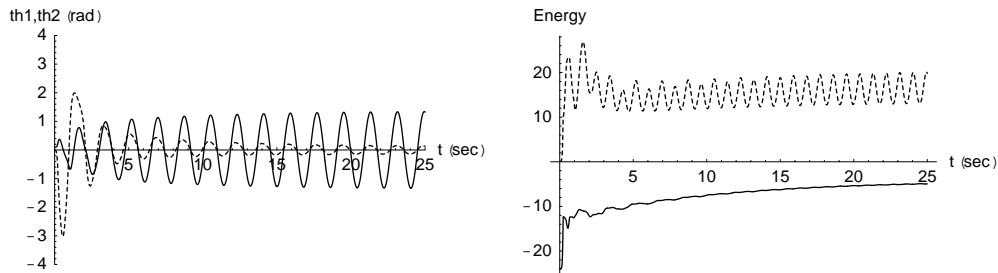
Figure 5.8: Joint trajectories (top, solid: θ_1, dashed: θ_2), Bottom: pseudo energy (dashed) and mechanical energy (solid) under the hybrid controller with the "wrong" choice of $\omega = 4.5$. In contrast, the total energy is bounded under the hybrid controller.

5.2.3   Simulations with Small Amplitude considering Experimental Implementation

In this section, we present numerical simulations in comparison to the experimental results of the implementation of the hybrid controller presented in Section 7.5. In our early attempts of the experimental implementation of the hybrid controller on the physical apparatus, we could not achieve the desired neutral orbit with the amplitude of $\theta^* = \frac{\pi}{2}$ swinging up to the "ceiling." In practice, this was largely due to the elbow actuator's torque limitation for such motions with the large desired amplitude. Therefore, we consider the desired neutral orbit with smaller amplitude originating in the "virtual ceiling" which is defined to be those configurations where the the angle of the virtual pendulum,θ, arising from the change of coordinates (2.10) reaches the specified amplitude of our interest, θ^*, as depicted in Figure 5.9. This "virtual ceiling" is parametrized by θ^* and d similar to the manner where the original ceiling is parametrized by d as discussed in Section 3.1.2. In the following simulations, we consider two cases, $\theta^* = \frac{\pi}{4}, d^* = 0.8$ and

Figure 5.9: The desired neutral orbit of the robot with small amplitude originating in the "virtual ceiling" parametrized by θ and d^*.

$\theta^* = \frac{\pi}{3}, d^* = 0.7$. The initial condition of the robot is $Tq_0 = [\, 0, \ 0, \ 0, \ 0.2 \,]^T$.
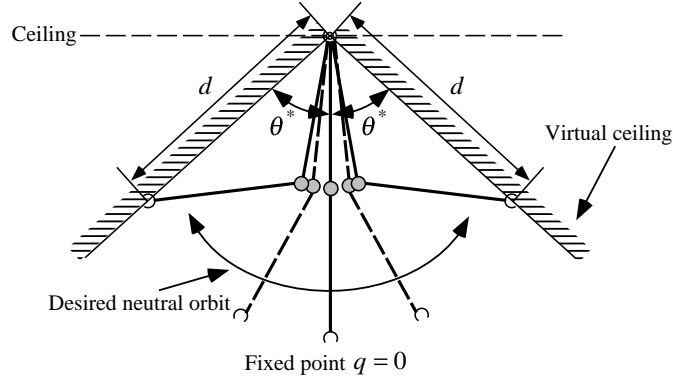
Case 1: $\theta^* = \frac{\pi}{4}, d^* = 0.8$ In this case, we use $\omega = 3.335$ which locates a neutral orbit supposing the robot starts swinging from the "virtual ceiling" with zero velocity parametrized by θ^* and d^*. The pseudo energy in the target dynamics is chosen as $\bar{E}^* = \frac{1}{2}\omega^2 \left(\frac{\pi}{4}\right)^2$ so that the robot achieves oscillation with the desired amplitude in θ. We choose to use the desired mechanical energy, $E^* = -20.51$, which corresponds to the potential energy of the system at the desired configuration of the robot in the "virtual ceiling." The energy gains are chosen empirically based on our experience in numerical simulations as $K_e = 10.0, K_{e2} = 20.0, K_{e3} = 2.0$.

Figure 5.10 shows a typical movement of the robot and Figure 5.11 shows joint trajectories and the voltage command to the motor driver under the hybrid controller. These results illustrate that the hybrid controller achieves good regulation of the desired swing behavior of the robot. In contrast, the original swing up controller yields "chaotic" behavior as depicted in Figures 5.12 and 5.13.

Case 2: $\theta^* = \frac{\pi}{3}, d^* = 0.7$ In this case, we use $\omega = 3.325$ which locates a neutral orbit supposing the robot starts swinging from the "virtual ceiling" with zero velocity parametrized by θ^* and d^*. The pseudo energy in the target dynamics is chosen as $\bar{E}^* = \frac{1}{2}\omega^2 \left(\frac{\pi}{3}\right)^2$ so that the robot achieves oscillation with the desired amplitude in θ. We choose to use the desired mechanical energy $E^* = -18.44$ which correspond to the potential energy of the system at the desired configuration of the robot in the "virtual ceiling." The energy gains are chosen empirically based on our experience in numerical simulations as $K_e = 20.0, K_{e2} = 20.0, K_{e3} = 2.0$.

Figure 5.14 shows a typical movement of the robot and Figure 5.15 shows joint trajectories and the voltage command to the motor driver under the hybrid controller. These results illustrate that the hybrid controller achieves good regulation of the desired swing behavior of the robot. In contrast, the original swing up controller yields "chaotic" behavior as depicted in Figures 5.16 and 5.17.

Figure 5.10: Typical movement of well regulated swing motion of the robot under the hybrid controller (simulation) from t=10 to t=15, where $\theta^* = \frac{\pi}{4}, d^* = 0.8$.

Figure 5.11: Simulation results of the hybrid controller, where $\theta^* = \frac{\pi}{4}, d^* = 0.8$. Left: Joint trajectories (solid: θ_1, dashed: θ_2), Right: Voltage command to the motor driver. Note that a near neutral orbit is achieved.

Figure 5.12: Typical movement of "chaotic" swing behavior of the robot under the original swing up controller controller (simulation) from t=10 to t=15, where $\theta^* = \frac{\pi}{4}, d^* = 0.8$.

Figure 5.13: Simulation results of "chaotic" behavior under the original swing up controller, where $\theta^* = \frac{\pi}{4}, d^* = 0.8$. Left: Joint trajectories (solid: θ_1, dashed: θ_2), Right: Voltage command to the motor driver.

5.3 Summary

This chapter is summarized as follows:

- We have introduced a hybrid controller combining the original target dynamics controller and the mechanical energy regulator.

- This hybrid controller guarantees boundedness of the total energy. Moreover, as the numerical simulations illustrate, we achieve good regulation of the swing motion of the robot, which suggests the desired orbit itself is also asymptotically stable (although we have yet to show this mathematically).

- Notwithstanding the favorable numerical results, it is not still clear how to choose suitable gains for the controller. Thus, further mathematical analysis will be required to truly understand the properties of the proposed controller.
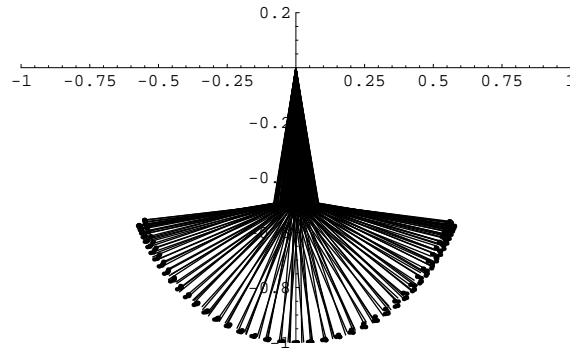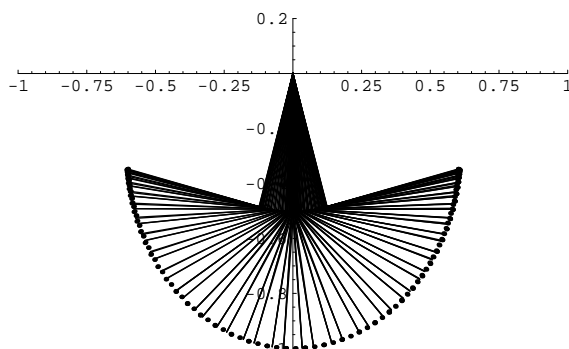
Figure 5.14: Typical movement of well regulated swing motion of the robot under the hybrid controller (simulation) from t=10 to t=15, where $\theta^* = \frac{\pi}{3}, d^* = 0.7$.
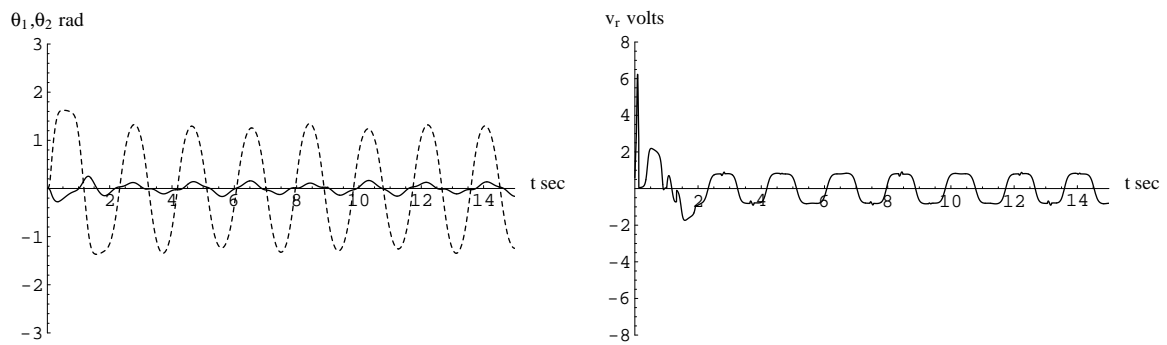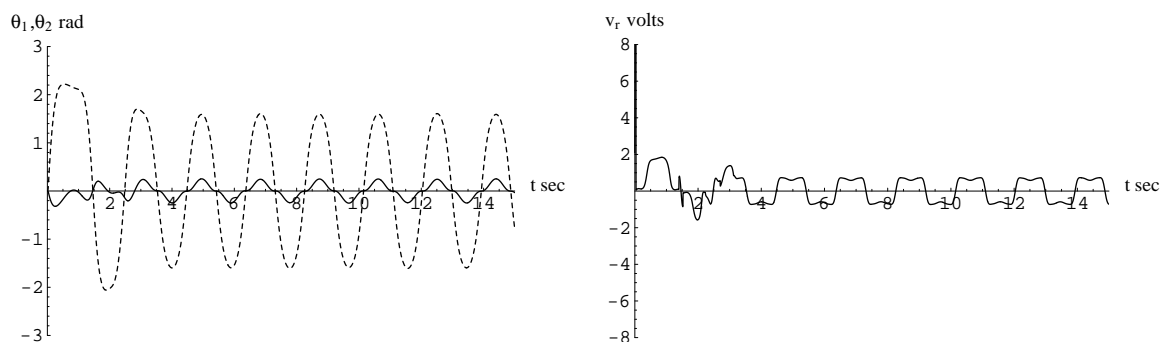

Figure 5.15: Simulation results of the hybrid controller, where $\theta^* = \frac{\pi}{3}, d^* = 0.7$. Left: Joint trajectories (solid: θ_1, dashed: θ_2), Right: Voltage command to the motor driver. Note that a near neutral orbit is achieved.
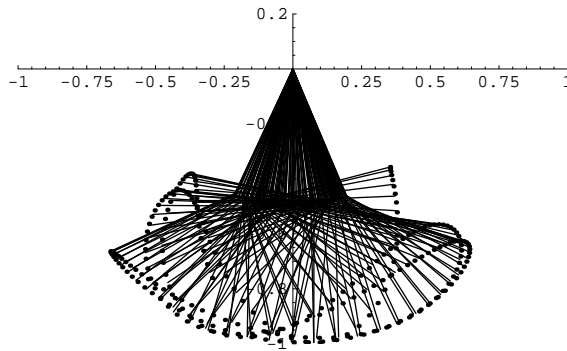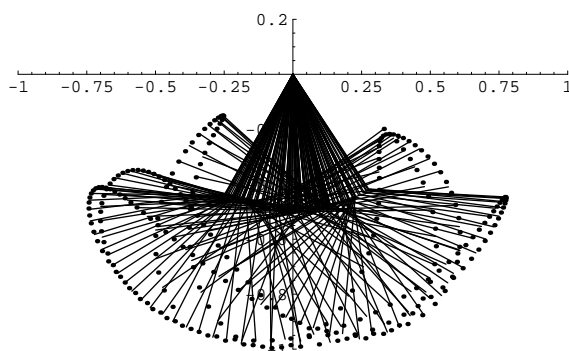

Figure 5.16: Typical movement of "chaotic" swing behavior of the robot under the original swing up controller controller (simulation) from t=10 to t=15, where $\theta^* = \frac{\pi}{3}, d^* = 0.7$.
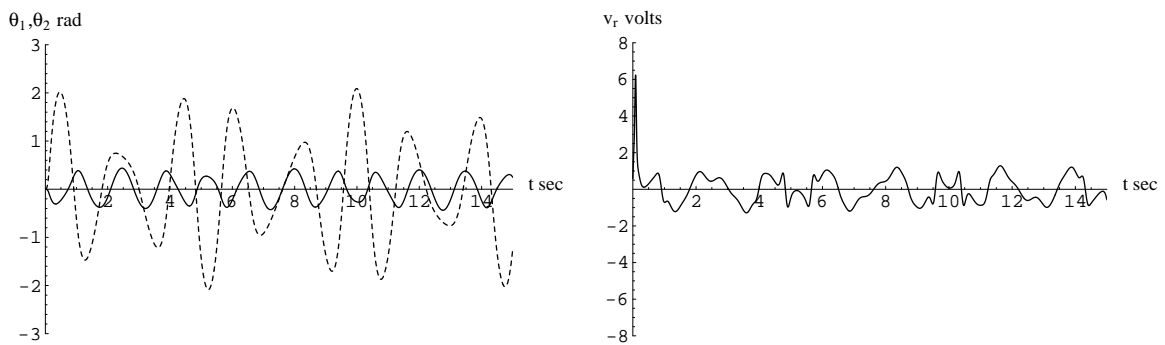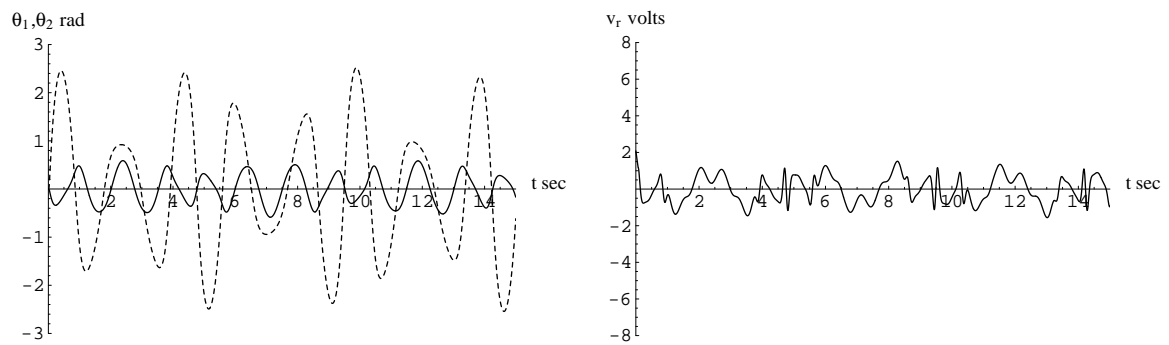
Figure 5.17: Simulation results of "chaotic" behavior under the original swing up controller, where $\theta^* = \frac{\pi}{3}, d^* = 0.7$. Left: Joint trajectories (solid: θ_1, dashed: θ_2), Right: Voltage command to the motor driver.

Chapter 6

Leap Problem

In this chapter, we present our preliminary studies on the leap problem arising from an ape's fast brachiation. The task considered here is to transfer from a handhold to the next which is far out of reach with a component of free flight. This is accomplished by swinging up from the suspended posture to gain enough velocity and energy for lift-off as well as controlling the posture of the robot to catch the target bar in the air. This problem seems analogous to a flip maneuver of a hopping robot [28], and also related to other problems of posture control of free flying systems [29, 49], space robots [48], gymnastic robots [79], and swing control of an underactuated manipulator addressing casting manipulation [6]. However, solving the leap problem seems to involve more task requirement than these problems. For instance, we need good regulation of a lift-off velocity and angular momentum in the swing phase to aim at the target bar. Furthermore, good control of posture and rotation of the body in the flight phase is necessary to catch the target bar in a very short period typically in a few of tenths of second. In Section 6.1, we consider the posture control problem of a simplified system in the flight phase equipped with a prismatic joint whose dynamics are much simpler than those of the two-link brachiating robot with a revolute joint. In Section 6.1, following the approach in [28], we first consider the simplest case assuming that the arm length can be changed instantaneously. Then, we consider the case where the arm length is changed at a fixed rate. In Sections 6.2 and 6.3, we propose a posture control strategy for the two-link brachiating robot in free flight following the preliminary studies of the simplified problems. Section 6.4 presents how the sequence of swing and flight motions are coordinated to achieve the desired maneuver. Numerical simulations presented in Section 6.5 suggest the effectiveness of the proposed strategy.

6.1   Preliminaries

6.1.1   Flight Dynamics of a Free-flying Planar n-link Kinematic Chain

Consider a free-flying planar n-link kinematic chain depicted in Figure 6.1 in the gravitational field. The equation of motion of the center of mass of the system is given by

$$\ddot{r}_c = \begin{bmatrix} 0 \\ -g \end{bmatrix} \tag{6.1}$$

Figure 6.1: Model of a free-flying planar n-link kinematic chain.

and the total angular momentum with respect to the center of mass of the system

$$H = \sum_{i=1}^{n} \{I_i \omega_i + \rho_{ci} \times m_i \dot{\rho}_{ci}\} = H_0 = const. \tag{6.2}$$

is conserved, where Σ_A is the inertial coordinate system, g is the gravitational constant, r_c is the position vector of the center of mass of the system from the origin Σ_A, r_{ci} is the position vector of the center of mass of each link from the origin Σ_A, ρ_{ci} is the position vector of the center of mass of each link from the center of the mass of the system, r_i is the position vector of the joint $i+1$, and ω_i is the angular velocity of each link. θ_i is the joint angle relative to the previous link, m_i and I_i is the mass and moment of inertia of each link, l_i is the link length, the center of mass of each link is located on the center line which passes through adjacent joints at a distance l_{ci}.

6.1.2 Simplified Pendulum with a Prismatic Joint

In this section, we discuss a control strategy in the flight phase for a simplified problem in order to gain insight into the development of the control strategy for the two-link brachiating robot.

Equation of Motion and Conservation of Angular Momentum

Consider a simplified pendulum with a prismatic joint with two point masses, $\frac{m}{2}$, located at the end of the massless link as depicted in Figure 6.2.

The equation of motion of the center of mass of the system is given by

$$\ddot{r}_c = \begin{bmatrix} 0 \\ -g \end{bmatrix} \tag{6.3}$$

and the conservation of angular momentum with respect to the center of mass of the system is reduced to

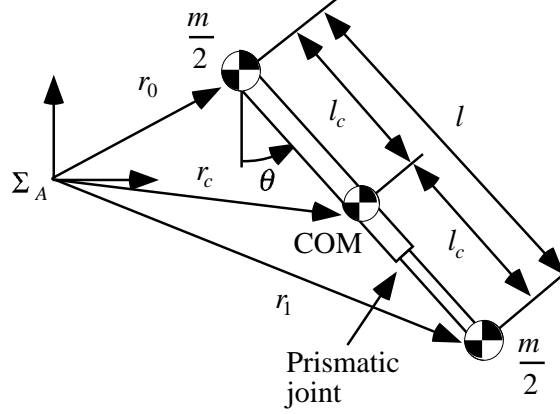$$H = ml_c^2 \dot{\theta} = H_0 = const. \tag{6.4}$$

Figure 6.2: Model of a simplified pendulum with a prismatic joint.

where m is the total mass of the system and the point mass, $\frac{m}{2}$, is located at the both ends of the link. l is the link length, and the center of mass of the system is located at a distance, $l_c = \frac{1}{2}l$. The body rotation during the flight from $t = t_0$ to $t = t_f$ is given by

$$\Delta\theta = \int_{t_0}^{t_f} \dot{\theta} dt = \int_{t_0}^{t_f} \frac{H_0}{ml_c^2} dt \tag{6.5}$$

arising from (6.4).

Development of Control Strategy in Flight Phase for RP System

Figure 6.3 shows a leaping maneuver of the simplified pendulum system with a prismatic joint depicted in Figure 6.2 in the flight phase. Given the interval between the bars, d, we consider that the lift-off condition and the control of body rotation are the key to the success of the desired maneuver. The lift-off condition is important since it determines the trajectory of the center of mass, and the angular momentum cannot be changed once in airborne. The body rotation during the flight needs to be synchronized with catching configuration of the robot by changing the arm length to control the angular velocity of the body.

Suppose the robot releases the bar at $t = 0$ with the lift-off condition $\theta(0) = \theta_0, \dot{\theta}(0) = \dot{\theta}_0$, $l_c(0) = l_{c0}$ and $\dot{l}_c(0) = 0$. The initial position and velocity of the center of mass are given by

$$r_{c0} = \begin{bmatrix} l_{c0}\sin\theta_0 \\ -l_{c0}\cos\theta_0 \end{bmatrix} \text{ and } v_{c0} = \dot{r}_{c0} = \begin{bmatrix} l_{c0}\cos\theta_0\dot{\theta}_0 \\ l_{c0}\sin\theta_0\dot{\theta}_0 \end{bmatrix} \tag{6.6}$$

respectively. Thus, by integrating (6.3), the trajectory of the center of mass is given by

$$r_c(t) = \begin{bmatrix} v_{c0x}t + r_{c0x} \\ -\frac{1}{2}gt^2 + v_{c0y}t + r_{c0y} \end{bmatrix} \tag{6.7}$$

and the initial angular momentum is $H_0 = ml_{c0}\dot{\theta}_0$.

We choose a candidate of the configuration of the robot at the grasp of the bar at $t = t_f$ which is the symmetric posture of the initial configuration about the axis $x = \frac{1}{2}d$ as shown in
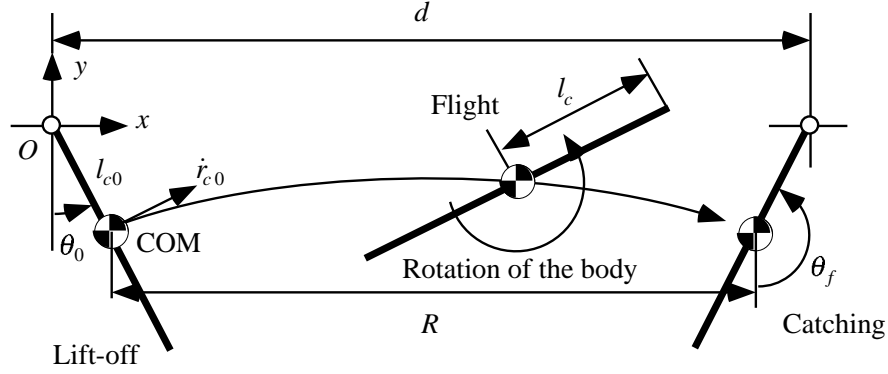
Figure 6.3: A leaping maneuver of the simplified system in the flight phase.

Figure 6.3 for simplicity. Namely, the final body angle, θ_f, and the range of the center of mass during the flight, R, are

$$\theta_f = \pi - \theta_0 \tag{6.8}$$

$$R = d - 2l_{c0} \sin \theta_0 \tag{6.9}$$

respectively. To synchronize the body rotation with catching, we equate the relationship of the position of the center of mass, (6.7) and (6.9), and the required rotation of the body, (6.5) and (6.8), at $t = t_f$ starting from $t_0 = 0$.

$$r_c(t_f) = \begin{bmatrix} v_{c0x} t_f + r_{c0x} \\ -\frac{1}{2} g t_f^2 + v_{c0y} t_f + r_{c0y} \end{bmatrix} = \begin{bmatrix} d - 2l_{c0} \sin \theta_0 \\ r_{c0y} \end{bmatrix} \tag{6.10}$$

$$\Delta\theta = \int_0^{t_f} \frac{H_0}{ml_c^2} dt = \theta_f - \theta_0 = \pi - 2\theta_0 \tag{6.11}$$

From (6.10), we have

$$t_f = \frac{2v_{c0y}}{g} = \frac{2l_{c0}\dot{\theta}_0 \sin \theta_0}{g} \tag{6.12}$$

and

$$\dot{\theta}_0^2 = \frac{g(d - 2l_{c0} \sin \theta_0)}{l_{c0}^2 \sin 2\theta_0}. \tag{6.13}$$

In the following sections, we present how these values are determined which satisfy (6.10) and (6.11) simultaneously to achieve successful a leaping maneuver when the interval between the bars, d, is given.

The Simplest Case

Suppose the arm length can be changed instantaneously from l_{c0} to l_c just after lift-off and back to l_{c0} instantaneously as well just before the grasp, and l_c is fixed during the flight. With this assumption, the angular velocity during the flight $\dot{\theta} = H_0/(ml_c^2)$ is constant and (6.11) is simplified to

$$\Delta\theta = \frac{H_0}{ml_c^2} t_f = \pi - 2\theta_0. \tag{6.14}$$

Thus, for given d, l_{c0} and θ_0, we can determine the state of the system during the flight by solving this equation for l_c with the substitution of (6.12), (6.13) and $H_0 = ml_{c0}{}^2$

$$l_c = \sqrt{\frac{l_{c0}(d - 2l_{c0}\sin\theta_0)}{(\pi - 2\theta_0)\cos\theta_0}} \tag{6.15}$$

and the initial angular velocity is determined by (6.13) as

$$\dot{\theta}_0 = \sqrt{\frac{g(d - 2l_{c0}\sin\theta_0)}{l_{c0}{}^2\sin 2\theta_0}}. \tag{6.16}$$

Changing Arm Length with a Fixed Rate

A simplified strategy presented above assumes instantaneous change of arm length and it is kept constant in the air so that the body rotates with the fixed angular velocity. In this section, we consider the case where the arm length is changed at a fixed rate motivated by the assumption in the study of a flip maneuver of a hopping robot [28] of lengthening the leg with a fixed rate in the flight.

Suppose we change the arm length from l_{c0} with a fixed rate, $\dot{l}_{ck}$, during the flight phase from $t = 0$ to $t = t_f$ as

$$l_c(t) = \dot{l}_{ck}t + l_{c0} \tag{6.17}$$

then (6.11) can be integrated in closed form as

$$\Delta\theta = \int_0^{t_f} \frac{H_0}{ml_c{}^2}dt = \int_0^{t_f} \frac{H_0}{m(\dot{l}_{ck}t + l_{c0})^2}dt = \left. -\frac{H_0}{\dot{l}_{ck}m(\dot{l}_{ck}t + l_{c0})} \right|_0^{t_f}. \tag{6.18}$$

Now we design a piecewise linear trajectory for the arm length, $l_c(t)$, as shown in Figure 6.4 during the flight. Namely,

$$l_c(t) = \begin{cases} \dot{l}_{ck}t + l_{c0} & 0 \leq t < t_1 \\ l_{c\max} = const. & t_1 \leq t < t_2 \\ -\dot{l}_{ck}(t - t_f) + l_{c0} & t_2 \leq t \leq t_f \end{cases} \tag{6.19}$$

where $t_f - t_2 = t_1$ and $\dot{l}_{ck} = (l_{c\max} - l_{c0})/t_1 = (l_{c\max} - l_{c0})/(t_f - t_2)$. Then, the total rotation of the body in the flight phase (6.11) in this problem setting can be integrated in closed form as we have discussed above

$$\begin{aligned} \Delta\theta &= \Delta\theta_1 + \Delta\theta_2 + \Delta\theta_3 \\ &= \int_0^{t_1} \frac{H_0}{m(\dot{l}_{ck}t + l_{c0})^2}dt + \int_{t_1}^{t_2} \frac{H_0}{ml_{c\max}{}^2}dt + \int_{t_2}^{t_f} \frac{H_0}{m[-\dot{l}_{ck}(t - t_f) + l_{c0}]^2}dt \\ &= \left. -\frac{H_0}{\dot{l}_{ck}m(\dot{l}_{ck}t + l_{c0})} \right|_0^{t_1} + \left. \frac{H_0\,t}{ml_{c\max}{}^2} \right|_{t_2}^{t_1} - \left. \frac{H_0}{\dot{l}_{ck}m(\dot{l}_{ck}t + l_{c0})} \right|_{t_2}^{t_f} \\ &= \theta_f - \theta_0 = \pi - 2\theta_0. \end{aligned} \tag{6.20}$$

Now, given d, θ_0 and l_{c0}, and if we choose some $t_1 = t_f - t_2$ such that $0 < t_1 < \frac{t_f}{2}$, we can solve (6.20) for $l_{c\max}$ substituting (6.12) in order to determine how the arm length should be changed during the flight to adjust the rotation of the body. And the initial angular velocity, $\dot{\theta}_0$, in (6.16) can be determined. This flight strategy for a simplified system is applied to the contol of the two-link brachiating robot in the air with a slight modification.
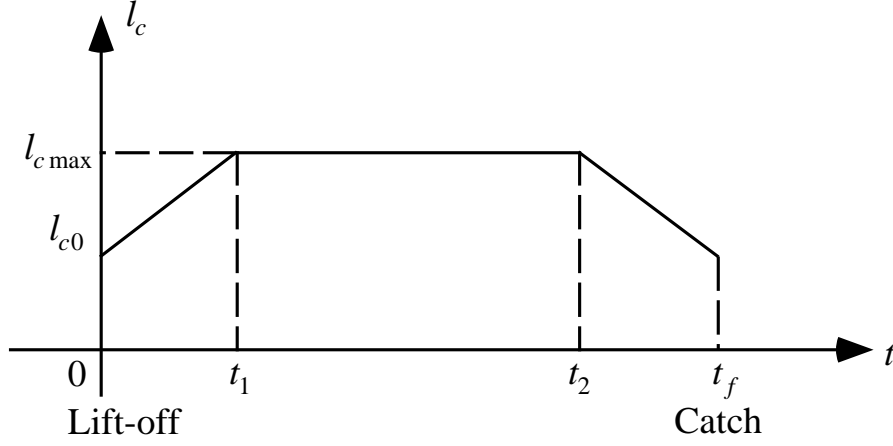
Figure 6.4: The arm length during the flight is changed according to this piecewise linear trajectory.

6.2   Two-link Brachiating Robot in the Flight Phase

Now, we move on to developing a control strategy for the two-link brachiating robot following preliminary studies on the simplified problems. Consider the two-link brachiating robot in a flight phase depicted in Figure 6.5. The equation of motion of the center of mass of the system is given by

$$\ddot{r}_c = \begin{bmatrix} 0 \\ -g \end{bmatrix} \tag{6.21}$$

and the total angular momentum with respect to the center of mass of the system

$$H = \sum_{i=1}^{n} \left\{ I_i \omega_i + \rho_{ci} \times m_i \dot{\rho}_{ci} \right\}$$
$$= c_1 \left[(c_2 + c_3 \cos \theta_2)\dot{\theta}_1 + (c_4 + c_5 \cos \theta_2)\dot{\theta}_2 \right] = H_0 = const. \tag{6.22}$$

is conserved, where

$$c_1 = \frac{1}{m_1 + m_2}$$
$$c_2 = m_1(I_1 + I_2) + m_2(I_1 + I_2 + m_1(l_1 - l_{c1})^2 + l_{c2}{}^2)$$
$$c_3 = 2m_1 m_2(l_1 - l_{c1})l_{c2}$$
$$c_4 = m_1 m_2 l_{c2}{}^2 + (m_1 + m_2)I_2$$
$$c_5 = m_1 m_2(l_1 - l_{c1})l_{c2}.$$

Assuming that θ_2 and $\dot{\theta}_2$ can be directly controlled by a torque input, τ, to the elbow joint, we consider how much θ_1 rotates, when a trajectory of θ_2 is given. Solving (6.22) for $\dot{\theta}_1$, we have

$$\dot{\theta}_1 = \frac{H_0}{c_1(c_2 + c_3 \cos \theta_2)} - \frac{c_4 + c_5 \cos \theta_2}{c_2 + c_3 \cos \theta_2}\dot{\theta}_2 \tag{6.23}$$
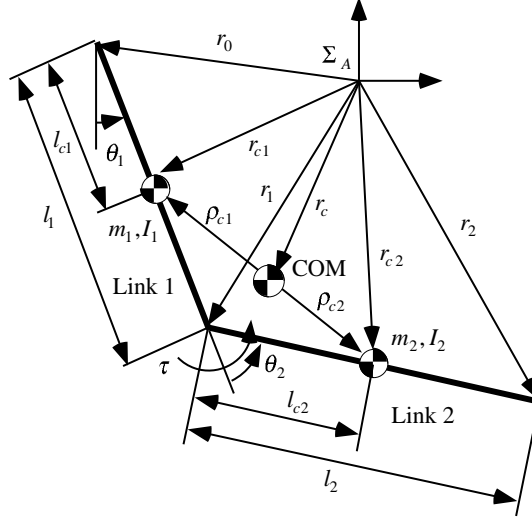
Figure 6.5: Model of a two-link brachiating robot in the flight phase.

when the initial angular momentum is H_0.

In the study of a flip maneuver of a hopping robot [28], they show that if the legs are lengthened at a fixed rate, the equation of the conservation of angular momentum resulting from an revolute-prismatic kinematics can be integrated in closed form. Thus, they can determine how much the body rotates in the flight phase. Although our equation (6.23) is much more complicated than their equation, similarly we find that if the angle of the elbow joint is changed with a fixed rate, (6.23) can be integrated in closed form as well. We find this observation useful in controlling the body rotation of the robot in the flight phase.

Suppose we change θ_2 with a fixed rate $\dot{\theta}_{2k}$ from $\theta_{20} = \theta_2(t_0)$ to $\theta_{2f} = \theta_2(t_f)$ as $\theta_2 = \dot{\theta}_{2k}t + \theta_{20}$, we obtain

$$\int \dot{\theta}_1 dt = -\frac{c_5(\dot{\theta}_{2k}t + \theta_{20})}{c_3} - \frac{1}{c_1 c_3 \dot{\theta}_{2k}\sqrt{-c_2{}^2 + c_3{}^2}}$$
$$\times \left[2\left(c_1\dot{\theta}_{2k}(-c_3 c_4 + c_2 c_5) + c_3 H_0\right)\tanh^{-1}\left(\frac{(c_2 - c_3)\tan\left(\frac{\dot{\theta}_{2k}t+\theta_{20}}{2}\right)}{\sqrt{-c_2{}^2 + c_3{}^2}}\right)\right] + C \quad (6.24)$$

using a symbolic integral command on *Mathematica*, where C is an integral constant. Thus, we can determine how much θ_1 rotates during this period evaluating the integral above

$$\Delta\theta_1 = \int_{t_0}^{t_f} \dot{\theta}_1 dt = \int_{t_0}^{t_f} \left(\frac{H_0}{c_1(c_2 + c_3\cos\theta_2)} - \frac{c_4 + c_5\cos\theta_2}{c_2 + c_3\cos\theta_2}\dot{\theta}_2\right) dt \quad (6.25)$$

in closed form[1].

In the sequel, we use the dynamical parameters of the robot, $m_1 = m_2 = 2.460$, $l_1 = l_2 = 0.5$, $l_{c1} = l_2 - l_{c2} = 0.335$ and $I_1 = I_2 = 0.1$. This is approximately equivalent to the lossless version the physical two-link brachiating robot we have used in this work having symmetry in the link parameters.

---

[1]In [21], it is described that the equivalent expression for a two-link spring board diver's model can be integrated in closed form for the special case when $H_0 = 0$.
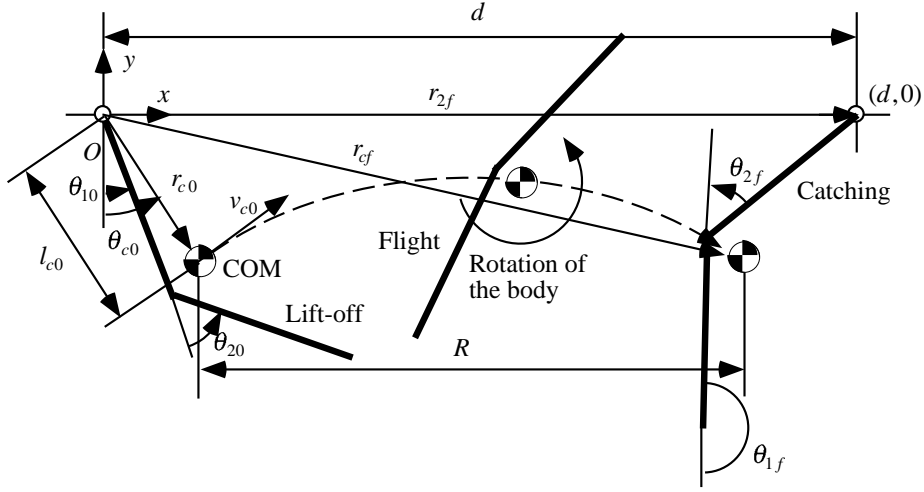
Figure 6.6: A leaping maneuver of the two-link brachiating robot.

6.3   Formulation of Flight Control Strategy for Brachiating Robot

This section presents a motion control strategy in the flight phase for a two-link brachiating robot. Suppose the robot releases the bar at $t = 0$ with the lift-off condition, $\theta_1(0) = \theta_{10}$, $\theta_2(0) = \theta_{20}$, $\dot{\theta}_1(0) = \dot{\theta}_{10}$ and $\dot{\theta}_2(0) = \dot{\theta}_{20}$ as depicted in Figure 6.6.

The trajectory of the center of mass is given by

$$r_c(t) = \begin{bmatrix} v_{c0x}t + r_{c0x} \\ -\frac{1}{2}gt^2 + v_{c0y}t + r_{c0y} \end{bmatrix} \tag{6.26}$$

where $r_{c0} = r_c(0)$ and $v_{c0} = v_c(0)$ are the initial states of the center of mass in the Cartesian coordinates.

Now, we consider a candidate of the condition at the grasp of the bar at $t = t_f$ as shown in Figure 6.6 such that the location of the center of mass is

$$r_{cf} = r_{c0} + \begin{bmatrix} R \\ 0 \end{bmatrix} \tag{6.27}$$

with the range

$$R = d - 2l_{c0} \sin \theta_{c0} \tag{6.28}$$

and the position of the gripper coincides the location of the next bar at $(d, 0)$,

$$r_{2f} = \begin{bmatrix} d \\ 0 \end{bmatrix}. \tag{6.29}$$

Given r_{cf} and r_{2f}, the configuration of the robot at the grasp can be determined by solving the inverse kinematics for θ_{1f} and θ_{2f}. In general, there exist two solutions, and we choose one of them which satisfies $\theta_{2f} = -\theta_{20}$ as shown in Figure 6.6 since we find it convenient when designing the desired trajectory for θ_2.
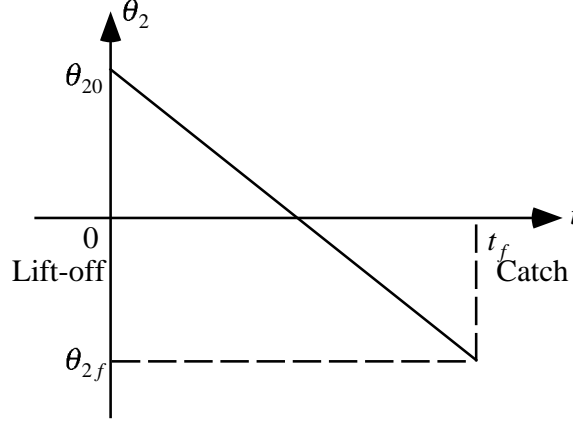
Figure 6.7: Design of the desired trajectory for θ_2 during the flight phase. θ_2 changes with a fixed angular velocity.

To synchronize the body rotation with catching, we design a trajectory for θ_2 from θ_{20} to θ_{2f} during the flight which satisfy the constraint from the conservation of angular momentum (6.23),

$$\Delta\theta_1 = \int_0^{t_f} \dot{\theta}_1 dt = \int_0^{t_f} \left(\frac{H_0}{c_1(c_2 + c_3\cos\theta_2)} - \frac{c_4 + c_5\cos\theta_2}{c_2 + c_3\cos\theta_2}\dot{\theta}_2 \right) dt \tag{6.30}$$

As discussed in section 6.2, when θ_2 changes with a fixed angular velocity $\dot{\theta}_{2k}$, (6.30) can be integrated in closed form. Thus, we change θ_2 at a constant rate from $\theta_2(0) = \theta_{20}$ to $\theta_2(t_f) = \theta_{2f}$ following the desired trajectory

$$\theta_2(t) = \dot{\theta}_{2k}t + \theta_{20} \tag{6.31}$$

where $\dot{\theta}_{2k} = (\theta_{2f} - \theta_{20})/t_f$, as depicted in Figure 6.7

Suppose we take the initial condition of the center of mass, $l_c(0) = l_{c0}$, $\dot{l}_c(0) = 0$, $\theta_c(0) = \theta_{c0}$ and $\dot{\theta}_c(0) = \dot{\theta}_{c0}$, in the polar coordinates, as depicted in Figure 6.7, namely,

$$r_{c0} = \begin{bmatrix} l_{c0}\sin\theta_{c0} \\ -l_{c0}\cos\theta_{c0} \end{bmatrix} \quad \text{and} \quad v_{c0} = \dot{r}_{c0} = \begin{bmatrix} l_{c0}\cos\theta_{c0}\dot{\theta}_{c0} \\ l_{c0}\sin\theta_{c0}\dot{\theta}_{c0} \end{bmatrix}. \tag{6.32}$$

Then, solving (6.26) and (6.27) for t_f and θ_{c0}, we have

$$t_f = \frac{2v_{c0y}}{g} = \frac{2l_{c0}\dot{\theta}_{c0}\sin\theta_{c0}}{g} \tag{6.33}$$

and

$$\dot{\theta}_{c0} = \sqrt{\frac{g(d - 2l_{c0}\sin\theta_{c0})}{l_{c0}^2\sin 2\theta_{c0}}}. \tag{6.34}$$

Thus, given d, l_{c0}, all the states of the robot parameterized by θ_{c0} can be determined by solving

$$\Delta\theta_1 = \theta_{1f} - \theta_{10} \tag{6.35}$$

arising from (6.30) for θ_{c0}. Since θ_{c0} appears in transcendental functions, we expect no closed form solution to this algebraic equation. Thus, we use a scalar numerical root finding method to

solve this equation. Notice that there is limitation on the distance which can be achieved since there is a trade-off between the control of rotation of the body resulting from the initial angular momentum and the horizontal/vertical velocity of the center of mass at lift-off.

6.4   Coordination of Sequence of Motions from Swing to Flight

In the development of the flight strategy discussed in Section 6.2, we first determine the configuration of the robot at the grasp, and then solve for the states of the robot parameterized by a initial state of the center of mass at lift-off assuming that the desired initial condition for the flight phase can be achieved. To initiate leaping, we need to achieve such required initial velocity of the center of mass and the desired configuration of the robot at lift-off. Numerical simulations suggest that leaping maneuver require fairly large lift-off initial velocity. Thus, we need to pump up larger amount of energy to the system for the flight resulting in much larger amplitude of oscillation in the swing motion than what we need for the regular swing locomotion from handhold to handhold in the ladder problem. To achieve such swing behaviors, we choose to use a hybrid swing up controller described in Chapter 5. However, in practice, we find it difficult to tune the hybrid swing up controller to achieve the "exact" values of the specified lift-off condition since we have yet to have full understanding of the swing up controller.

   Under these circumstances, we slightly modify the flight strategy discussed in Section 6.2 so that the the body rotation is adjusted for the approximated lift-off conditions. Then, we present how the hybrid swing up controller is tuned to obtain the appropriate center of mass trajectory in the flight coordinating the sequence of the swing and flight motions.

6.4.1   Adjustment of Body Rotation in Flight Phase

Suppose the robot releases the bar at lift-off with an initial condition, $\theta_1(0) = \theta_{10}$, $\theta_2(0) = \theta_{20}$, $\dot{\theta}_1(0) = \dot{\theta}_{10}$ and $\dot{\theta}_2(0) = \dot{\theta}_{20}$, obtained using an appropriately tuned swing up controller, assuming that the resulting center of mass trajectory (6.26) passes near the target bar located at a distance, d, such that the robot can reach it as depicted in Figure 6.8.

   Consider a candidate of the configuration of the robot at the grasp when the trajectory of the center of mass approaches the bar at some time $t = t_f$ such that the location of the center of mass is

$$r_{cf} = \begin{bmatrix} v_{c0x}t_f + r_{c0x} \\ -\frac{1}{2}gt_f{}^2 + v_{c0y}t_f + r_{c0y} \end{bmatrix} \tag{6.36}$$

and the position of the gripper, r_{2f}, coincides the location of the bar at $(d, 0)$. Given r_{cf} and r_{2f}, the configuration of the robot at the grasp can be determined by solving the inverse kinematics for θ_{1f} and θ_{2f} and taking one of the solutions as shown in Figure 6.8. Now we design the desired trajectory for θ_2 during the flight from $\theta_2(0) = \theta_{20}$ to $\theta_2(t_f) = \theta_{2f}$ as

$$\theta_2(t) = \dot{\theta}_{2k}t + \theta_{20} \tag{6.37}$$

where $\dot{\theta}_{2k} = (\theta_{2f} - \theta_{20})/t_f$. By choosing this trajectory for θ_2 with the fixed angular velocity, the body rotation during the flight $\Delta\theta_1$ in (6.30) can be evaluated in closed form as discussed in Section 6.2. To adjust the body rotation, we solve the equation

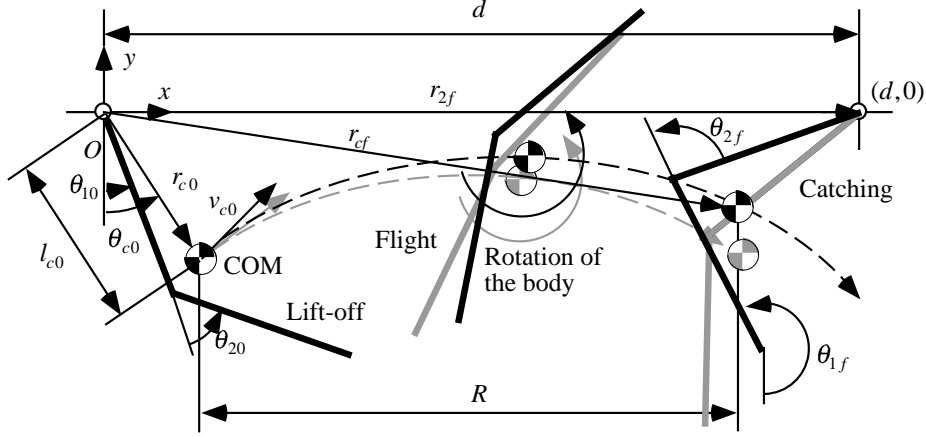$$\Delta\theta_1 = \theta_{1f} - \theta_{10} \tag{6.38}$$

Figure 6.8: A modified leaping maneuver of the robot in the flight phase. The body rotation is adjusted when the exact value of the desired initial condition for the flight phase cannot be achieved because of difficulty in the tuning of the hybrid swing up controller.

for t_f, and all the states of the robot during the flight which are parameterized by t_f can be determined. Since t_f appears in transcendental functions, we expect no closed form solution to this algebraic equation. Thus, we solve this equation using a scalar numerical root finding method.

6.4.2 Swing Control and Lift-off Condition

To accomplish a successful leaping maneuver, it is important to achieve an appropriate lift-off states by swing up. However, because of theoretical difficulty associated with the swing up problem, we have yet to have an automatic tuning procedure of the hybrid swing up controller in a systematic way. Thus, we tune the parameter of the hybrid swing up controller manually and make decision for lift-off empirically based on our physical intuition and understanding of the problem in the coordination of the sequence of motions from swing to flight.

It seems important to us to control the following in swing up for a successful leap:

- amplitude of swing motion to obtain enough energy for lift-off

- timing of lift-off to determine the initial velocity of the center of mass for flight

In practice, we specifically adjust the pseudo energy gain, K_e, and the pseudo energy level, $\bar{E}^*$, of the hybrid swing up controller, which seem to be the two key parameters to achieve proper lift-off condition leaving the rest of them at a fixed value. First, we tune the pseudo energy gain, K_e, in (3.22) to control the rate of energy pumping adjusting the number of swings required for swing up until lift-off. We choose to use the value $K_e = 0.1$. In so doing, a small "kick" velocity, θ_{20}, to the second joint is introduced in the desired direction to initiate swing motion since the bottom state with zero velocity is an equilibrium state of the closed loop dynamics. Then, we tune the desired pseudo energy level, $\bar{E}^*$, defined in (3.22) to control the corresponding amplitude of the swing, $\theta_{amp} = \frac{\pi}{2} + \phi$, parameterized by ϕ. In order to achieve a large center of mass velocity,

Case	d (m)	ϕ (rad)	θ_{c0} (rad)	$\dot{\theta}_{20}$ (rad/s)	t_{lo} (sec)
1	$0.86 \sim 1.08$	0.6	1.0	-0.2	5.207
2	$1.0 \sim 1.16$	0.6	0.8	-0.2	5.162
3	$1.15 \sim 1.27$	0.9	0.6	0.2	4.288
4	$1.23 \sim 1.34$	0.9	0.65	0.2	6.327
5	$1.32 \sim 1.41$	1.2	0.45	-0.2	8.034
6	$1.4 \sim 1.47$	1.1	0.5	0.2	11.324
7	$1.46 \sim 1.49$	1.2	0.5	-0.2	10.674
8	$1.48 \sim 1.50$	1.26	0.5	-0.2	11.508

Table 6.1: The sets of tuned parameters of the hybrid controller and lift-off conditions used for a given distance between the bars, d. The desired pseudo energy level, $\bar{E}^*$, is parameterized by ϕ as in (6.39). θ_{c0} is the selected angle of the virtual pendulum with respect to the center of mass at lift-off as depicted in Figure 6.8. A kick velocity to the second joint, $\dot{\theta}_{20}$, is given to the desired direction to initiate swing up motion from the suspended posture at rest. t_{lo} is the lift-off timing determined empirically as a result of the application of these parameters to the hybrid controller. We choose to use the pseudo energy gain $K_e = 0.1$ for all cases.

we simply increase the desired pseudo energy level

$$\bar{E}^* = \frac{1}{2}\omega^2 \left(\frac{\pi}{2} + \phi \right)^2 \tag{6.39}$$

by changing ϕ, which results in a large swing amplitude. Lastly, we select the timing of releasing the bar by observing the angle of the virtual pendulum, θ_c, with respect to the the center of mass as shown in Figure 6.8 to determine the lift-off velocity of the center of mass.

The values of these parameters and the lift-off timing are adjusted recursively until the robot achieves a successful leap in numerical simulations by solving (6.38) with the selected lift-off conditions and observing the resulting sequence of motions. In this procedure each decision is made empirically in our numerical experience. Although this procedure seems ad hoc, we nevertheless find that it is relatively straightforward to adjust the desired sets of parameters and lift-off conditions since they are fairly physically intuitive.

Finally, in Table 6.1 we present the specified sets of the parameter in the hybrid controller, ϕ, the lift-off condition, θ_{c0}, and the direction of the initial kick velocity, $\dot{\theta}_{20}$, and the resulting timing of lift-off, t_{lo}, for a given interval between the bars, d. The rest of the parameters of the hybrid controller are fixed as $\omega = 3.36$, $E^* = 3.301$, $E_{max1} = E^* + 10.0$, $E_{max2} = E_{max1} + 10.0$, $K_{e2} = 0.6$ and $K_{e3} = 1.0$.

6.5   Simulation

We present numerical simulations of the application of the swing and flight strategies to achieve the desired leaping maneuver. Consider the case where the interval between the bars is $d = 1.3$. We use the set of the parameters for the hybrid controller and lift-off conditions #5 in Table 6.1.

The robot starts swing up with the initial condition, $Tq_0 = [\, 0,\ 0,\ 0,\ 0.2\,]^T$, at $t = 0$, and lifts off at $t = 6.327$ with the states of the robot in joint space, $Tq = [\, 0.5652,\ 0.5193,\ 5.7371,\ 0.8373\,]^T$,
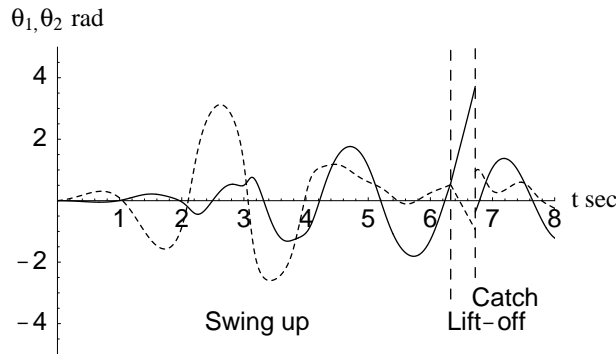
Figure 6.9: Simulation results of a leaping maneuver when $d = 1.3$. Joint trajectories (solid: θ_1, dashed: θ_2). The robot lifts off at $t = 6.327$ and catches the bar at $t = 6.722$. θ_1 and θ_2 are switched after the catch.

Figure 6.10: Pictures of the movement of the robot (simulation) when $d = 1.3$. 1. Initial state at t=0. 2. Swing phase at t=3.74. 3. Lift-off at t=6.35. 4. Flight phase at t=6.53. 5. Catching the next bar at t=6.69

after several swings. They correspond to the states of the virtual pendulum with respect to the center of mass, $[\, l_c, \; \theta_c, \; \dot{l}_c, \; \dot{\theta}_c \,]^T = [\, 0.491, \; 0.65, \; -0.0413, \; 5.863 \,]^T$. The time in the flight phase is 0.395 sec and the robot catches the next bar at $t = 6.722$. Figure 6.9 shows the joint trajectories. Figure 6.10 are the pictures of the motion of the robot at t=0 (initial state), t=3.74 (swing phase), t=6.35 (lift-off), t=6.53 (flight phase) and t=6.69 (grasp of the next bar) respectively. Figures from 6.10 to 6.13 depict the sequence of the motion of the leaping maneuver.

6.6 Summary

This chapter is summarized as follows:

- We have formulated a control strategy for the two-link brachiating robot to achieve a leaping maneuver. The key observation in the flight strategy is that the equation of body rotation can be integrated in closed form with piecewise linear trajectories for the elbow joint inspired by the analysis of mechanics of a flip in [28].

- Numerical simulations suggest the effectiveness of the proposed strategy. Further analytical work will be required to truly understand the properties of the behavior of the system particularly associated with theoretical difficulties in the analysis of the closed loop dynamics
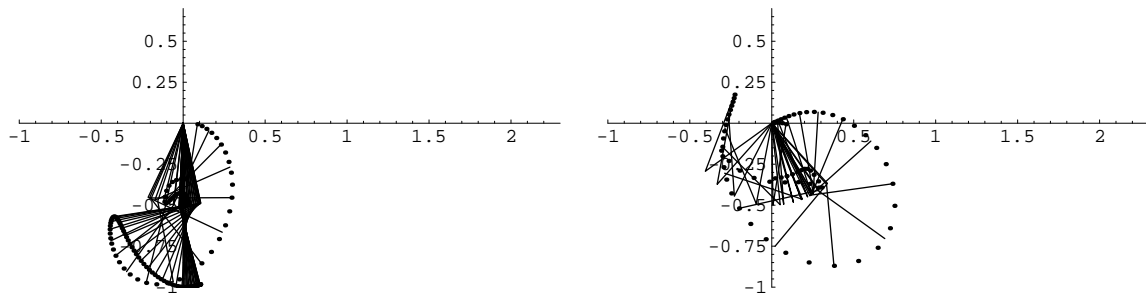
Figure 6.11: Simulation results of a leaping maneuver when $d = 1.3$. (Swing phase) Left: t=0 $\sim$ 2.5, Right: t=2.5 $\sim$ 3.5.
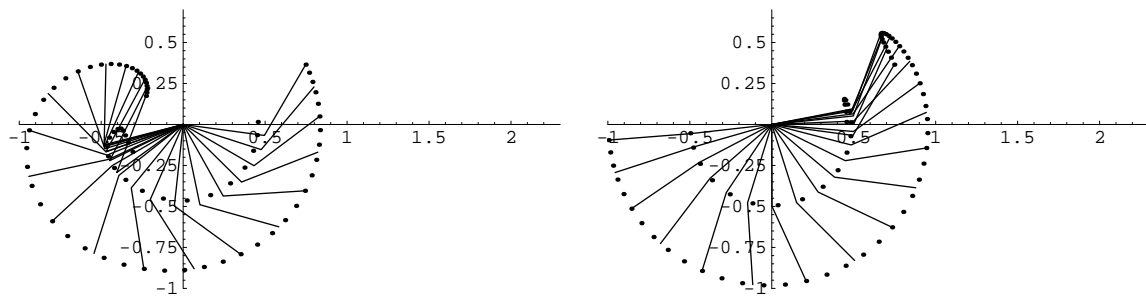

Figure 6.12: Simulation results of a leaping maneuver when $d = 1.3$. (Swing phase) Left: t=3.5 $\sim$ 4.5. Right: t=4.5 $\sim$ 5.5.
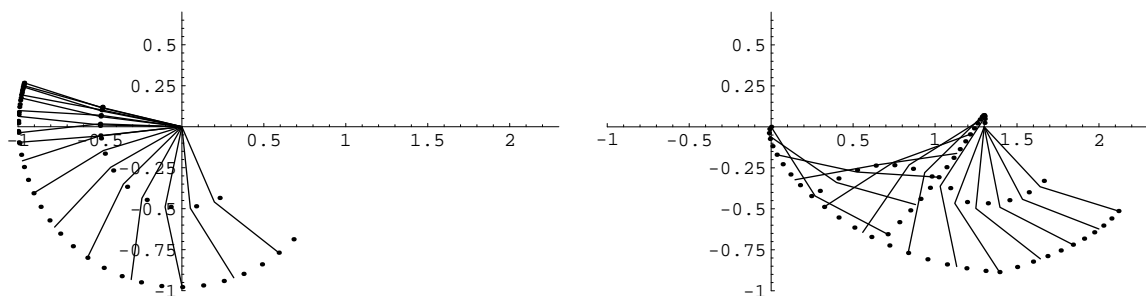

Figure 6.13: Simulation results of a leaping maneuver when $d = 1.3$. The robot lifts off at t=6.327. Left: t=5.5 $\sim$ 6.327, Right: flight phase and catch t=6.327 $\sim$ 7.22

in swing up.

- We are as well interested in a future exploration of consecutive leaping "gaits" over several branches which seems analogous to running and hopping.

Chapter 7

Experiments

We present results of the experimental implementation of the target dynamics controller in order to validate our control strategy. The proposed algorithm is applied to the uniform/irregular ladder and swing up problems. However, the rope problem cannot be experimentally carried out with the robot considered in this work because of the structure of the gripper. We have achieved swing locomotion on a ladder with uniform and irregular intervals, various swing up behaviors from a suspended posture, and repeated locomotion over several rungs. We also present results of the experimental implementation of the hybrid swing up controller to suggest its effectiveness.

7.1 Uniform Ladder Problem

This section considers the uniform ladder problem—brachiation on a set of evenly spaced bars at the same height. In the experimental setting, the next bar is located at a distance of 0.6m.

As discussed in Section 3.1, the symmetry property of neutral orbits solves the uniform ladder problem. We need to choose ω in the target dynamics (2.9) for a given ladder distance, d^*. For our experimental setting, ω is tuned to be $\omega = 3.36$ according to the mapping depicted in Figure 3.2

Early attempts to implement the controller (3.21) were not successful. Swing motion close to the desired behavior was achieved, but the gripper did not come close enough to the target bar to catch it[1]. A central component contributing to these failures was the model mismatch. Therefore, we tuned the parameters of the model manually. Some experience is helpful in the refinement of these parameters: we choose to use $m_1 = 3.39, m_2 = 1.30, c_2 = 0.73$ and $b_2 = 0.33$ instead of the values in Table 2.1 for the ladder problem. This assignment yielded success.

A typical motion of the physical robot is plotted in Figure 7.1, while the joint trajectories and the voltage commands sent to the driver are shown in Figure 7.2. The mean locomotion time of ten runs is 0.973 seconds with ± 0.015 second error[2], which is very close to its analytically calculated value, $t = \frac{\pi}{\omega} = 0.935$ seconds. Notice that the symmetry of the neutral orbit is not

---

[1] In practice, we need to consider the time lag in opening the gripper when the robot initiates locomotion, something not taken into account in the analytical work. It takes approximately 0.08 to 0.1 seconds to release the bar after the command to open the gripper is sent. Empirically, we have observed that this time affects the swing behavior of the robot. As a result, we choose to send the open command of the gripper 0.08 seconds before the target dynamics controller is turned on.

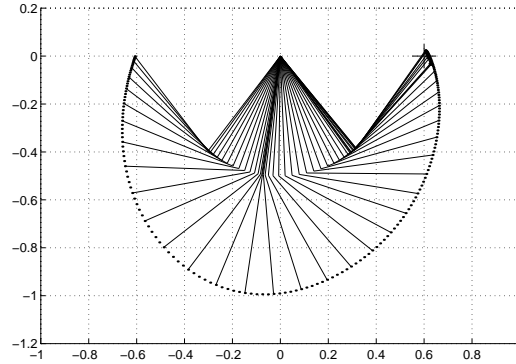[2] In the sequel, the error refers to the maximum deviation from the mean.

Figure 7.1: Movement of the robot (experiment). The target bar is located at a distance of 0.6m marked by the "+".
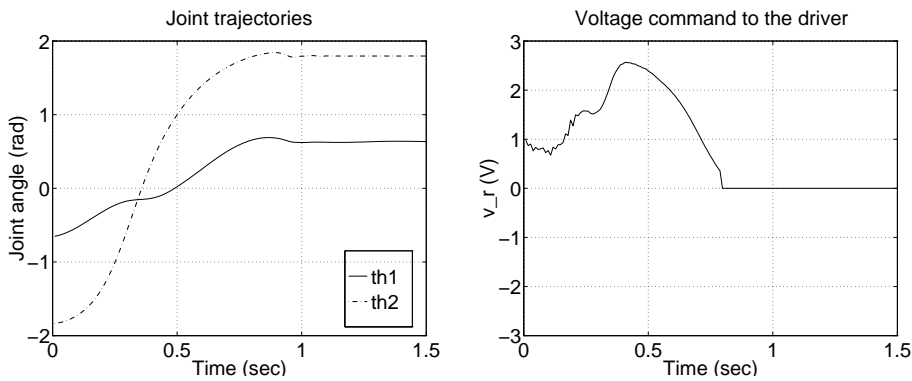

Figure 7.2: The experimental results of the ladder problem. Left: Joint trajectories, Right: Voltage command to the motor driver

perfectly achieved in the motion of the robot. We discuss the discrepancy between the simulation and experimental results in Appendix C.

7.2 Swing up Problem

As we have mentioned, the swing up problem represents the task of swinging up from the suspended posture at rest and catching the next bar. The results of the experimental implementation of the proposed controller are presented. In order to achieve the task, we need to bring the effective actuated portion of the state, θ, to the right pseudo energy level, while simultaneously ensuring that the unactuated degree of freedom, r, coincide with the regulated length between the bars, d^*.

What follows is a presentation of the different swing up behaviors resulting from changes in the rate of energy pumping, as characterized by K_e. The distance between the bars is 0.6m. We consider three cases where $K_e = 0.03, 0.47$ and 0.9. These parameters are chosen manually based on our experience in numerical simulation and experiments. In order to successfully swing up, we have found it necessary to slightly modify the desired pseudo energy level and some of

the model parameters. The nominal pseudo energy is chosen to be $\bar{E}^*_{nom} = \frac{1}{2}\omega^2\left(\frac{\pi}{2}\right)^2$ so that the gripper reaches the height of the bar, which corresponds to the condition, $\theta = \frac{\pi}{2}$, when $\dot{\theta} = 0$. In the initial attempts using the nominal pseudo energy level, we found that the gripper of the robot came close to the bar, but did not reach the enough height up to the ceiling to catch it. Thus, we introduce a slight modification to this value as $\bar{E}^* = 1.1\bar{E}^*_{nom}$ to increase the amplitude of the oscillation so that the gripper reaches the height of the bar, and we choose to use $m_1 = 3.39, m_2 = 1.30$ instead of the values in Table 2.1. The initial direction of the swing motion depends solely upon the initial states of the system since the motion of the robot is governed by the closed loop dynamics. Only small deviation from the origin on the phase plane determines this direction. Thus, we introduce an impulse-like initial torque before the controller is turned on so that the robot starts its swing motion in the desired direction at every run. The experimental results of swing up problem do not exactly match those of numerical simulations presented in Section 3.2. We investigate this matter in Appendix C.

Slow Swing up ($K_e = 0.03$)   Consider the case where $K_e = 0.03$. Figure 7.3 shows the joint trajectory and the voltage command to the motor driver. The mean time of ten runs for this slow swing up behavior is 7.474 seconds with ± 0.080 second error.

Fast Swing up ($K_e = 0.47$)   Consider the case where $K_e = 0.47$. Figure 7.4 shows the joint trajectory and the voltage command to the motor driver. This choice K_e yields relatively fast swing up. The mean swing up time of ten runs for this swing up is 3.843 seconds with ± 0.146 second error.

Faster Swing up ($K_e = 0.9$)   Consider the case where $K_e = 0.9$. Figure 7.5 shows the joint trajectory and the voltage command to the motor driver. This choice of K_e yields a "faster" swing up maneuver. The mean swing up time of ten runs for this movement is 2.913 seconds with ± 0.025 second error. In this case, the initial impulse-like torque is applied in the opposite direction to the previous two cases in order to start swinging in the CCW direction.

7.3   Irregular Ladder Problem

This section presents the experimental implementation of the proposed control strategy for the irregular ladder problem discussed in Section 4.2. We consider the same ladder intervals as specified in Table 4.1.

As we have experienced in our experimental work in the ladder problem presented above, we refine the dynamical parameters in the controller and the timing of bar release manually so that the robot successfully achieves the desired brachiation because of the parameter mismatch and a delay in the actuator mechanism the gripper. The command to close the gripper is sent and the voltage command to the motor driver is turned off simultaneously when the gripper approaches the target bar. Some experience is helpful in these refinements.

Case 1: $d[k] = 0.4, d[k+1] = 0.6$ A typical movement of the robot is depicted in Figure 7.6, while the joint trajectories and the voltage commands sent to the driver are shown in Figure 7.7. We choose to use the dynamical parameters, $m_1 = 3.39, m_2 = 1.30, c_2 = 0.65, b_2 = 0.9$, instead of
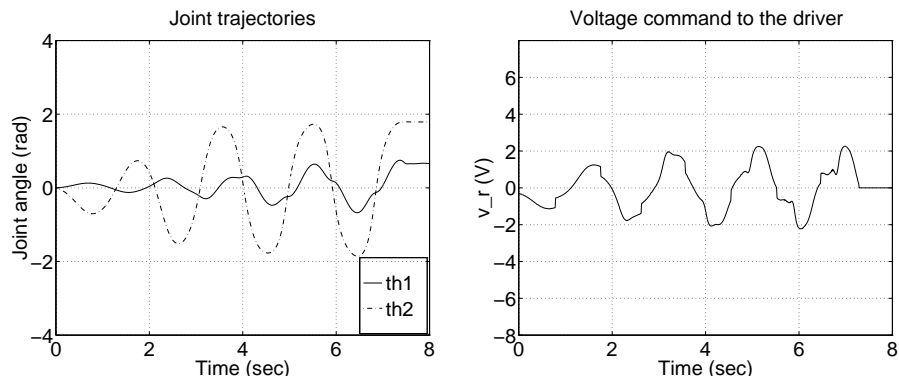
Figure 7.3: Experimental results of slow swing up behavior ($K_e = 0.03$). Left: Joint trajectories, right: Voltage command to the motor driver. The robot captures the bar when $t \sim 7.5$ seconds.
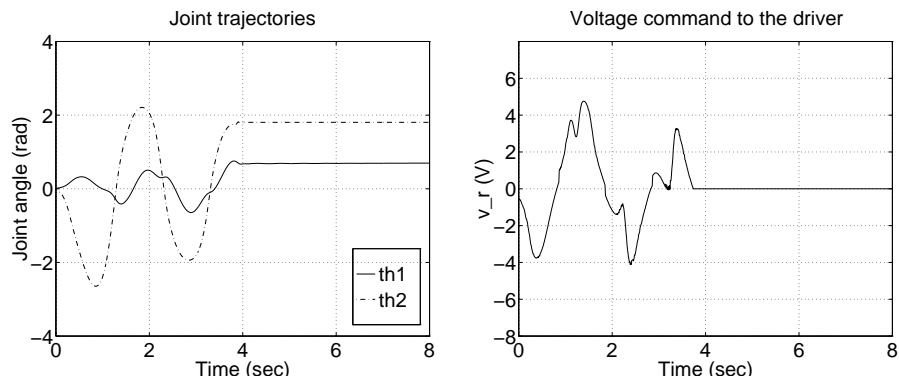

Figure 7.4: Experimental results of fast swing up behavior ($K_e = 0.47$). Left: Joint trajectories, right: Voltage command to the motor driver. The robot captures the bar when $t \sim 3.8$ seconds.
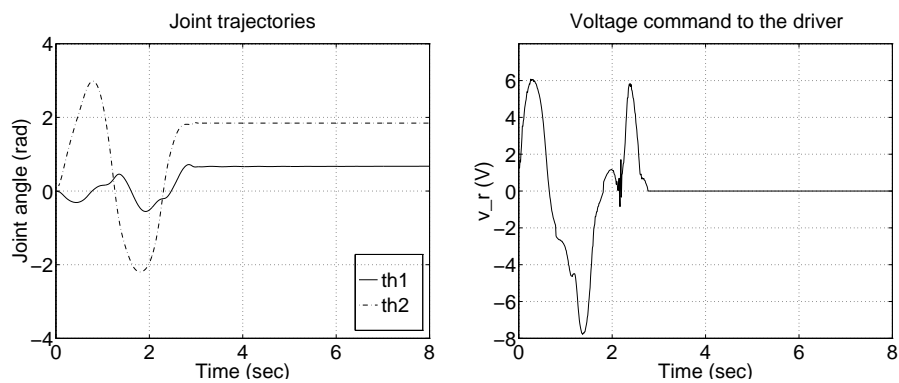

Figure 7.5: Experimental results of faster swing up behavior ($K_e = 0.9$). Left: Joint trajectories, right: Voltage command to the motor driver. The robot captures the bar when $t \sim 2.9$ seconds.
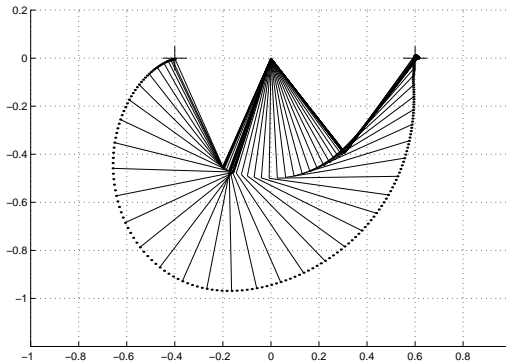
Figure 7.6: Movement of the robot (experiment), where $d[k] = 0.4, d[k+1] = 0.6$.
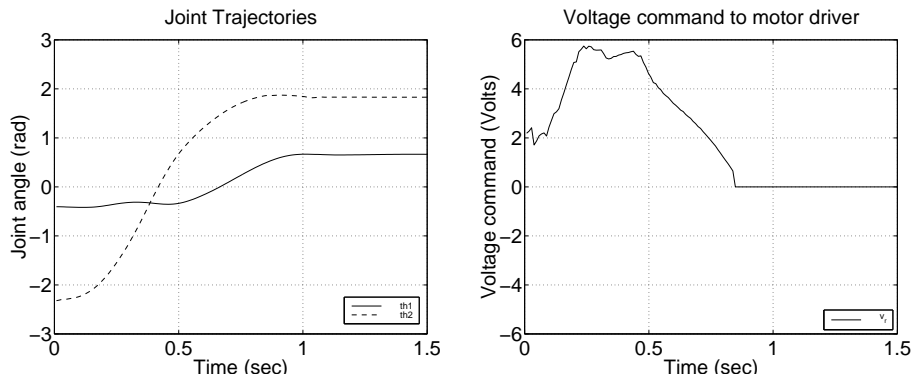

Figure 7.7: The experimental results, where $d[k] = 0.4, d[k+1] = 0.6$. Left: Joint trajectories (solid: θ_1, dashed: θ_2) , Right: Voltage command to the motor driver.

the values shown in Table 2.1. The mean time of ten runs at which the robot reaches the ceiling is 0.949 seconds with ± 0.04 second error, which is close to its analytical value, $t = \frac{\pi}{\omega} = 0.854$ seconds.

Case 2: $d[k] = 0.5, d[k+1] = 0.6$ A typical movement of the robot is depicted in Figure 7.8, while the joint trajectories and the voltage commands sent to the driver are shown in Figure 7.9. We choose to use the dynamical parameters, $m_1 = 3.39, m_2 = 1.30, c_2 = 0.73, d_2 = 0.6$, instead of the values shown in Table 2.1 and send the command to open the gripper 0.01 seconds before the controller is turned on. The mean locomotion time of ten runs is 0.870 seconds with ± 0.03 second error, which is close to its analytically calculated value, $t = \frac{\pi}{\omega} = 0.905$ seconds.

Case 3: $d[k] = 0.6, d[k+1] = 0.5$ A typical movement of the robot is depicted in Figure 7.10, while the joint trajectories and the voltage commands sent to the driver are shown in Figure 7.11. We choose to use the dynamical parameters, $m_1 = 3.39, m_2 = 1.30, c_2 = 0.73, b_2 = 0.33$, instead of the values shown in Table 2.1 and send the command to open the gripper 0.08 seconds before the controller is turned on. The mean locomotion time of ten runs is 0.841 seconds with ± 0.08 second error, which is very close to its analytical value, $t = \frac{\pi}{\omega} = 0.965$ seconds.
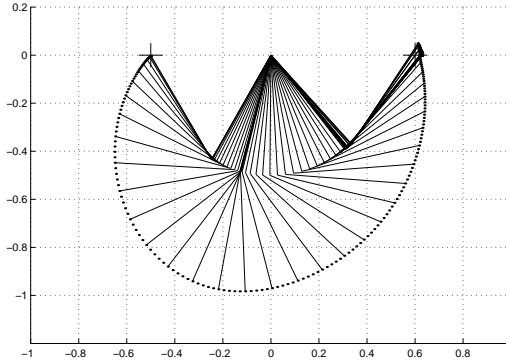
Figure 7.8: Movement of the robot (experiment), where $d[k] = 0.5, d[k+1] = 0.6$.
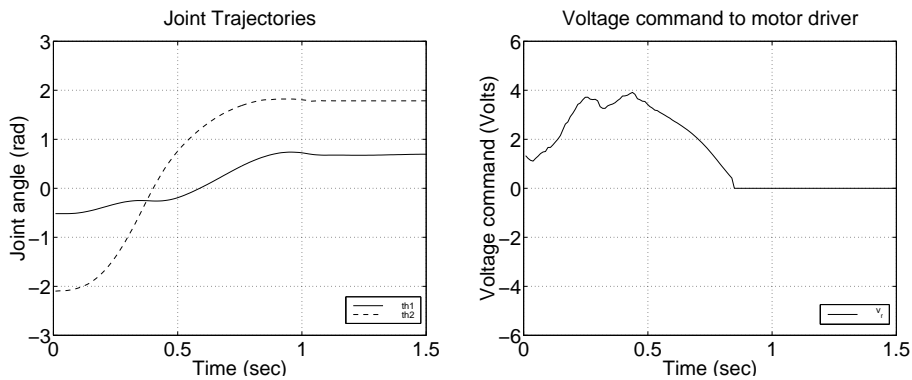

Figure 7.9: The experimental results, where $d[k] = 0.5, d[k+1] = 0.6$. Left: Joint trajectories (solid: θ_1, dashed: θ_2) , Right: Voltage command to the motor driver.

7.4   Continuous Locomotion

Here we exhibit the demonstration of continuous locomotion over several rungs of the ladder. Figure 7.12 depicts repeated locomotion of the robot initiated at the ceiling and moving from left to right. This motion can be considered as the iteration of the ladder trajectory. After each swing, the initial condition is reset, and the function of each arm is switched. This switching is done manually by looking at the motion of the robot to make sure that the it does not fall off from the ladder by mistakenly releasing the grasping bar before catching the next bar with some automated manner, which may result in serious damage to the robot. Due to the symmetrical structure of the robot, the same model is used in each swing where the configuration of the robot is "flipped over." In Figure 7.13, we show a picture of continuous locomotion initiated from the suspended posture. This is a combination of the "faster" swing up maneuver and the iterated ladder trajectory. First, the robot swings three times—going forth (1) and back (2) to gain momentum, and again swinging forward (3) to catch the bar—with the swing up controller ($K_e = 0.9$) described above. Then the control law is switched into the locomotion controller.
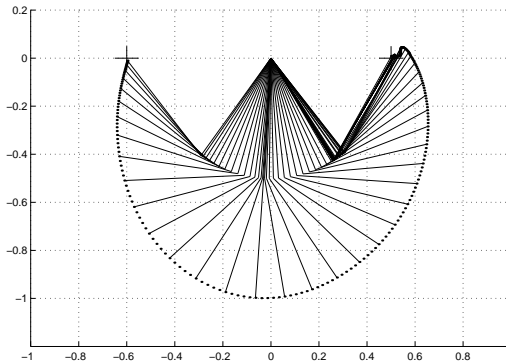
Figure 7.10: Movement of the robot (experiment), where $d[k] = 0.6, d[k+1] = 0.5$.
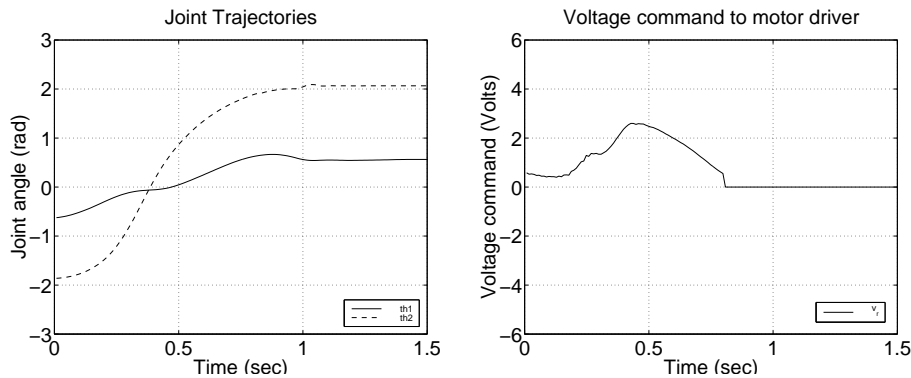

Figure 7.11: The experimental results, where $d[k] = 0.6, d[k+1] = 0.5$. Left: Joint trajectories (solid: θ_1, dashed: θ_2) , Right: Voltage command to the motor driver.

7.5 Hybrid Swing up Controller

In this section, we present results in the experimental implementation of the hybrid swing up controller (5.7). Our early attempts to achieve the desired neutral orbit swinging up to the "ceiling" with the amplitude of $\theta^* = \frac{\pi}{2}$ were not successful largely because of the torque saturation problem of the elbow actuator. Thus, we consider the desired neutral orbit with smaller amplitude parametrized by θ^* and d^* as depicted in Figure 5.9. In the following experiments, we consider two cases, $\theta^* = \frac{\pi}{4}, d^* = 0.8$ and $\theta^* = \frac{\pi}{3}, d^* = 0.7$, which correspond to the numerical simulations presented in Section 5.2.3. We use the dynamical parameters of the robot in Table 2.1 for the controller.

The preliminary experimental results presented below demonstrate that the hybrid controller achieves the desired swing motion of the robot while the original swing up controller yields "chaotic" behavior. Although we have favorable results in achieving the near desired orbit, practically we find that the choice of large energy gains in the controller induces torque commands with undesirable large amount of noise caused by noisy measurement of $\dot{\theta}_2$ generated through the numerical differentiation of θ_2 as seen in Figures 7.19 and 7.21. We tried to avoid this by using a discrete version of a filtered numerical differentiation to obtain $\dot{\theta}_2$ or by filtering the voltage
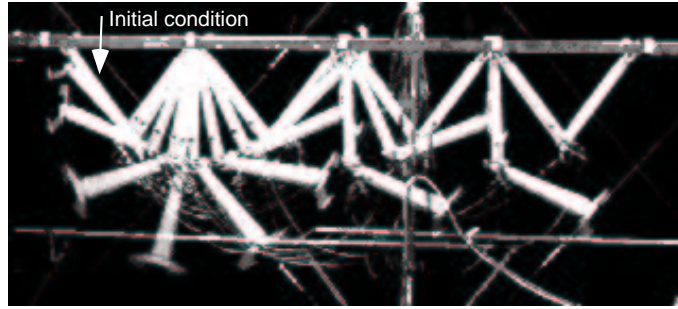
Figure 7.12: A Picture of continuous locomotion started in the ceiling. The robot iterates brachiation three times moving from left to right.
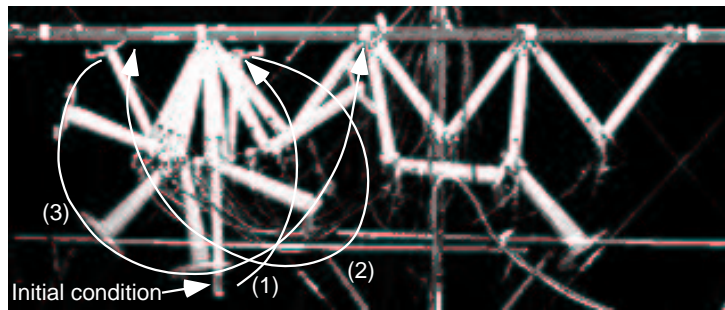

Figure 7.13: A Picture of continuous locomotion initiated from the suspended posture. First, the robot swings three times—going forth (1) and back (2) to gain momentum, and again swinging forward (3) to catch the bar—with the swing up controller ($K_e = 0.9$) described above. Then the control law is switched into the locomotion controller.

command to the motor driver. However, we were unable to eliminate the undesirable noise in the voltage command. In practice, we find that it seems somewhat effective to increase the sampling rate of the controller. Thus, in the following experiments, the control law is evaluated at a rate of 1250Hz. We suspect that use of a tachometer to measure the angular velocity of the second joint would be preferable.

Case 1: $\theta^* = \frac{\pi}{4}, d^* = 0.8$ In this case, we use $\omega = 3.335$ which locates a neutral orbit supposing the robot starts swinging from the desired configuration with zero velocity in the "virtual ceiling." The pseudo energy in the target dynamics is chosen as $\bar{E}^* = \frac{1}{2}\omega^2\left(\frac{\pi}{4}\right)^2$ so that the robot achieves oscillation with the desired amplitude in θ. We choose to use the desired mechanical energy $E^* = -20.51$ which correspond to the potential energy of the system at the desired configuration of the robot in the "virtual ceiling." The energy gains are chosen empirically based on our experience in numerical simulations as $K_e = 10.0, K_{e2} = 20.0, K_{e3} = 2.0$.

Figure 7.14 shows a typical movement of the robot and Figure 7.15 shows joint trajectories and the voltage command to the motor driver under the hybrid controller. These results illustrate that the hybrid controller achieves good regulation of the desired swing behavior of the robot. In contrast, the original swing up controller yields "chaotic" behavior as depicted in Figures 7.16
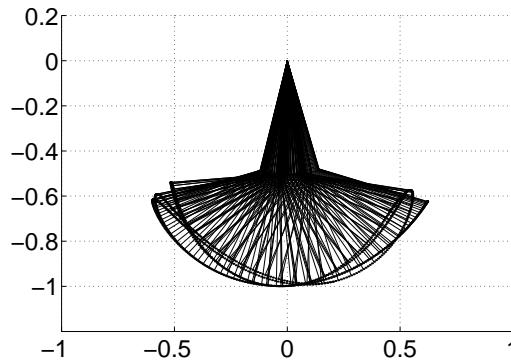
and 7.17.

Figure 7.14: Typical movement of well regulated swing motion of the robot under the hybrid controller (experiment) from t=10 to t=15, where $\theta^* = \frac{\pi}{4}, d^* = 0.8$.
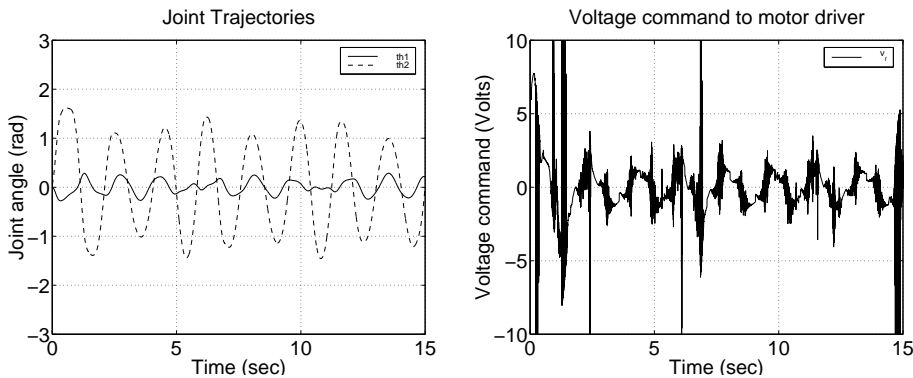

Figure 7.15: Experimental results of the implementation of the hybrid controller, where $\theta^* = \frac{\pi}{4}, d^* = 0.8$. Left: Joint trajectories (solid: θ_1, dashed: θ_2), Right: Voltage command to the motor driver. Note that the desired near neutral orbit is achieved.

Case 2: $\theta^* = \frac{\pi}{3}, d^* = 0.7$ In this case, we use $\omega = 3.325$ which locates a neutral orbit supposing the robot starts swinging from the desired configuration with zero velocity in the "virtual ceiling." The pseudo energy in the target dynamics is chosen as $\bar{E}^* = \frac{1}{2}\omega^2 \left(\frac{\pi}{3}\right)^2$ so that the robot achieves oscillation with the desired amplitude in θ. We choose to use the desired mechanical energy $E^* = -18.44$ which correspond to the potential energy of the system at the desired configuration of the robot in the "virtual ceiling." The energy gains are chosen empirically based on our experience in numerical simulations as $K_e = 20.0, K_{e2} = 20.0, K_{e3} = 2.0$.

Figure 7.18 shows a typical movement of the robot and Figure 7.19 shows joint trajectories and the voltage command to the motor driver under the hybrid controller. These results illustrate that the hybrid controller achieves good regulation of the desired swing behavior of the robot. In contrast, the original swing up controller yields "chaotic" behavior as depicted in Figures 7.20 and 7.21. In these cases, the choice of large energy gains induces undesirable large noise in the
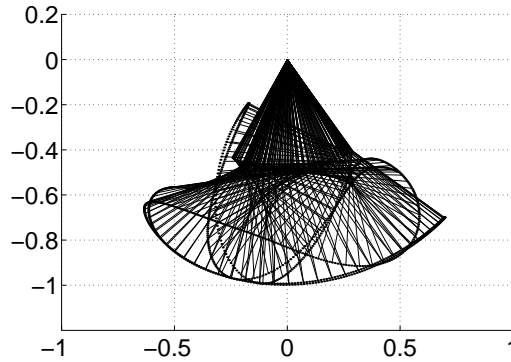
Figure 7.16: Typical movement of "chaotic" swing behavior of the robot under the original swing up controller controller (experiment) from t=10 to t=15, where $\theta^* = \frac{\pi}{4}, d^* = 0.8$.

Figure 7.17: Experimental results of "chaotic" behavior under the original swing up controller, where $\theta^* = \frac{\pi}{4}, d^* = 0.8$. Left: Joint trajectories (solid: θ_1, dashed: θ_2), Right: Voltage command to the motor driver.

voltage command to the motor driver.

7.6 Summary

This chapter is summarized as follows:

- We have presented our empirical success in the implementation of the target dynamics method to the two-link brachiating robot. The proposed algorithm is applied to the uniform/irregular ladder and swing up problems. We achieved swing locomotion in the ladder problem and various swing up behaviors with different rates of energy pumping characterized by K_e. We demonstrated continuous locomotion over several rungs of the ladder as well. We also had favorable results in the experimental implementation of the hybrid swing up controller.

- The experimental success bears out the validity of our control strategy in spite of the presence of model mismatches and physical effects previously unconsidered. Even so, some
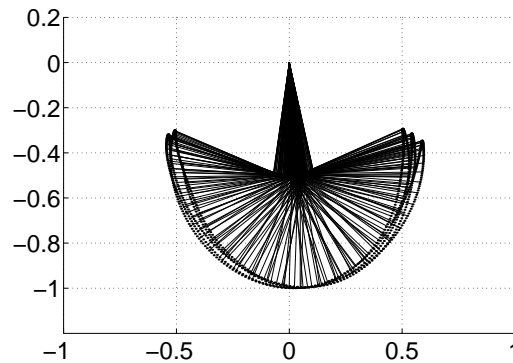
Figure 7.18: Typical movement of well regulated swing motion of the robot under the hybrid controller (experiment) from t=10 to t=15, where $\theta^* = \frac{\pi}{3}, d^* = 0.7$.
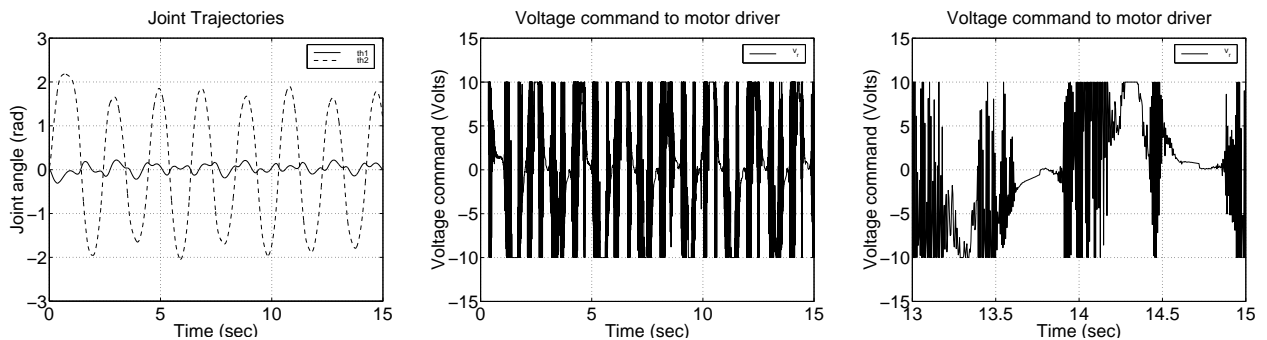
Figure 7.19: Experimental results of the implementation of the hybrid controller, where $\theta^* = \frac{\pi}{3}, d^* = 0.7$. Left: Joint trajectories (solid: θ_1, dashed: θ_2). Note that the desired near neutral orbit is achieved. Center: Voltage command to the motor driver. Large amount of noise is induced by the noisy measurement of $\dot{\theta}_2$ obtained through numerical differentiation of θ_2. Note that we set an upper limit of the voltage command at ± 10 Volts according to the range of the D/A board (± 10 Volts). Right: A sample of the voltage command from $t = 13$ to $t = 15$.

manual tuning was required to implement our ideas.

- We have yet to experimentally implement the proposed leaping strategy because of a number of technical difficulties. In fact, the robot is not originally designed for performing a leaping maneuver, which requires a fairly large torque/power and precise control of the elbow actuator in swing up, and sensing devices to measure the location and posture of the body in the flight phase. The harmonic drive DC motor at the elbow joint exhibits very complicated friction and it cannot produce enough torque for the required swing up. Moreover, an additional problem of dexterous grasp, which involves hand-eye coordination, needs to be considered, and failure of catching the target branch results incurs disastrous damage to the robot.
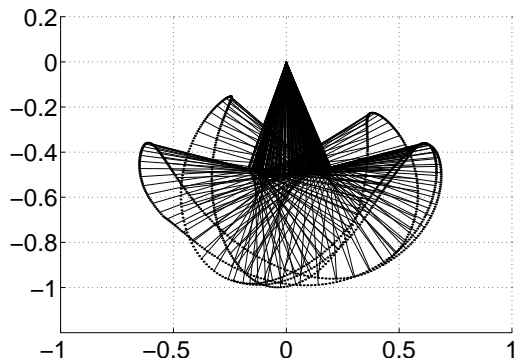
Figure 7.20: Typical movement of "chaotic" swing behavior of the robot under the original swing up controller controller (experiment) from t=10 to t=15, where $\theta^* = \frac{\pi}{3}, d^* = 0.7$.
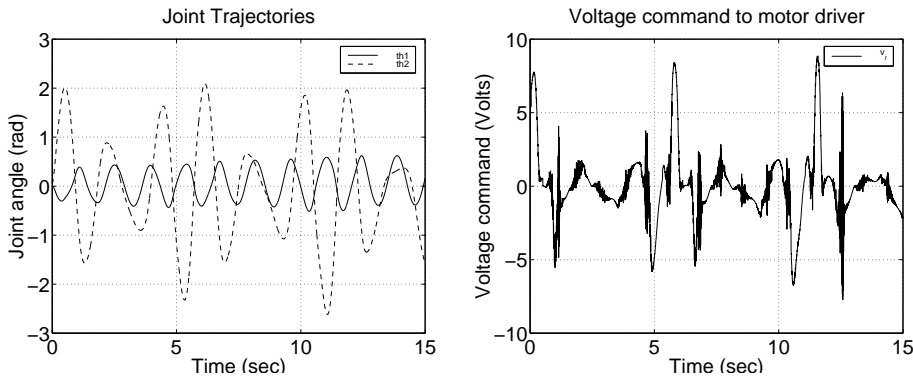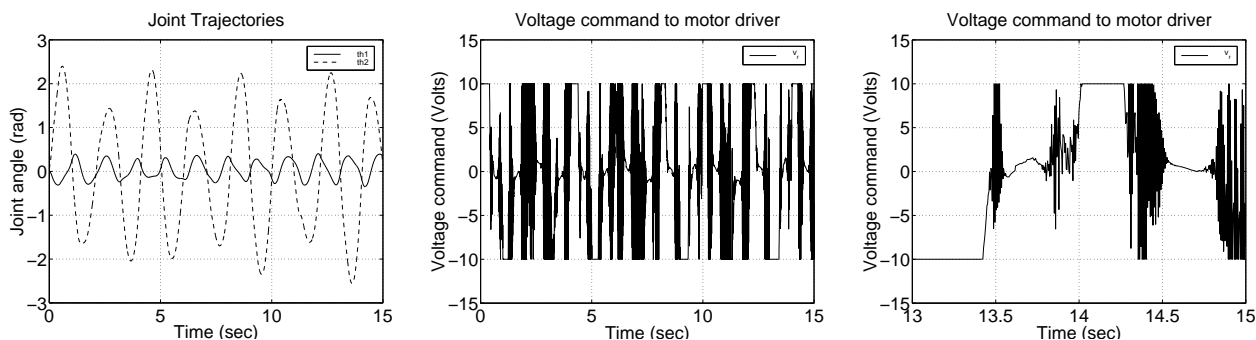

Figure 7.21: Experimental results of "chaotic" behavior under the original swing up controller, where $\theta^* = \frac{\pi}{3}, d^* = 0.7$. Left: Joint trajectories (solid: θ_1, dashed: θ_2), Center: Voltage command to the motor driver. Large amount of noise is induced by the noisy measurement of $\dot{\theta}_2$ obtained through numerical differentiation of θ_2. Note that we set an upper limit of the voltage command at ± 10 Volts according to the range of the D/A board (± 10 Volts). Right: A sample of the voltage command from $t = 13$ to $t = 15$.

Chapter 8

Conclusion

We have presented preliminary studies of a new brachiating controller for a simplified two-link robot. The algorithm uses a target dynamics method to solve a number of brachiation problems such as the ladder, swing up and rope problems. These tasks are encoded as the output of a target dynamical system inspired by the pendulum-like motion of an ape's (slow) brachiation. We have also introduced a hybrid controller combining the original target dynamics controller and a mechanical energy regulator as well as a control strategy for solving the leap problem arising from ape's fast brachiation. We provide numerical simulations suggesting the effectiveness of the proposed algorithm. We also present our empirical success in the implementation of the target dynamics method to a physical two-link brachiating robot. The proposed algorithm is applied to achieve the ladder and swing up behaviors. We achieve swing locomotion in the ladder problem and various swing up behaviors with different rates of energy pumping characterized by K_e. We demonstrate repeated locomotion over several rungs of the ladder as well. The experimental success bears out the validity of our control strategy in spite of the presence of model mismatches and physical effects previously unconsidered, although some manual tuning is required to implement these ideas.

In Section 8.1 we review some of the open questions this raises and in Section 8.2 we address future work.

8.1 Open Problems

These numerical simulations and experimental results suggest that the proposed algorithm is effective for solving robot brachiation problems. They are far from conclusive: a formal mathematical analysis will be required in order to truly understand how these ideas work. Most importantly, we need to consider the internal boundedness of the states of the closed loop system. The unactuated dynamics of our closed loop take the form of a one degree of freedom mechanical system forced by a periodic input. Such problems of parametric resonance are known to be complex. Furthermore, although we have favorable numerical results in the swing up problems, it is not still clear how to choose suitable parameters particularly for the hybrid swing up controller. A second open problem concerns the swing map. Numerical studies suggest the local stability of the fixed point d^* but this must be verified analytically, and the extent of the domain of attraction must be characterized.

8.2   Future Work

The controller developed in this dissertation requires exact model knowledge of the robot. "Passive" and, hence, less model dependent strategies will be addressed in our future work pursuing the analogy between the brachiation problem and the control of hopping robots. This analogy becomes particularly useful as we begin to contemplate studies of robot brachiation using more complicated models with higher degrees of freedom, where modelling of such systems is much more difficult. Specifically in Schwind's study on the control of simplified spring loaded inverted pendulum (SLIP) hopping robots [68, 69], a particular choice of a spring law allows us to integrate the system's dynamical equation of the stance phase analytically, and gives us the stance map in closed form. We suspect a similar approach may make the slow brachiation problem more analytically tractable. Finally, experimental implementation of the leaping strategy seems compelling. For reasons discussed in Section 7.6, this lies in the more distant future.

We believe there are generalizable principles of brachiation which may be established through the study of this simplified two degree of freedom model. In the longer run, we believe that the ideas presented in this dissertation may have wider application to such areas of robotics as dexterous manipulation, legged locomotion and underactuated mechanisms.

Bibliography

[1] Abraham, R. and Marsden, J. E., *Foundations of Mechanics*, The Benjamin/Cummings Publishing Company, Inc, 1978.

[2] Andersson, R. L., *A Robot Ping-Pong Player: Experiment in Real-Time Intelligent Control*, MIT Press, 1988.

[3] Arai, H., "Controllability of a 3-DOF manipulator with a passive joint under a nonholonomic constraint," In *IEEE International Conference on Robotics and Automation*, pages 3707–3713, 1996.

[4] Arai, H., Tanie, K., and Shiroma, N., "Time-scaling control of an underactuated manipulator," In *IEEE International Conference on Robotics and Automation*, pages 2619–2626, 1998.

[5] Arimoto, S., *Control Theory of Non-linear Mechanical Systems —A Passivity-based and Circuit-theoretic Approach*, Oxford University Press, 1996.

[6] Arisumi, H., Kotoku, T., and Komoriya, K., "Swing motion control of casting manipulation," *IEEE Control Systems Magazine*, vol. 19, no. 4, pp. 56–64, August 1999.

[7] Arnold, V. I., *Mathematical Methods of Classical Mechanics*, Springer-Verlag, 1989.

[8] Beek, P. J. and Lerbel, A., "The science of juggling," *Scientific American*, vol. 273, no. 5, pp. 92–97, November 1995.

[9] Berkemeier, M. D. and Fearing, R., "Tracking fast inverted trajectories of the underactuated acrobot," *IEEE Transactions on Robotics and Automation*, vol. 15, no. 4, pp. 740–750, August 1999.

[10] Bloch, A. M., Leonard, N. E., and Marsden, J. E., "Stabilization of the pendulum on a robot arm by the method of controlled lagrangian," In *IEEE International Conference on Robotics and Automation*, pages 500–505, May 1999.

[11] Bloch, A. M., Reyhanoglu, M., and McClamroch, N. H., "Control and stabilization of nonholonomic dynamic systems," *IEEE Transactions on Automatic Control*, vol. 37, no. 11, pp. 1746–1757, November 1992.

[12] Brockett, R. W., "Asymptotic stability and feedback stabilization," In Brockett, R. W., Millman, R. S., and Sussmann, H. J., editors, *Differential Geometric Control Theory*, pages 181–191. Birkhäuser, 1983.

[13] Brockett, R. W., "Nonlinear systems and differential geometry," *Proceedings of the IEEE*, vol. 64, no. 1, pp. 61–72, 1976.

[14] Bühler, M., Koditschek, D. E., and Kindlmann, P. J., "Planning and control of a juggling robot," *International Journal of Robotics Research*, vol. 13, no. 2, pp. 101–118, 1994.

[15] Bühler, M., Koditschek, D. E., and Kindlmann, P. J., "A family of robot control strategies for intermittent dynamical environments," *IEEE Control Systems Magazine*, vol. 10, no. 2, pp. 16–22, February 1990.

[16] Burridge, R. R., Rizzi, A. A., and Koditschek, D. E., "Sequential composition of dynamically dexterous robot behaviors," *International Journal of Robotics Research*, vol. 18, no. 6, pp. 534–555, June 1999.

[17] Carpenter, C. R., *Naturalistic Behavior of Nonhuman Primates*, The Pennsylvania State University Press, 1964.

[18] Eimerl, S. and DeVore, I., *The Primates*, TIME-LIFE BOOKS, 1966.

[19] Fernendes, C., Gurvits, L., and Li, Z. X., "Attitude control of space platform/manipulator system using internal motion," In *IEEE International Conference on Robotics and Automation*, pages 893–898, 1992.

[20] Fleagle, J., "Dynamics of a brachiating siamang [*Hylobates (Symphalangus) syndactylus*]," *Nature*, vol. 248, pp. 259–260, March 1974.

[21] Frohlich, C., "Do springboard divers violate angular momentum conservation?," *American Journal of Physics*, vol. 47, no. 7, pp. 583–592, July 1979.

[22] Frohlich, C., "The physics of somersaulting and twisting," *Scientific American*, vol. 242, no. 3, pp. 154–164, March 1980.

[23] Fukuda, T., Hosokai, H., and Kondo, Y., "Brachiation type of mobile robot," In *Fifth International Conference on Advanced Robotics*, pages 915–920, June 1991.

[24] Fukuda, T., Saito, F., and Arai, F., "A study on the brachiation type of mobile robot (heuristic creation of driving input and control using CMAC," In *IEEE/RSJ International Workshop on Intelligent Robots and Systems*, pages 478–483, 1991.

[25] Furuta, K., Yamakita, M., and Kobayashi, S., "Swing-up control of inverted pendulum using pseudo-state feedback," *Proceedings of the Institution of Mechanical Engineers, Part I, Journal of Systems and Control Engineering*, vol. 206, no. I 4, pp. 263–269, 1992.

[26] Goldstein, H., *Classical Mechanics, 2nd edition*, Addison-Wesley, 1980.

[27] Hauser, J. and Murray, R. M., "Nonlinear controllers for non-integrable systems: the acrobot example," In *American Control Conference*, pages 669–671, 1990.

[28] Hodgins, J. K. and Raibert, M. H., "Biped gymnastics," *International Journal of Robotics Research*, vol. 9, no. 2, pp. 115–132, April 1990.

[29] Kamon, M. and Yoshida, K., "3D attitude control methods of free-flying dynamic system with initial angular momentum," *Journal of Robotics Society of Japan*, vol. 16, no. 2, pp. 223–231, 1998, (in Japanese).

[30] Kane, T. R. and Scher, M. P., "A dynamical explanation of the falling cat phenomenon," *International Journal of Solids and Structures*, vol. 5, pp. 663–670, 1969.

[31] Kawamura, T., Yamafuji, K., and Kobayashi, T., "A study on posture control and soft landing of a free falling robot (3rd report, fall experiment with cat turning motion)," *Transactions of the Japan Society of Mechanical Engineers, Series C*, vol. 58, no. 552, pp. 2495–2500, 1992, (in Japanese).

[32] Keith, A., "On the chimpanzees and their relationship to the gorillas," In *Proceedings of the Zoological Society of London*, pages 296–312, 1899.

[33] Khalil, H. K., *Nonlinear Systems, Second Edition*, Prentice-Hall, 1996.

[34] Kobayashi, K., Imura, ichi J., and Yoshikawa, T., "Controllability of planar manipulators with one unactuated joint," *Journal of Robotics Society of Japan*, vol. 17, no. 8, pp. 1167–1172, 1999, (in Japanese).

[35] Koditschek, D. E., "Natural motion for robot arms," In *IEEE Conference of Decision and Control*, pages 733–735, 1984.

[36] Koditschek, D. E., "Dynamically dexterous robots," In Spong, M. W., Lewis, F. L., and Abdallah, C. T., editors, *Robot Control: Dynamics, Motion Planning and Analysis*, pages 487–490. IEEE Press, 1993.

[37] Koditschek, D. E. and Bühler, M., "Analysis of a simplified hopping robot," *International Journal of Robotics Research*, vol. 10, no. 6, pp. 587–605, December 1991.

[38] Lewis, A. D. and Murray, R. M., "Configuration controllability of simple mechanical control systems," *SIAM Journal on Control and Optimization*, vol. 35, no. 3, pp. 766–790, 1997.

[39] Li, P. Y. and Horowitz, R., "Control of smart exercise machines—part I: Problem formulation and nonadaptive control," *IEEE/ASME Transactions on Mechatronics*, vol. 2, no. 4, pp. 237–247, December 1997.

[40] Li, P. Y. and Horowitz, R., "Control of smart exercise machines—part II: Self-optimizing control," *IEEE/ASME Transactions on Mechatronics*, vol. 2, no. 4, pp. 248–258, December 1997.

[41] Li, P. Y. and Horowitz, R., "Passive velocity field control of mechanical manipulators," *IEEE Transactions on Robotics and Automation*, vol. 15, no. 4, pp. 751–763, August 1999.

[42] Lynch, K. M. and Mason, M. T., "Dynamic nonprehensile manipulation: Controllability, planning and experiments," *International Journal of Robotics Research*, vol. 18, no. 1, pp. 64–92, January 1999.

[43] Lynch, K. M., Shiroma, N., Arai, H., and Tanie, K., "Motion planning for a 3-DOF robot with a passive joint," In *IEEE International Conference on Robotics and Automation*, pages 927–932, 1998.

[44] Mareczek, J., Buss, M., and Schmidt, G., "Robust global stabilization of the underactuated 2-DOF manipulator R2D1," In *IEEE International Conference of Robotics and Automation*, pages 2640–2645, 1998.

[45] Marilier, T. and Richard, J. A., "Non-linear mechanic and electric behavior of a robot axis with a 'harmonic-drive' gear," *Robot. Computer Integrated Manufact.*, vol. 5, no. 2–3, pp. 129–136, 1989.

[46] M'Closkeys, R. T. and Burdick, J. W., "Periodic motions of a hopping robot with vertical and forward motion," *International Journal of Robotics Research*, vol. 12, no. 3, pp. 197–218, June 1993.

[47] Nakamura, Y., "Non-holonomic robot systems, part 1–5," *Journal of Robotics Society of Japan*, vol. 11, no. 4–7, 1993, vol. 12, no. 2, 1994 (in Japanese).

[48] Nakamura, Y. and Mukherjee, R., "Nonholonomic path planning of space robots via a bidirectional approach," *IEEE Transactions on Robotics and Automation*, vol. 7, no. 4, pp. 500–514, August 1991.

[49] Nakano, E. and Tsuchiya, M., "A study on the control of rotational maneuvers of a robot in midair," *Journal of Robotics Society of Japan*, vol. 11, no. 1, pp. 91–99, 1993, (in Japanese).

[50] Napier, J. R. and Napier, P. H., *A Handbook of Living Primates*, Academic Press, 1967.

[51] Napier, J., "Brachiation and brachiators," In Napier, J. and Barnicot, N. A., editors, *The Primates: the Proceedings of the Symposium held on 12th–14th April 1962 at the Offices of The Zoological Society of London*, pages 183–195. London, The Society, 1963.

[52] Nonaka, K., Yamakita, M., and Furuta, K., "Swing up control of double pendulum," In *IEEE International Conference on Robotics and Automation, Conference Video Proceedings*, 1993.

[53] Oriolo, G. and Nakamura, Y., "Free-joint manipulators: Motion control under second-order nonholonomic constraints," In *IEEE/RSJ International Workshop on Intelligent Robots and Systems*, pages 1248–1253, November 1991.

[54] Owen, R., "On the orang, chimpanzee and gorilla," In *Appendix B to On the Classification and Geographical distribution of the Mammalia (Reade Lecture, Cambridge, May 1859)*, pages 64–103. Parker, London, 1859.

[55] Parsons, P. E. and Taylor, C. R., "Energetics of brachiation versus walking: A comparison of a suspended and an inverted pendulum mechanism," *Physiological Zoology*, vol. 50, no. 3, pp. 182–188, July 1977.

[56] Preuschoft, H. and Demes, B., "Biomechanics of brachiation," In Preuschoft, H., Chivers, D. J., Brockelman, W. Y., and Creel, N., editors, *The Lesser Apes*, pages 96–118. Edinburgh University Press, 1984.

[57] Raibert, M. H., *Legged Robots that Balance*, MIT Press, 1986.

[58] Rathinam, M. and Murray, R. M., "Configuration flatness of lagrangian systems underactuated by one control," *SIAM Journal on Control and Optimization*, vol. 36, no. 1, pp. 164–179, 1998.

[59] Rizzi, A. A. and Koditschek, D. E., "Dynamically dexterous robotics: The two juggle," In *IEEE International Conference on Robotics and Automation, Conference Video Proceedings*, 1993.

[60] Rizzi, A. A. and Koditschek, D. E., "Further progress in robot juggling: The spatial two-juggle," In *IEEE International Conference on Robotics and Automation*, pages 919–924, 1993.

[61] Rizzi, A. A., Whitcomb, L. L., and Koditschek, D. E., "Distributed real-time control of a spatial robot juggler," *IEEE Computer*, vol. 25, no. 5, pp. 12–24, May 1992.

[62] Saito, F., *Motion Control of the Brachiation Type of Mobile Robot*, PhD thesis, Nagoya University, March 1995, (in Japanese).

[63] Saito, F. and Fukuda, T., "Brachiation robot," In *IEEE International Conference on Robotics and Automation, Conference Video Proceedings*, 1993.

[64] Saito, F. and Fukuda, T., "A multi-link brachiation robot," In *IEEE International Conference on Robotics and Automation, Conference Video Proceedings*, 1996.

[65] Saito, F., Fukuda, T., and Arai, F., "Movement control of brachiation robot using CMAC between different distance and height," In *IMACS/SICE International Symposium on Robotics, Mechatronics and Manufacturing Systems*, pages 35–40, 1992.

[66] Saito, F., Fukuda, T., and Arai, F., "Swing and locomotion control for a two-link brachiation robot," *IEEE Control Systems Magazine*, vol. 14, no. 1, pp. 5–12, February 1994.

[67] Schaal, S. and Atkeson, C. G., "Robot juggling: Implementation of memory-based learning," *IEEE Control Systems Magazine*, vol. 14, no. 1, pp. 57–71, February 1994.

[68] Schwind, W. J. and Koditschek, D. E., "Control of the forward velocity of the simplified planner hopping robot," In *IEEE International Conference on Robotics and Automation*, pages 691–696, 1995.

[69] Schwind, W. J. and Koditschek, D. E., "Characterization of monoped equilibrium gaits," In *IEEE International Conference on Robotics and Automation*, pages 1986–1992, 1997.

[70] Simons, E. L., *Primate Evolution: An Introduction to Man's Place in Nature*, Macmillan, 1972.

[71] Slotine, J.-J. E. and Li, W., *Applied Nonlinear Control*, Prentice-Hall, 1991.

[72] Spong, M., "Partial feedback linearization of underactuated mechanical systems," In *IEEE/RSJ International Conference on Intelligent Robots and Systems*, pages 314–321, September 1994.

[73] Spong, M., "The swing up control problem for the acrobot," *IEEE Control Systems Magazine*, vol. 15, no. 1, pp. 49–55, February 1995.

[74] Stoer, J. and Bulirsch, R., *Introduction to Numerical Analysis*, Springer-Verlag, 1980.

[75] Strogatz, S. H., *Nonlinear Dynamics and Chaos*, Addison-Wesley, 1994.

[76] Sussmann, H. J., "A general theorem on local controllability," *SIAM Journal on Control and Optimization*, vol. 25, no. 1, pp. 158–194, January 1987.

[77] Suzuki, T., Koinuma, M., and Nakamura, Y., "Chaos and nonlinear control of a nonholonomic free-joint manipulator," In *IEEE International Conference on Robotics and Automation*, pages 2668–2675, April 1996.

[78] Suzuki, T. and Nakamura, Y., "Control of manipulators with free-joints via the averaging method," In *IEEE International Conference on Robotics and Automation*, pages 2998–3005, April 1997.

[79] Takashima, S., "Control of gymnast on a high bar," In *IEEE/RSJ International Conference on Intelligent Robots and Systems*, pages 1424–1429, November 1991.

[80] Trevor, J. C., "The history of the word "brachiator" and a problem of authorship in primate nomenclature," In Napier, J. and Barnicot, N. A., editors, *The Primates: the Proceedings of the Symposium held on 12th–14th April 1962 at the Offices of The Zoological Society of London*, pages 197–198. London, The Society, 1963.

[81] Tuttle, T. D. and Seering, W. P., "A nonlinear model of a harmonic drive gear transmission," *IEEE Transactions on Robotics and Automation*, vol. 12, no. 3, pp. 368–374, June 1996.

[82] Vakakis, A. F., Burdick, J. W., and Caughey, T. K., "An "interesting" strange attractor in the dynamics of a hopping robot," *International Journal of Robotics Research*, vol. 10, no. 6, pp. 606–618, December 1991.

[83] Nieuwstadt, van M., Rathinam, M., and Murray, R. M., "Differential flatness and absolute equivalence of nonlinear control systems," *SIAM Journal on Control and Optimization*, vol. 36, no. 4, pp. 1225–1239, 1998.

[84] Yamakita, M., Iwashiro, M., Sugagara, Y., and Furuta, K., "Robust swing up control of double pendulum," In *American Control Conference*, pages 290–295, June 1995.

Appendix A

Publications

Title	Publication	Authors
I. Journals and Transactions		
1. Analytical Approach to Studies of Two-link Brachiating Robot Control (in Japanese)	Journal of the Robotics Society of Japan, vol. 16, No. 3, pp. 361–368 (1998)	Jun Nakanishi Toshio Fukuda Daniel E. Koditschek
2. Study on the Control of Two-link Brachiating Robot— Experimental Implementation of a Target Dynamics Controller— (in Japanese)	Journal of the Robotics Society of Japan, vol. 17, No. 1, pp. 110–117 (1999)	Jun Nakanishi Toshio Fukuda Daniel E. Koditschek
3. Study on the Control of a Two-link Brachiating Robot (Brachiation on a Ladder with Irregular Intervals via Target Dynamics) (in Japanese)	Transactions of the Japan Society of Mechanical Engineers, Series C, Vol. 65, No. 639, pp. 4387–4394 (1999)	Jun NAKANISHI Toshio FUKUDA Daniel E. KODITSCHEK
4. A Brachiating Robot Controller	IEEE Transactions on Robotics and Automation (to appear) (1999)	Jun Nakanishi Toshio Fukuda Daniel E. Koditschek
II. International Conferences		
1. Preliminary Studies of a Second Generation Brachiation Robot Controller	1997 IEEE International Conference on Robotics and Automation, pp. 2050–2056, Albuquerque, USA (1997)	Jun Nakanishi Toshio Fukuda Daniel E. Koditschek
2. Experimental Implementation of a "Target Dynamics" Controller on a Two-link Brachiating Robot	1998 IEEE International Conference on Robotics and Automation, pp. 787–792, Leuven, Belgium (1998)	Jun Nakanishi Toshio Fukuda Daniel E. Koditschek
3. Brachiation on a Ladder with Irregular Intervals	1999 IEEE International Conference on Robotics and Automation, pp. 2717–2722, Detroit, USA (1999)	Jun Nakanishi Toshio Fukuda Daniel E. Koditschek
4. A Hybrid Swing up Controller for a Two-link Brachiating Robot	1999 IEEE/ASME International Conference on Advanced Intelligent Mechatronics, pp. 549–554, Atlanta, USA (1999)	Jun Nakanishi Toshio Fukuda Daniel E. Koditschek
5. A Leaping Maneuver for a Brachiating Robot	2000 IEEE International Conference on Robotics and Automation San Francisco, USA (2000) (accepted for presentation)	Jun Nakanishi Toshio Fukuda

Appendix B

Parameter Identification

We need to identify the dynamical parameters corresponding to the robot's Lagrangian dynamics. We initially considered an off-line least squares estimation method with torque filtering [71], but were unable to obtain a good estimate of the parameter set with this scheme. This may be because of somewhat inaccurate and noisy sensory data particularly obtained with the rate gyro[1]. In consequence, we resorted to a rather simple identification procedure, where the inertia parameters are obtained either or direct measurement or from the manufacturer's data, and the preliminary estimate of the friction coefficients are obtained from the natural dissipation of the system. These parameters were refined iteratively by comparing step and sinusoid responses obtained experimentally to those generated by simulations using the "best" parameters. In this comparison, we considered step response with various amplitude as well as sinusoid response with various amplitude and frequencies. The results of the parameter identification are listed in Table 2.1. Here, the mass of the two motors at the elbow joint is included in the first link, however, we could also derive an equivalent model having symmetry in the link parameters since there is redundancy in the inertia parameters. The efficacy of this parameter identification approach is illustrated in Figure B.1 which shows examples of the comparison between experimental runs and simulations using the parameters of Table 2.1 in Chapter 2.

---

[1]Standard least squares method is susceptible to noise and inaccuracy in the measurement. Numerical studies suggests that we indeed obtain good estimation of the set of dynamical parameters with the absence of error and noise in the measurement.
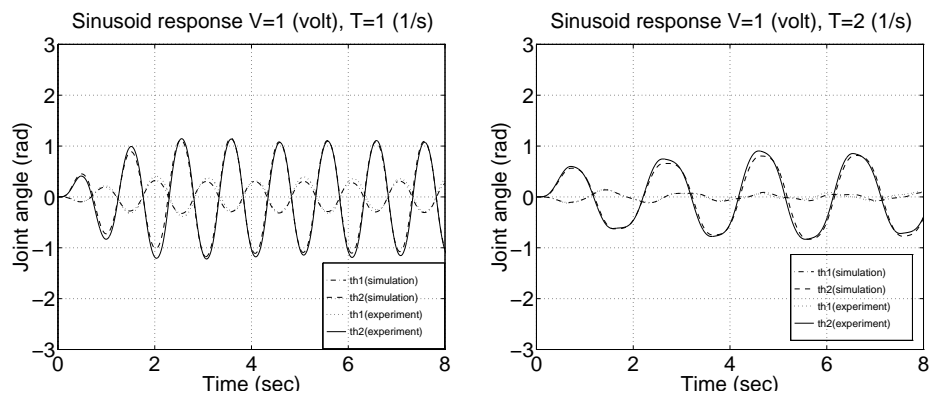
Figure B.1: Examples of the comparison between experimental runs and simulations. Left: voltage command $v_r = \sin(2\pi t)$, right: voltage command $v_r = \sin(\pi t)$. These plots show close matching between the numerical simulations using the obtained model and experiments.

Appendix C

Discrepancy between Simulations and Experiments

C.1 Unmodelled Nonlinear Characteristics of Harmonic Drive DC Motors

We see some discrepancy in the motion of the robot and the choices of K_e to achieve similar swing up behavior of the robot between the numerical simulations and experiments presented above. This section presents our efforts to understand how various physical effects and model mismatch affect the behavior of the robot.

The proposed controller using input/output linearization technique aggressively cancels non-linearities in the plant dynamics to achieve the target dynamics, which requires exact model knowledge of the system. As we have pointed out, harmonic drives bear complicated nonlinear dynamics [81]. We suspect that unmodelled nonlinear characteristics of the harmonic drive DC motors at the elbow joint, such as nonlinear viscous friction, stiction and torque saturation, may be one of the main reasons of such discrepancy. Consider a slightly modified friction model, which includes coulomb friction, linear and cubic viscous friction and stiction, denoted by

$$\tau_{fric} = c_2 \text{sgn}(\dot{\theta}_2) + b_2 \dot{\theta}_2 + \bar{b}_2 \dot{\theta}_2^3 + s_2 \text{sgn}(\dot{\theta}_2) e^{-\kappa |\dot{\theta}_2|} \tag{C.1}$$

where c_2 is the coulomb friction coefficient, b_2 and $\bar{b}_2$ are the viscous friction coefficients, s_2 represents stiction torque, and κ denotes the lubrication coefficient [5]. The introduction of the cubic term in (C.1) seems to be reasonable as described in the study on the modelling of harmonic drive gear transmission mechanisms [81]. We assume that torque produced by the actuator saturates when torque commands exceeds the regular operating range of the motor.

C.2 Simulation

In the following numerical studies, we present our effort to reproduce the circumstances in the experiments in order to understand the reasons for the discrepancy. For the plant model, we use the dynamics denoted by (2.1), but the friction terms of the second joint are substituted by (C.1). The inertia parameters shown in Table 2.1, and the friction parameters, $c_1 = 0.02, b_1 = 0.02, c_2 = 0.22, b_2 = 0.14, \bar{b}_2 = 6.02 \times 10^{-3}, s_2 = 0.5$ and $\kappa = 20$ are used for the robot. However, we choose
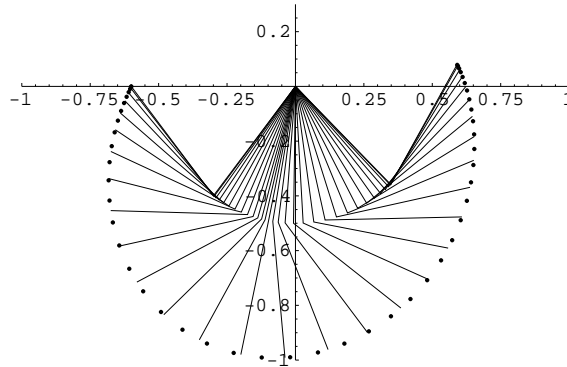
Figure C.1: Movement of the robot considering unmodelled characteristics of the actuator. The numerical simulations closely match the corresponding experimental results.

to use $\bar{b}_2 = 0$ for the slow swing up case ($K_e = 0.03$) since we have found in numerical simulation that setting $\bar{b}_2 = 0$ gives better match. In fact, as discussed in [81], harmonic drives have other complicated characteristics such as variation of friction depending on the position of harmonic-drive output and dramatic increase of dissipation at some operating ranges that excite system resonance, which are difficult to model. Furthermore, [81] points out that friction in some drives can actually decrease over some velocity ranges as reported in [45]. In the following simulations, the torque saturation is introduced at ± 5.2Nm[1]. For the controller, we use the same control law (3.21) and the same dynamical parameters that are used for the experimental implementation. Although we have yet to gain full understanding of the circumstances, the following simulations do, indeed, match closely with observed experimental results suggesting that our assumptions of unmodelled dynamics and torque saturation of the actuator may be reasonable for the explanation of some of the causes of the discrepancy we have seen.

C.2.1   Uniform Ladder Problem

Consider the same case as the experiments presented in section 7.1. The next bar is located at the distance of $d^* = 0.6$ and we choose $\omega = \hat{\lambda}(0.6) = 3.36$. The same parameters are used for the controller as we have chosen in the experiments. The movement of the robot is depicted in Figure C.1, while the joint trajectories and the voltage commands sent to the driver are shown in Figure C.2. The gripper reaches $d = 0.623$ at $t = 0.810$ seconds. The numerical simulation closely match the experimental results.

C.2.2   Slow Swing up ($K_e = 0.03$)

The same parameters are used for the controller as we have chosen in the experiments (K_e and dynamical parameters of the robot). Figure C.3 shows the joint trajectory and the voltage command to the motor driver. The gripper reaches at $d = 0.532$ at $t = 7.36$ seconds. The numerical simulations closely match the experimental results.

---

[1]According to the manufacturer's data, the rated torque of this motor is 3.2Nm, the instantaneous maximum torque is 14Nm, and the rated current is 1.8A which corresponds to the torque about 5.26Nm.
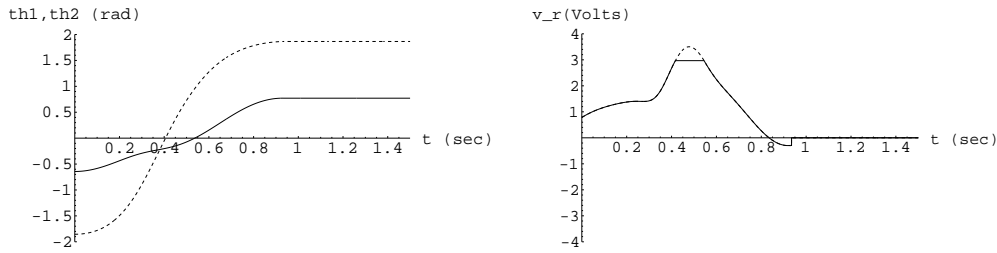
Figure C.2: The simulation results of the ladder problem considering unmodelled characteristics of the actuator. Left: Joint trajectories (θ_1: solid, θ_2: dashed). Right: Voltage command to the motor driver. Solid line corresponds to the produced torque by the actuator considering saturation. Dashed line denotes the voltage command. The numerical simulation closely match the corresponding experimental results in Figure 7.2.
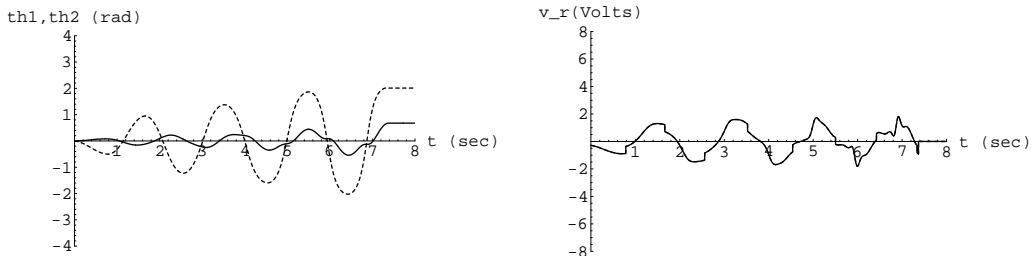

Figure C.3: Simulation results of slow swing up behavior ($K_e = 0.03$) considering unmodelled characteristics of the actuator. Left: Joint trajectories (θ_1: solid, θ_2: dashed). Right: Voltage command to the motor driver. Solid line corresponds to the produced torque by the actuator considering saturation. Dashed line denotes the voltage command.The numerical simulations closely match the corresponding experimental results.

C.2.3 Fast Swing up ($K_e = 0.47$)

Consider the same case of the fast swing up ($K_e = 0.46$) as the experiments presented in section 7.2. The same parameters are used for the controller as we have chosen in the experiments (K_e and dynamical parameters of the robot). Figure C.4 shows the joint trajectory and the voltage command to the motor driver. The gripper reaches at $d = 0.599$ at $t = 3.83$ seconds. The numerical simulations closely match the experimental results.

C.2.4 Faster Swing up ($K_e = 0.9$)

Consider the same case of the faster swing up ($K_e = 0.9$) as the experiments presented in Section 7.2. The same parameters are used for the controller as we have chosen in the experiments (K_e and dynamical parameters of the robot). Figure C.5 shows the joint trajectory and the voltage command to the motor driver. The gripper reaches at $d = 0.645$ at $t = 2.79$ seconds. The simulation closely matches the experimental results.
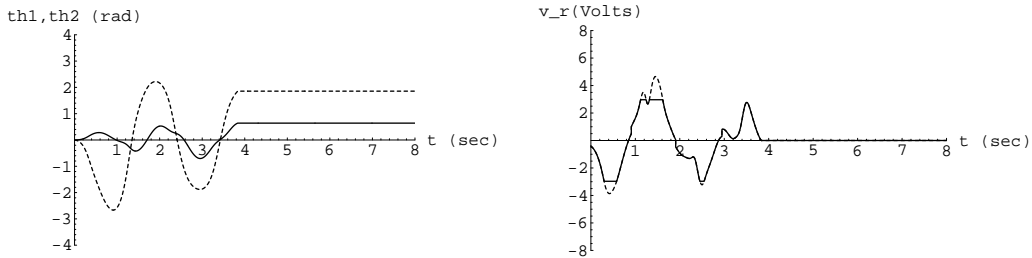
Figure C.4: Simulation results of fast swing up behavior ($K_e = 0.47$) considering unmodelled characteristics of the actuator. Left: Joint trajectories (θ_1: solid, θ_2: dashed). Right: Voltage command to the motor driver. Solid line corresponds to the produced torque by the actuator considering saturation. Dashed line denotes the voltage command. The numerical simulations closely match the corresponding experimental results.
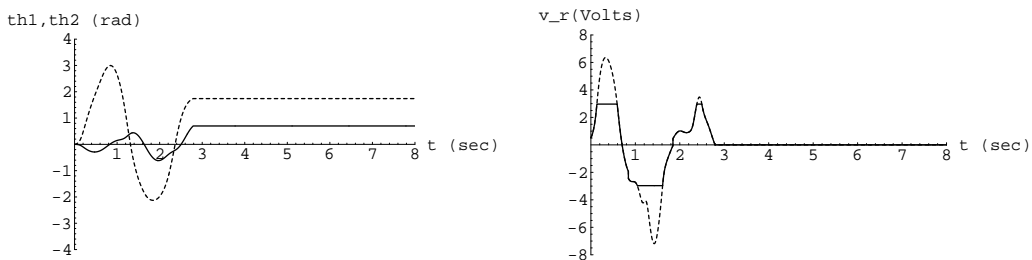
Figure C.5: Simulation results of faster swing up behavior ($K_e = 0.9$) considering unmodelled characteristics of the actuator. Left: Joint trajectories (θ_1: solid, θ_2: dashed). Right: Voltage command to the motor driver. Solid line corresponds to the produced torque by the actuator considering saturation. Dashed line denotes the voltage command.The numerical simulations closely match the corresponding experimental results.

Appendix D

Specifications of the Hardware Elements

Type		RH–8–6006	RH–14–6002
Rated Power	W	8.6	20.3
Rated Voltage	A	24	24
Rated Current	A	1.0	1.8
Rated Torque	N·m	1.4	3.2
Rated Rotational Speed	rpm	60	60
Instantaneous Maximum Current	A	1.6	5.4
Instantaneous Maximum Torque	N·m	2.7	14
Maximum Rotational Speed	rpm	100	100
Gear Ratio	1 : R	1 : 50	1 : 50

Table D.1: The specifications of the motors (Harmonic Drive Systems, DC servo actuator RH series).

Rated Output Voltage	± 30 V
Rated Output Current	± 3.8 A
Maximum Output Voltage	± 45 V
Maximum Output Current (Continuous)	± 16.7 A
Maximum Output Power (Continuous)	± 750 W
Power Supply Requirements	DC 12 V ∼ 48 V
Reference Voltage Signals	± 10 V
Outline Dimensions	100 × 90 × 35 mm
Weight	130 g

Table D.2: The specifications of th motor driver circuit (Titech Robot Driver). Since we do not require the maximum output current as large as 16.7A, we adjusted the range of output current between ±5A for the grippers and ±6A for the elbow actuator as directed in the manual of this motor driver circuit.

Power Supply Requirements	DC 8 ∼ 13.5 V
Maximum Angular Velocity	± 90 deg/s
Sensitivity	± 45 deg/s/V
Output Signals	2.5 V at zero angular velocity
	± 2.0 V at maximum angular velocity
Linearity	within 0.1 % of maximum angular velocity
Hysteresis	None
Offset Temperature	within 0.1 % / °C of maximum angular velocity
Drift	within 0.2 % / h of maximum angular velocity
Outline Dimensions	24 × 24 × 58 mm
Weight	41 g

Table D.3: The specifications of the gyro (Murata Manufacturing, ENV-05S). Originally, the range of measurable angular velocity of this gyro is up ±90 deg/s. However, this is insufficient for our applications, where the estimated maximum angular velocity for the first link can be over 160 deg/s. Thus, we had our gyros adjusted by the manufacture so that we can measure the angular velocity up to ±200 deg/s.